12-2001

A Molecular Investigation of Absorption onto Mineral Pigments

Brian J. Ninness

A MOLECULAR INVESTIGATION OF ADSORPTION ONTO MINERAL PIGMENTS

By

Brian J. Ninness

B.S. University of Pittsburgh, 1995

M.S. University of Maine, 1997

A THESIS

Submitted in Partial Fulfillment of the

Requirements for the Degree of

Doctor of Philosophy

(in Chemical Engineering)

The Graduate School

The University of Maine

December, 2001

Advisory Committee:

Carl Tripp, Associate Professor of Chemistry and LASST, Co-Advisor
Douglas Bousfield, Professor of Chemical Engineering, Co-Advisor
Bill DeSisto, Assistant Professor of Chemical Engineering
William Unertl, Professor of Physics and LASST
Adriaan van Heiningen, Professor of Chemical Engineering

A MOLECULAR INVESTIGATION OF ADSORPTION ONTO MINERAL PIGMENTS

By Brian J. Ninness

Thesis Co-Advisors: Dr. Carl P. Tripp and Dr. Douglas W. Bousfield

An Abstract of the Thesis Presented
in Partial Fulfillment of the Requirements for the
Degree of Doctor of Philosophy
(in Chemical Engineering)
December, 2001

Pigment suspensions are important in several processes such as ceramics, paints, inks, and coatings. In the wet state, pigments are combined with a variety of chemical species such as polymers, surfactants, and polyelectrolytes which produce a complex colloidal system. The adsorption, desorption, and redistribution of these species at the pigment – aqueous solution interface can have an impact on the behavior in both the wet state or its final dried state. The goal of this work is to establish a molecular picture of the adsorption properties of these pigmented systems.

A novel *in situ* infrared technique has been developed which allows the detection of adsorbed surface species on pigment particles in an aqueous environment. The technique involves the use of a polymeric binder to anchor the colloidal pigment particles to the surface of an internal reflection element (IRE). The binder only weakly perturbs about 25% of the reactive surface sites (hydroxyl groups) on silica. The reaction of succinic anhydride with an aminosilanized silica surface has been quantified using this technique.

The adsorption dynamics of the cationic surfactant cetyltrimethylammonium bromide (C_{16}TAB) at the TiO_2 – aqueous solution interface has been investigated using Fourier transform infrared – attenuated total reflection spectroscopy (FTIR-ATR) and electrokinetic analysis. At low bulk concentrations, C_{16}TAB is shown to adsorb as isolated islands with a "defective" bilayer structure. Anionic probe molecules are shown to effectively "tune" the adsorbed surfactant microstructure. The results indicate that the structure of the adsorbed surfactant layer, and not the amount of adsorbed surfactant, dictates the subsequent adsorption behavior of the system.

Atomic Layer Deposition is used to deposit a TiO_2 layer onto the surfaces of silica and kaolin pigments. The process involves the cyclic reaction sequence of the vapors of $TiCl_4$ and H_2O. Three complete deposition cycles are needed before the surfaces of the modified pigments are dominated by the presence of TiO_2. The modified kaolin pigments display increased dispersion stability as compared to the parent kaolin. The electrokinetic behavior of the modified kaolin is shown to be identical to that of pure TiO_2 pigments.

ACKNOWLEDGEMENTS

The author wishes to express his most sincere appreciation to the advisors of this project, Dr. Carl Tripp and Dr. Douglas Bousfield. Dr. Bousfield has provided continuing guidance and support throughout both the author's M.S. and Ph.D. programs, along with leading a nationally recognized research program in the field of Paper Surface Science. A special thanks is due to Dr. Tripp for providing such a stimulating environment for advanced research, for devoting countless hours to pertinent discussions relating to this project, and also for being a compassionate friend as well as advisor.

The author would also like to express a sincere thanks to Dr. Bill DeSisto, Dr. William Unertl, and Dr. Adriaan van Heiningen for the time which was devoted to help lead direction in this project, and for the time devoted to reading and commenting on this thesis.

The funding for this research was provided by the industrial sponsors of the Paper Surface Science Program at the University of Maine, and by a grant from the Department of the Navy, Naval Surface Warfare Center, Dohlgren Division.

Finally, this work would not have been possible without the never-ending support, patience, and love of my wife Dora. She has provided the foundation on which this research was built, and for which I am deeply thankful.

This dissertation is dedicated to my daughter Hailey, who blessed the final moments of its preparation with her emergence into this world.

TABLE OF CONTENTS

LIST OF TABLES

LIST OF FIGURES

LIST OF EQUATIONS

CHAPTER 1. INTRODUCTION

1.1. Paper Coating

Pigmented coatings are applied to the surface of paper in order to improve or enhance the optical and printing properties of the surface. Paper coatings consist mainly of (greater than 99% by weight) mineral pigments, binders and water. The remaining constituents can be considered functional additives, whose purpose is to impart a desired property characteristic to the wet or dry state of the coating. This combination of ingredients produces a complex colloidal system made up of a number of chemical species, each with its own set of physical and chemical properties. It is the molecular interactions between these various chemical species that will ultimately dictate certain macroscopic properties such as viscosity, dewatering behavior, and ink receptivity. Establishing a molecular picture of the adsorption properties of these systems is important to developing an understanding of the complex colloidal behavior of these coating systems.

An applied paper coating is a porous, composite material, primarily based on a pigment and binder, and whose structure and properties is primarily determined by the pigment "skeleton". These coatings are typically formulated with just enough binder in order to promote minimum coating cohesion and adhesion to the underlying paper substrate. The ultimate choice of binder level depends on the end-use properties of the coated paper. In this way coatings are often compared by their pigment volume concentration (PVC). The PVC is defined as the volume of pigment per total volume of pigment and binder, as illustrated in Equation 1.1.

(1.1) PVC = Pigment Volume / [Total Volume of Pigment + Binder]

The critical pigment volume concentration (CPVC) is the concentration at which the binder, or fluid, just fills the interstitial voids between the pigment particles. At concentrations below the CPVC the pigment is dispersed in a "sea" of binder. Above the CPVC there is not enough binder present to fill the interstitial spaces between pigments, and therefore air voids are present. Most paper coatings are formulated above the CPVC, where the presence of voids positively contributes to the optical properties of the coating. It is the voids that are responsible for the scattering of the incident light which contributes to the opacity of the final coated sheet. The improved optical properties are somewhat offset by the degradation of mechanical strength caused by the lack of binder. This performance-property relationship is illustrated in Figure 1.1.

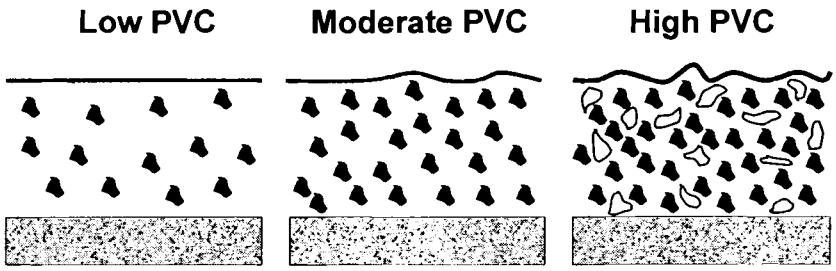

Performance			
Mechanical:	Strong	Weak	Very Weak
Chemical:	Strong	Moderate	Very Poor
Optical:	Weak	Strong	Very Opaque

Figure 1.1. Effects of pigment volume concentration (PVC).

1.2. Pigments

The pigment particles are the building blocks of the final coated layer, and as a result, their role is of the utmost importance. In the wet state the pigments typically constitute greater than 80% of the total formulation, with the remaining 20% being the binder and various additives. Different types of pigments are used in order to confer some desired property to the finished product (i.e. gloss, printability, smoothness). The performance of a specific pigment depends on a multitude of both physical and chemical properties such as chemical composition, particle morphology, refractive index, and reactivity. Kaolin and $CaCO_3$ are by far the most widely used. Other pigments include amorphous silica, titanium dioxide, and more recently plastic pigments. Amorphous silica dominates the ink-jet coated paper market, while titanium dioxide is frequently added to kaolin based coatings in order to achieve target levels of opacity and sometimes brightness.

1.2.1. Kaolin

The term kaolin, as used in the paper coating industry, refers to a clay material comprised mainly of the mineral kaolinite. Structurally, kaolin is a 1:1 layered aluminosilicate that consists of a tetrahedral silica surface and an octahedral alumina surface. The theoretical structural formula of kaolin is $Al_2O_3 \bullet 2SiO_2 \bullet 2H_2O$, and has a theoretical composition of 46.5% SiO_2, 39.5% Al_2O_3, and 14% H_2O [1]. Kaolin is a natural, mined pigment and is classified as coming from either primary or secondary deposits. Primary deposits are found in close association with the parent rocks, and therefore have a high proportion of other minerals and impurities which must be removed

before the kaolin is ready for coating applications. On the other hand, secondary deposits have been transported, by water, away from their original source, and consist of mainly beds of pure clay.

In paper coating applications kaolin finds widespread use in the wood-containing sector, especially for lightweight, coated grades (LWC) [2]. The sheet-like atomic structure of kaolin produces flat plate-like pigment particles, which allow coated gloss to be achieved readily. Also, since the particle packing behavior of these plate-like particles is quite poor, the resulting coating is quite bulky and open. This produces a compressible coating layer which is advantageous in the gravure printing process. The compressible nature of the kaolin coating enables good contact to be made with the ink contained in the recessed cavities of the gravure printing cylinder.

1.2.2. Calcium Carbonate

Calcium carbonate ($CaCO_3$) occurs naturally in two crystalline structures, calcite and aragonite. The only thermodynamically stable form of these two is calcite. As a paper coating pigment $CaCO_3$ is classified as either a natural or synthetic product. The natural products are produced by grinding of the naturally occurring rock materials limestone, marble, and chalk. Pigments derived from these sources are termed ground calcium carbonate (GCC). Precipitated calcium carbonate (PCC) is a synthetically prepared pigment, produced by reacting a calcium-containing material with a carbonate or with carbon dioxide gas [2]. By maintaining control of the reaction conditions the particle size and shape of the PCC can be controlled.

The main use of $CaCO_3$ pigments in paper coating applications is to achieve a bright, white coating layer. The superior particle packing of $CaCO_3$ pigments, as compared to kaolin particles, dismisses their use for gravure printed grades. The $CaCO_3$ pigments find widespread use in wood-free offset grades. The natural pigments (GCC) are also used in many applications as a pre-coat layer.

1.2.3. Titanium Dioxide

Titanium dioxide is the premier opacifying pigment used in both paint and coating applications. It is a synthetic pigment, and as such is probably the most expensive ingredient used in paper coating formulations. There are two common procedures used for the manufacture of TiO_2 pigments. In the first process, the "sulfate process", the ore ilmenite ($FeO \bullet TiO_2$) is leached with sulfuric acid, and the resulting solution is subsequently hydrolyzed. The hydrated product is then calcined at high temperature to form titanium dioxide. In the second process, the "chloride process", the ilmenite is reacted with carbon and a chlorinating agent. The titanium tetrachloride that is formed is heated in a stream of air at high temperature to produce TiO_2 [3].

The main use of TiO_2 in paper coatings is to provide opacity. Opacification by TiO_2 is due mainly to the scattering of visible light. The property which makes TiO_2 such a good scatterer of visible light is its high refractive index. TiO_2 may exist in one of three crystalline forms; brookite, anatase, and rutile. Brookite is quite unstable and of no practical use. The rutile crystalline form of TiO_2 possesses a higher refractive index than the anatase form (2.74 vs. 2.56), and as such is the predominant choice for a coating pigment [4].

1.2.4. Silica

The vast majority of coated paper destined for the ink-jet printing market is based on a silica pigment and poly(vinyl alcohol) binder. The hydrogen bonding between the surface silanol groups of silica and the alcohol groups of PVOH , results in a strong, hydrophilic substrate necessary for the fast immobilization of the water-based ink-jet inks. Like TiO_2, the amorphous silica pigments are synthetic in nature. There are four main types of synthetic silica pigments which find use in paper coating formulations; colloidal silica, fumed silica, silica gel, and precipitated silica [5].

Colloidal silica is a stable dispersion of non-porous, dense phase primary particles in water. These range in size from 10 nm to over 100 nm. Fumed silica is produced by the flame hydrolysis of silica tetrachloride. This process produces small primary particles ranging in size from 7 nm to 40 nm. The primary particles adhere through hydrogen bonding and form aggregates, which in turn bond together to form micron sized agglomerates. The surface area can be quite high ($\approx 400\ m^2/g$), and is considered to be totally external. Silica gels are produced by acidification of concentrated sodium silicate. The small primary particles (≈ 25 Å) are chemically bonded together to form a three dimensional structure. This structured network results in a very high specific surface area ($\approx 800\ m^2/g$) which consists almost exclusively of internal surface area. Precipitated silica is produced in a similar fashion to the silica gels, however the mixture is continuously sheared during the reaction. The result being that the structured network is continuously broken down, resulting in small primary particles with less internal

porosity. These primary particles pack together as in fumed silica, and can also possess a very high specific surface area ($\approx 600\ m^2/g$).

1.3. Adsorption Phenomena in Coating Systems

In the typical preparation of a paper coating formulation the pre-dispersed pigment slurry is first mixed with a binder. The binder may be a natural product such as starch or protein, or may be a synthetic binder such as poly(vinyl alcohol) or a styrene-butadiene latex. In addition there are usually a number of additional chemical species (additives) which are added in order to impart some desired property characteristic to the wet or dry state of the coating. An example of a water-soluble polymer added to formulations is carboxymethyl cellulose (CMC), used as either a co-binder or a water retention modifier. Calcium stearate, a surfactant, is used as a paper coating lubricant in order to alter the wet-state flow properties of the coating. In most cases the pigments are dispersed with polyelectrolytes such as polyphosphates or polyacrylates. Synthetic binders such as styrene-butadiene latex contain surfactants to ensure their own stability. As we have seen the pigment particles comprise the largest portion of a coating formulation, and due to their small particle size, introduce a substantial amount of available surface area for the adsorption of the many chemical species present.

Therefore, this combination of high surface-area pigment particles, polyelectrolytes, surfactants, and polymers can lead to a complex colloidal system when mixed together to form a coating formulation. These species will interact both physically and chemically, and knowledge of the associative behavior and adsorption properties of these species will aid in the proper formulation of these complex colloidal systems.

The literature is extremely rich with work pertaining to the adsorption of chemical species onto mineral pigments. Therefore this review is focused only on those studies where both the adsorbate and adsorbent surface are of relevance to the paper coating community. Moreover, since paper coatings are water based systems, only adsorption from aqueous systems is reviewed.

1.3.1. Adsorption of Sodium Polyacrylate (NaPA)

The sodium salt of polyacrylic acid, sodium polyacrylate (NaPA), is the primary pigment dispersant used in coating formulations today. Most all pigments received on site from the suppliers have already been pre-dispersed with NaPA. This dispersant is a polyelectrolyte with the general formula;

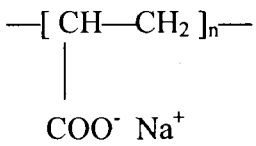

where n represents the number of repeating units and reveals the molecular weight.

The adsorption of NaPA onto titanium dioxide (anatase crystalline form) has been studied by Foissy et al [6]. Particular attention was focused on the influence of pH, average molecular weight of the polyelectrolyte, and the influence of the concentration of calcium ions. The amount of NaPA adsorbed was calculated by the difference between the NaPA introduced and its concentration in the supernatant, after elimination of the solid phase by centrifugation. The results presented are for equilibrium adsorption values, as no time dependence of adsorption was studied. The evolution of surface

charging was followed with electrophoretic mobility measurements, and dispersion stability was monitored by sedimentation techniques. Three different molecular weights of NaPA were investigated; 4000, 2000, and 700. It was found for the pH range from 2.8 to 9.8 that the order of increasing adsorption was also the order of increasing molecular weight. Since the isoelectric point of the TiO_2 was found to be 6.2, the forces leading to adsorption are of a different type at alkaline and acidic pH. In the presence of calcium ions at alkaline pH the enhancement of adsorption is attributed to the formation of complexes in solution, along with a decrease in electrical repulsion of the NaPA.

Extending the work of Foissy, Bohmer [7] incorporated calorimetry into the study of NaPA adsorption onto TiO_2. At low pH, below the isoelectric point of TiO_2, exothermic heats of adsorption were measured. At high pH, and in salt solutions of $CaCl_2$ and NaCl, endothermic heats of adsorption were measured. Calcium ion effects are partly responsible for the results, especially the Ca^{2+} – PA interactions.

A few researchers have studied the adsorption of NaPA onto ground calcium carbonate. Mäkinen and Laakso [8] used a serum cell apparatus to monitor the adsorption onto ground calcium carbonate (GCC), that already had preadsorbed NaPA present from the pigment supplier. The serum cell is essentially a vessel with a fine membrane filter at the bottom. The dispersion is mixed with a magnetic stirrer and the serum from the aqueous medium is passed through the membrane using air pressure. The serum can then be analyzed for the concentration of the adsorbate. The researchers found considerable adsorption of NaPA onto the commercial pigment, indicating that the total adsorption capacity of commercial $CaCO_3$ slurries exceeds the normal NaPA content of the slurries as delivered. Therefore these commercial slurries can possess a high capacity

for adsorbing NaPA from other pigments when these are mixed with the GCC slurries. The other part of this study was concerned with the competitive adsorption of NaPA and polyvinyl alcohol (PVOH) onto the $CaCO_3$ surface. The results show that NaPA and PVOH do not affect each others adsorption behavior onto the $CaCO_3$. The conclusion is that NaPA and PVOH adsorb onto different surface sites of the $CaCO_3$, or adsorb by forming chemical layers on the $CaCO_3$ surface.

Järnström [9] studied the effect of adsorption of NaPA onto GCC on the viscosity of the pigment slurry. In the pH range investigated (8.2 – 8.8) the interaction between NaPA and the $CaCO_3$ was explained as electrostatic attraction. The adsorption of NaPA leads to a reversal of the pigment's surface charge, as measured by electrophoretic mobility. This electrostatically induced adsorption is hypothesized to yield a flat conformation, with the polyion tightly bound to the surface. It was found that the amount of NaPA needed to achieve the lowest dispersion viscosity was independent of the specific surface area for adsorption. In addition the amount of NaPA needed for minimum viscosity did not change when half of the $CaCO_3$ was replaced with kaolin. The conclusion is that a pure adsorption mechanism is not solely responsible for the amount of NaPA needed to achieve a minimum slurry viscosity. It was also reported that the calcium ion concentration had an impact on the adsorption process by binding to the polyelectrolyte in solution. The increase in colloidal stability with increasing NaPA concentration is attributed to two mechanisms; the decrease in the number of bound calcium ions per monomer, and the increase in the adsorbed amount.

Järnström [10] also investigated the adsorption of NaPA onto sodium kaolinite, and for kaolinite in the presence of carboxymethyl cellulose (CMC). The ionic strength

and the specific counter ions in solution were shown to have a pronounced impact on the adsorption of NaPA. $CaCl_2$ was found to increase adsorption almost four-fold compared to NaCl at the same ionic strength. This increased adsorption is attributed to the screening effect of the divalent cations. The repulsion between the anionic groups of the NaPA are reduced and its configuration becomes less extended in solution, thereby reducing its solubility. This reduction in solubility may then allow the polyelectrolyte to pack more closely on the pigment surface. The researchers also point out that adsorbed calcium ions could create active sites on the pigment surface to which NaPA could bind strongly. Adsorbed NaPA on kaolin was found to influence the subsequent adsorption of CMC. It was found that the maximum adsorption of CMC on kaolin is considerably reduced by the presence of NaPA on the surface. This reduced adsorption was attributed to the partial blocking of adsorption sites of CMC on kaolin by the NaPA.

1.3.2. Adsorption of Polyvinyl Alcohol

Polyvinyl alcohol (PVOH) is one of the strongest binders used in the paper coating industry [2]. It is manufactured by the hydrolysis of polyvinyl acetate. It is also the predominant binder used in ink-jet coatings. Hydrogen bonding between PVOH hydroxyl groups and the silanol groups on the silica pigment causes increased final coating viscosity, with only small increases in solids concentration. This phenomena limits solid concentrations of ink-jet coatings to the 25 – 30 % range [11]. Because of its excellent binding strength PVOH is also finding more use as a co-binder in $CaCO_3$ and kaolin based coatings.

Tadros [12] investigated the adsorption of PVOH onto silica pigments. Three types of silica were chosen for examination; precipitated silica, fumed silica, and a 40% aqueous silica sol. Three grades of PVOH were also used; a 98% hydrolyzed grade with a MW of 55,000, an 88% hydrolyzed grade with a MW of 45,000, and a 99% hydrolyzed grade also with a MW of 45,000. It was found that heat treatment of the precipitated silica was necessary before any adsorption of PVOH could be detected. The silica sample lost 12.5% of its original weight after heating at 350° C for 15 hours. This loss in weight is attributed to the removal of physisorbed water and also condensation of surface silanol groups. In all cases the adsorption of PVOH decreased with an increase in the pH of the dispersion. PVOH adsorption was found to increase rapidly as the silica heat treatment surpassed 400° C. The optimum temperature for maximum adsorption was found to be 700° C for the fumed silica investigated. These results indicate that the important adsorption sites for PVOH are both the isolated silanol groups and the siloxane groups.

Järnström et al [13] investigated aggregation in coatings based on kaolin and PVOH. The addition of small amounts of PVOH to kaolin dispersions results in an increase in the viscosity. However, as more PVOH is added the viscosity begins to decrease. This phenomenon is attributed to a bridging mechanism. Bridging flocculation occurs when the kaolin particles are incompletely covered by the PVOH. At complete coverage repulsion between particles is reestablished and stability is enhanced. Adsorption of PVOH onto a NaPA treated kaolin was also found to depend on the degree of hydrolysis. PVOH with a MW of 48,000 and a degree of hydrolysis of 88% adsorbed to a greater extent than a PVOH with a degree of hydrolysis of 98%, also with a MW of

48,000. Adsorption increased with increasing MW when the degree of hydrolysis remained constant.

1.3.3. Adsorption of Protein

Protein-pigment interactions, and their effect on rotogravure printing properties has been investigated by Shaw [14]. One major aim of this work was to characterize the interaction of chemically modified proteins with pigment surfaces. This interaction was monitored by measuring the adsorption of the protein onto the pigment surface. Proteins have a net negative charge at normal coating pH (9 – 10), however cationic sites are present because of their amino acid composition. Therefore the molecular weight of the protein, and the presence of these cationic sites are expected to affect the degree of interaction with the pigment surface, and also potentially the resultant coating structure. Adsorption of protein onto kaolin was found to decrease as the square root of protein concentration in the aqueous phase. As total protein is increased up to about 8%, based on clay, a decreasing percentage of the protein is associated with the clay. Therefore, considering only binder-pigment interactions, maximum utilization of the protein is obtained at the lower addition levels. As more protein is present in the aqueous phase, water retention of the coating increases. Thus the protein-pigment interaction and the controlled water retention can be modified by the proper choice of type and amount of modified protein.

1.3.4. Adsorption of Surfactants

An interesting study of the competitive adsorption behavior of model paper coating systems was performed by Stenius et al [15]. A model coating system of a kaolin pigment and polystyrene latex as binder was used. Latex binders are usually stabilized by anionic or nonionic surfactants. Therefore the goal was to study the redistribution of these adsorbed species in the model coating. The anionic surfactant used was sodium dodecyl sulfate (SDS). The nonionic surfactants were polyethyleneoxide nonylphenol ethers ($NPEO_n$), sodium hexametaphosphate (SHMP), and polyethylene oxide (PEO). For the polyethylene oxides of molecular weights exceeding 1,500 (about 35 EO units) the maximum adsorption did not depend on melecular weight. This indicates that the adsorbed molecules are lying flat on the surface. The $NPEO_n$ surfactants show a large maximum adsorption with a low EO content, with the maximum adsorbed amount decreasing as the EO content increased. It was found that at high EO content the maximum adsorption of polyethylene oxide and $NPEO_n$ coincide. These results indicate that as the EO content decreases (surfactants become more hydrophobic), the mode of adsorption changes. The free energy of adsorption of these nonionic surfactants on polystyrene latex and kaolin are very similar. This implies that if a pure kaolin is added to a latex dispersion stabilized with these surfactants, the surfactant may desorb from the latex and adsorb onto the kaolin. This could cause a previously stable latex to coagulate. Competitive adsorption of $NPEO_{10}$ and SDS on polystyrene latex reveals that the nonionic surfactant ($NPEO_{10}$) is preferentially adsorbed onto the latex surface. SHMP is found to desorb from the kaolin surface when exposed to $NPEO_{10}$ in solution. The hypothesis is that the NPEO and SHMP complex strongly in solution.

1.4. Motivation

A review of the literature has demonstrated the importance of understanding the adsorption, and competitive adsorption, phenomena occurring in pigmented coating systems. To date the majority of this work has focused on the bulk equilibrium properties (adsorption isotherms) of the adsorption processes. However, it is the molecular interactions between these various chemical species and the pigment surfaces that will ultimately dictate certain observable macroscopic properties such as viscosity, dewatering behavior, and ink receptivity. Establishing a detailed molecular picture of the adsorption properties of these systems is important to understand of the colloidal behavior of these systems.

In this work we are interested in using vibrational spectroscopic methods, along with electrokinetic measurements, to characterize the dynamic adsorption characteristics of aqueous based surfactants and polyelectrolytes on mineral pigments used in the paper coating industry (TiO_2, silica, kaolin). In addition, we are also interested in techniques which will allow the surface chemistry of these pigments to be modified in order to elucidate how these surface properties can influence the pigment's behavior in aqueous based systems.

1.5. Thesis Layout

To address the objectives put forth in the preceding section this thesis is the culmination of three separate publications (Chapter 3, Chapter 4, and Chapter 5). Chapter 2 will introduce the various analytical techniques that are used to study the surface behavior (adsorption) of these mineral pigments. In Chapter 3 a novel technique

is described which allows adsorption onto mineral pigments to be studied by an infrared technique from aqueous solutions. This chapter has been published in the journal "Applied Spectroscopy" [16]. In Chapter 4 the importance of adsorbed surfactant structure is discussed, and a technique involving the use of probe molecules to uncover the underlying surfactant microstructure is introduced. This chapter has been accepted for publication in the journal "Colloids and Surfaces A: Physicochemical and Engineering Aspects", and is currently in press [17]. In Chapter 5 a technique for modifying the surfaces of kaolin and silica pigments is discussed. The work comprising Chapter 5 has also been submitted for publication in the journal "Colloids and Surfaces A: Physicochemical and Engineering Abstracts" [18]. Finally, Chapter 6 includes an overall summary of this research along with recommendations for future work in this area.

CHAPTER 2. EXPERIMENTAL METHODS

2.1. Attenuated Total Reflection Spectroscopy (ATR)

Attenuated total reflection spectroscopy (ATR) is an advantageous method of obtaining the infrared spectrum of a species located near the surface of a sample. It is particularly well suited for *in situ* measurements conducted in the aqueous phase, since the shallow sampling depth reduces the strong absorption of infrared light by water. To fully understand this surface sensitive technique we must first understand the general phenomenon of the total reflection of light at the interface of two different media.

2.1.1. Theory of Internal Reflection

Figure 2.1 shows a light wave of intensity I_{IN} travelling from a more dense region (region 1) and impinging, with an angle of incidence θ, at the interface with a less dense region (region 2). In order to obtain internal reflectance the angle of the incident radiation, θ, must exceed the critical angle, θ_c. The critical angle is a function of the refractive indices of the two media, and is defined as

(2.1) $$\theta_C = \sin^{-1} (n_2/n_1)$$

where n_1 is the refractive index of the more dense region and n_2 is the refractive index of the less dense region. The reflectivity, R, is defined as the ratio of the reflected intensity to that of the incident intensity.

(2.2) $$R = (I_{OUT} / I_{IN})$$

If the substance comprising the less dense region (region 2) does not absorb light, then a total internal reflection occurs with $I_{OUT} = I_{IN}$ and $R = 1$. However, if region 2 is absorbing then an attenuated total reflection occurs in which R is now less than unity. The light beam is attenuated (reduced in intensity) due to the absorption of a portion of the light wave by the rarer medium.

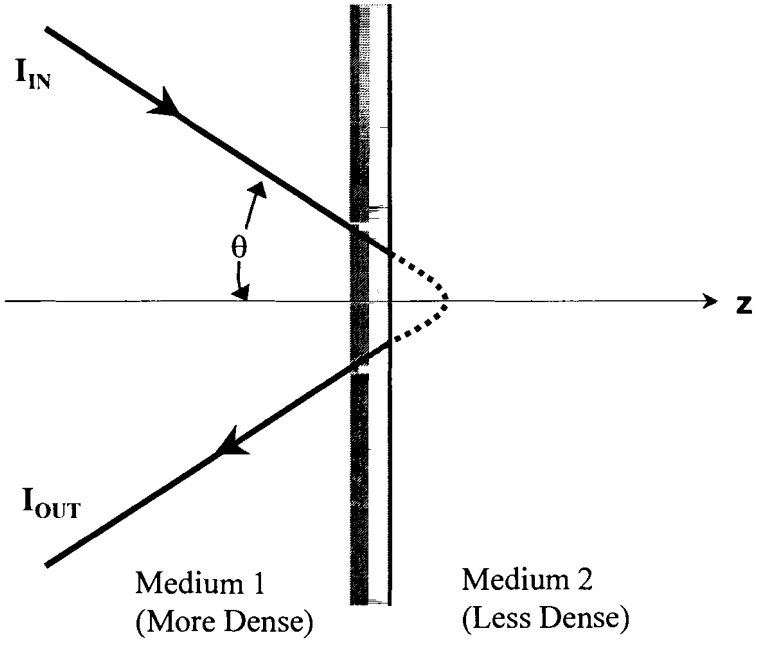

Figure 2.1. Schematic representation of a ray of light undergoing a total internal reflection.

A total internal reflection sets up a standing wave pattern at the interface due to interference of the incoming and outgoing waves. This standing wave amplitude pattern is shown in Figure 2.2. The wave amplitude extending into the less dense region is not constant, but decays exponentially with distance from the interface. This is called an evanescent wave.

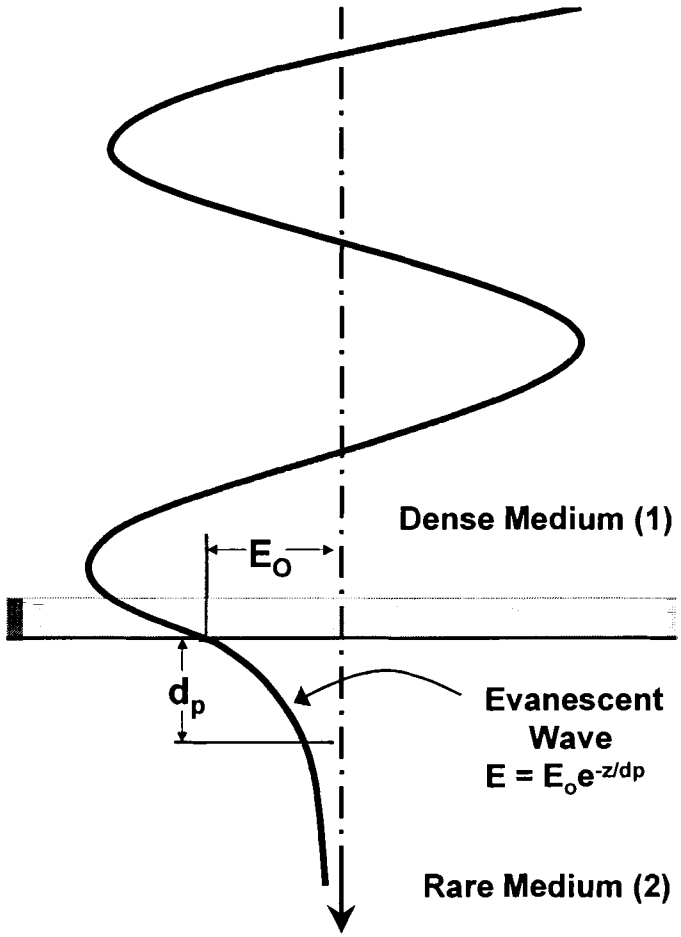

Figure 2.2. Standing wave amplitude pattern established near a totally reflecting interface.

If E_O is the value of the amplitude at the interface, then this exponential decay can be described by the equation

$$E = E_O e^{-z/dp} \tag{2.3}$$

where d_p is defined as the depth of penetration. d_p is the depth at which the amplitude has decreased to 1/e of its value at the surface (i.e. $E \cong 37\%E_O$). The depth of penetration, d_p, as given by Harrick [19] can be represented by the following expression

$$d_p = \frac{\lambda_1}{2\pi(\sin^2\theta - n_{21}^2)^{1/2}} \tag{2.4}$$

where $\lambda_1 = \lambda/n_1$, $n_{21} = n_2/n_1$, and θ is the angle of incidence. Another useful expression when working with ATR measurements is the "effective depth". The effective depth is that thickness which would give the same amount of absorption in a transmission experiment. The effective depth, as defined by Harrick [19], is given by the expression

$$d_e = \frac{n_{21}E_O^2 d_p}{2\cos\theta} \tag{2.5}$$

This last expression gives some insight into the differences between absorption measurements conducted via transmission, and absorption measurements conducted via ATR techniques. For transmission studies the decrease in intensity of the light is due simply to the amount of light absorbed by the sample. In transmission experiments the intensity would remain constant if the material were nonabsorbing. However, for ATR

measurements the intensity is decreasing for two reasons; first because light is being absorbed by the sample, and second because it is an evanescent wave.

As we have seen, a property of the evanescent wave, which makes ATR a powerful technique, is that the intensity of the wave decays exponentially with distance form the surface of the ATR crystal. This distance, which is usually on the order of microns, makes ATR generally insensitive to sample thickness, allowing for the analysis of thick and/or strongly absorbing samples (aqueous solutions). However, for the detection of dilute species in aqueous solutions, this shallow sampling depth can lead to low sensitivity. Therefore it is typical to utilize ATR crystals which allow multiple internal reflections. A typical geometry used for *in situ* adsorption studies is the parallelepiped. This geometry is shown in Figure 2.3, and depicts a light beam undergoing 4 internal reflections.

The material of construction of the internal reflection element (IRE) depends on a multitude of factors. As mentioned in the theoretical section, it is necessary for the refractive index of the IRE to be greater than that of the sample to be analyzed. Secondly, the material of construction must possess a useful transmission range for the identification of the vibrational frequencies of interest. Finally, the IRE must be compatible with the sample. The most common materials used for the construction of internal reflection elements, and their associated properties are listed in Table 2.1. ZnSe is the most widely used material for aqueous based systems due to its wide transmission range and its insolubility in water.

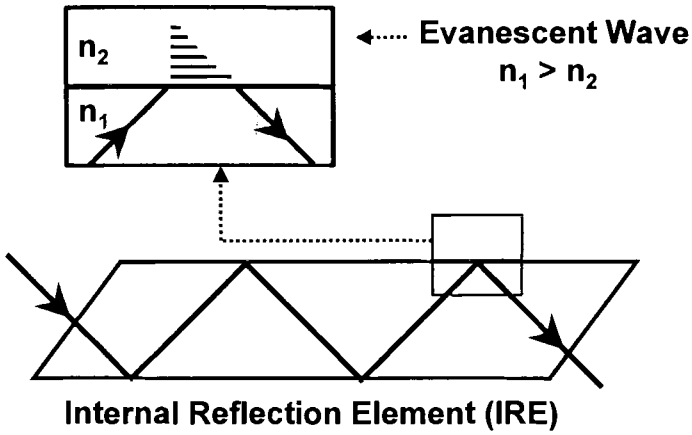

Figure 2.3. Schematic of a light beam undergoing multiple internal reflections.

Material	ATR Transmission Range (cm^{-1})	Refractive Index @ 1000 cm^{-1}	Water Solubility (g/100 g H_2O)
ZnSe	20,000 – 650	2.4	Insoluble
Ge	5,500 – 830	4.0	Insoluble
ZnS	17,000 – 950	2.2	Insoluble
Diamond	4,200 – 200	2.4	Insoluble
Si	8300 – 1500	3.4	Insoluble
KRS-5	20,000 – 400	2.4	0.05
Sapphire	50,000 - 1780	1.7	Insoluble

Table 2.1. Typical materials of construction for internal reflection elements (IRE).

2.1.2. Modification of IRE Surfaces for Adsorption Studies

Unless one is interested in studying adsorption and surface phenomena related to one of the materials listed in Table 2.1, then techniques must be used in order to modify the surface to mimic the desired mineral surface of interest. A detailed literature review of this subject is covered in Chapter 3 of this thesis, however a general discussion of a few of the most common methods, as detailed by Kellar et al [20], is pertinent at this juncture.

2.1.2.1. Method 1: Particulate Suspension with Inert IRE.

This method involves the application, and subsequent dewatering, of a particulate suspension onto the surface of an inert IRE. This method is illustrated in Figure 2.4. One of the main advantages of this technique is the ability to significantly increase the available surface area for adsorption, due to the use of high-surface-area particulate matter. Also, scattering losses that are common to transmission and diffuse reflectance techniques are minimized due to the short pathlength of the evanescent wave.

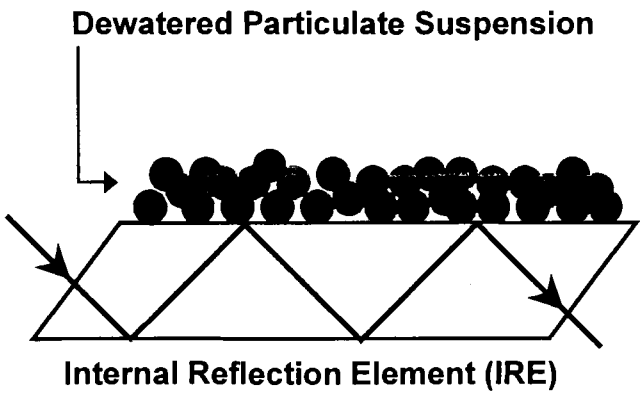

Figure 2.4. Modification of IRE surface using a dewatered particulate suspension.

The biggest disadvantage of this method is the ability of the particulate matter to form a dense, water stable film, which is strongly anchored to the IRE surface. The particulate suspension technique has proven well suited to the study of surfactant adsorption at the TiO_2 – aqueous solution interface, and this is covered in more detail in Chapter 4 of this thesis. For the study of surface reactions on silica particles in aqueous solutions, however, this method has shown to not be applicable. The silica films so formed are easily removed from the IRE surface when placed in contact with the aqueous solution. Therefore a novel technique has been developed which allows the study of adsorption onto particulate silica surfaces from aqueous solutions, and this is the focus of Chapter 3 of this thesis.

2.1.2.2. Method 2: Surface Coating of Inert IRE

In this method the desired mineral is coated onto the surface of an inert IRE, usually by vacuum deposition or sputtering. An example is the deposition of copper and nickel metallic films by evaporation onto a germanium internal reflection element [21]. The metal film thickness (3 – 4 nm) on the germanium IRE is approximately two orders of magnitude less than the penetration depth of the evanescent wave. A disadvantage of this method is the problem of achieving proper adhesion of the deposited coating to the IRE surface. As stated earlier, ZnSe is an ideal choice for the material of construction of an IRE for water based adsorption studies, due mainly to its expanded spectral range advantages. However, thin TiO_2 films (1000 Å) sputtered onto the surface of a ZnSe IRE began to crack and lift off the surface when exposed to water. For certain materials this can be overcome to a certain extent by using a thin buffer layer to promote adhesion to

the IRE surface. This is illustrated by the work of Sperline et al [22] in which silicon was sputtered as a thin film onto a thin Al_2O_3 buffer layer, which had been previously sputtered onto a ZnSe IRE to improve adhesion of the silicon layer. A major disadvantage, as compared to the particulate coating technique, is the inherently low surface are of these vacuum deposited coatings, which reduces the sensitivity of detecting adsorbed species, especially at very low adsorbate concentrations.

2.1.2.3. Method 3: Reactive Internal Reflection Elements

When the material of interest can be fabricated into an internal reflection element, and also still posses a wide enough spectral window, surface reactions and surface adsorption phenomena can be monitored directly, *in situ*, at the IRE surface. Obvious systems that are facilitated by this technique include any solid/solution interfacial phenomena occurring with the standard materials of construction commercially available; Si, Ge, ZnSe, sapphire etc. An example of a non-typical IRE used for adsorption studies is the use of the mineral fluorite. Kellar et al [23] studied the adsorption of the surfactant oleate at the surface of a fluorite IRE. A single crystal fluorite was machined and polished into a 50 x 10 mm internal reflection element. The use of reactive internal reflection elements allows the real-time acquisition of a number of surface adsorption related phenomena. This is illustrated in Figure 2.5 [20].

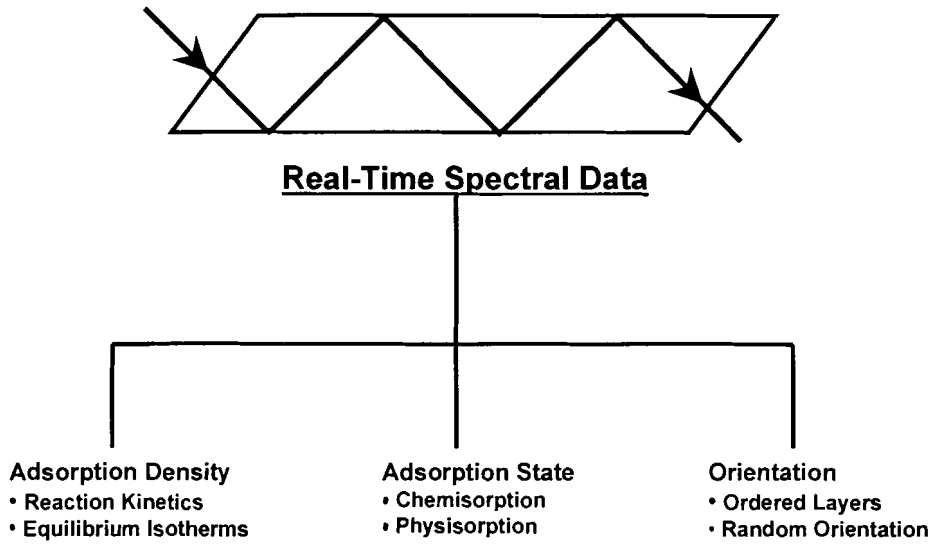

Figure 2.5. Application of ATR spectroscopy for the study of surface phenomena.

An example of the quantitative information that can be obtained from using reactive internal reflection elements is the determination of the adsorption density (surface excess). Sperline et al [24] developed the necessary equations for interpretation of the ATR spectra of adsorbed surfactants for the determination of the Gibbs surface excess. By using a calibrated cylindrical IRE, the researchers were able to obtain quantitative values of the surface excess for the surfactant cetylpyridinium chloride (CPC), adsorbed from water, onto the surface of a ZnSe IRE.

The resulting equation relating the absorbance to the surface excess is given by

(2.6) $A/N = \epsilon C d_e + \epsilon(2000 d_e/d_p)\Gamma$

where A = integrated absorbance

ϵ = molar analyte absorptivity

C = bulk analyte concentration

N = number of ATR reflections

Γ = surface excess

d_e = effective thickness

d_p = depth of penetration

For this derivation a cylindrical IRE was used, and therefore the effective number of reflections had to be independently determined by a calibration procedure. Kellar et al [23] extended this work to include a flat IRE, where the number of reflections can be calculated from geometric considerations according to the relationship

(2.7) $N = (l/t) \cot \theta$

where l is the length of the IRE, t is the thickness, and θ represents the angle of incidence. By using this defined geometry the following relationship for the surface excess is established.

(2.8) $$\Gamma = [A/(l/t)\cot\theta - \epsilon C d_e] / [1000\epsilon(2d_e/d_p)]$$

The development of these relationships thus allows the direct calculation of adsorbate adsorption densities for different equilibrium concentrations, from the real-time spectral data. The utility of ATR spectroscopy for the study of adsorption phenomena is well founded. The above relationships allow the determination of the adsorption isotherms for various chemical systems to be obtained, and the use of Fourier transform infrared spectroscopy also allows rapid spectral acquisition, which facilitates the determination of the kinetics of adsorption as well.

2.2. Electrokinetic Measurements for Adsorption Studies

2.2.1. Origin of Surface Charge

Almost all colloidal particles, when dispersed in water or an aqueous solution, will develop an electrical charge at their surface. This surface charge may be acquired in a number of ways, depending on both the properties of the surface and the properties of the dispersing medium. A few of the most common charging mechanisms, and those of particular relevance to mineral pigments, will be briefly covered here.

In the case of differential ion solubility, a preferential solubilization of one of the surface ions comprising the solid can lead to the accumulation of an opposite charge at the surface. This mechanism assumes that the solid particle is insoluble, or only sparingly soluble in the dispersing medium. The classic example of this charging mechanism is the behavior of silver iodide particles in water. The ions dissolve from the surface until the product of their concentrations is equal to the solubility product of AgI.

For the case of equally dissolving Ag^+ and I^- ions, the net effect would be a surface charge of zero. However, the Ag^+ ions are more readily dissolved, leaving a higher proportion of I^- ions at the surface. The overall effect is the accumulation of a net negative charge on the surface.

For materials that contain surface groups that can be directly ionized, but in which one of the ions is permanently bound to the surface, represents another important mechanism for the accumulation of surface charge. For the metal oxides (SiO_2, TiO_2, and Al_2O_3) the surface charging is due to the presence of ionizable surface hydroxyl groups [25]. The dissociation of these hydroxyl groups is pH dependent and can be represented by;

$$MOH_2^+ \overset{H^+}{\leftrightarrow} MOH \overset{H^+}{\leftrightarrow} MO^- \tag{2.9}$$

Therefore for metal oxides in water the OH^- and H^+ ions are the potential-determining ions. At low pH values the surfaces of metal oxides are positively charged, and at high pH negatively charged. At some intermediate pH, which varies depending on the oxide, the net charge on the surface is zero. This pH value is known as the point-of-zero-charge (PZC) or the isoelectric point (IEP). Table 2.2 lists the PZC of a few common metal oxides [26]. For certain polymeric materials containing carboxylic acid groups, such as latex particles, ionization can lead to the accumulation of a net negative charge when dispersed in water.

OXIDE	PZC
SiO_2 (precipitated)	2 – 3
SiO_2 (quartz)	3.7
TiO_2 (anatase)	6.2
TiO_2 (rutile)	5.7 – 5.8
Al_2O_3 (corundum)	9.0

Table 2.2. PZC values of some common metal oxides.

For many minerals, and especially clay minerals, isomorphous substitution can be an important mechanism of surface charging. Kaolin is a layered aluminosilicate ($Al_2O_3 \bullet 2SiO_2 \bullet 2H_2O$) comprised of tetrahedral silica layers and octahedral gibbsite (alumina) layers. In this mechanism structural ions are substituted by ions with a valency less than the original ion. Substitution of Al^{3+} for Si^{4+} in the silica layers, or Mg^{2+} for Al^{3+} in the alumina layers results in a net negative charge which is independent of solution conditions such as pH [27]. However, the basal planes of clay platelets are not the only surfaces responsible for the overall surface charge. The atomic structure of the edges is entirely different from that of the basal planes. At the edges the silica and alumina sheets are disrupted and primary bonds broken. The edge sites are therefore akin to silica and alumina sites, and their charging properties are pH dependent [28].

Finally, and probably most pertinent to the work contained in this thesis, is the charge conferred to particles due to the specific adsorption of ions. An example is the

specific adsorption of surfactant ions onto the surface of mineral pigments. For an initially uncharged particle the adsorption of cationic surfactants would lead to a positively charged surface, while the adsorption of anionic surfactants would lead to a negatively charged surface. Also, a combination of charging mechanisms may be responsible for the observed behavior in aqueous solutions. A metal oxide particle below its isoelectric point would carry a positive surface charge due to the adsorption of H^+ ions as the potential determining ions. The addition of an anionic surfactant could lead to surface charge neutralization, or even surface charge inversion, depending on the extent of adsorption.

2.2.2. Electrokinetic Phenomena

The term "electrokinetic" encompasses both the effects of motion and electrical phenomena, more specifically the mutual effects of an electric field and the tangential motion of two phases with respect to each other. These effects may arise from the motion of a particle relative to its dispersing medium, or conversely it could be the solution phase which moves relative to a stationary solid boundary. There are four phenomena which are usually grouped under the umbrella of electrokinetic phenomena; electrophoresis, electroosmosis, streaming potential, and sedimentation potential. The phenomena associated with each of these, along with its cause, are summarized in Table 2.3 [25].

SOLID PHASE	CAUSE	PHENOMENON	NAME
Particles	Electric Field	Motion of Dispersed Phase	Electrophoresis
Particles	Gravitational Field	Potential Gradient	Sedimentation Potential
Tube Wall or Packed Bed	Electric Field	Motion of Medium	Electroosmosis
Tube Wall or Packed Bed	Motion of Medium	Potential Gradient	Streaming Potential

Table 2.3. Electrokinetic phenomena.

In each of the above techniques an experimentally determined quantity known as the zeta potential, ζ, can be calculated. As will be discussed next, the zeta potential is an empirically equivalent parameter to the actual potential at the surface. This value has important implications for the stability of colloidal systems, and is also used as an indirect means of evaluating the adsorption of species onto colloidal particles. In this work we are primarily concerned with the theory and use of electrophoresis for the study of colloidal pigment systems.

2.2.3. Electrophoresis

Electrophoresis is concerned with the movement of a particle (and any material attached to the surface of the particle) relative to a stationary dispersing medium under the influence of an applied electric field. Therefore, if an electric field is applied across an electrolyte, charged particles suspended in the electrolyte will be attracted towards the electrode of opposite charge. The charged particle will move with a certain velocity which depends on the strength of the applied electric field, the properties of the solution (dielectric constant and viscosity) and the zeta potential. In electrophoretic measurements it is the electrophoretic mobility of the particle that can be experimentally measured. The zeta potential being obtained only after resorting to theoretical arguments. The electrophoretic mobility, u, is defined as the velocity of the moving particle per unit of applied electric field.

(2.10) $$u = v/E$$

2.2.3.1. Definition of Zeta Potential

At the solid/liquid interface in a solution containing ions there will be a variation in the ion density near the interface. This distribution of ion density leads to a distribution of electrical charges at the phase boundary. This distribution of electrical charges then leads us to the development of an electrical double layer, with a potential that varies with distance from the interface. Much theoretical work has been devoted to the understanding of the distribution of electrical charge near the interface, and many models of this double layer have been proposed. One such theory that is used extensively

in the field of electrophoresis is the Stern double layer model [29]. In the Stern model the aqueous part of the double layer is divided by a hypothetical boundary known as the *Stern surface*. The *Stern surface* is drawn through the ions which are most strongly adsorbed to the charged surface. This model is illustrated in Figure 2.6.

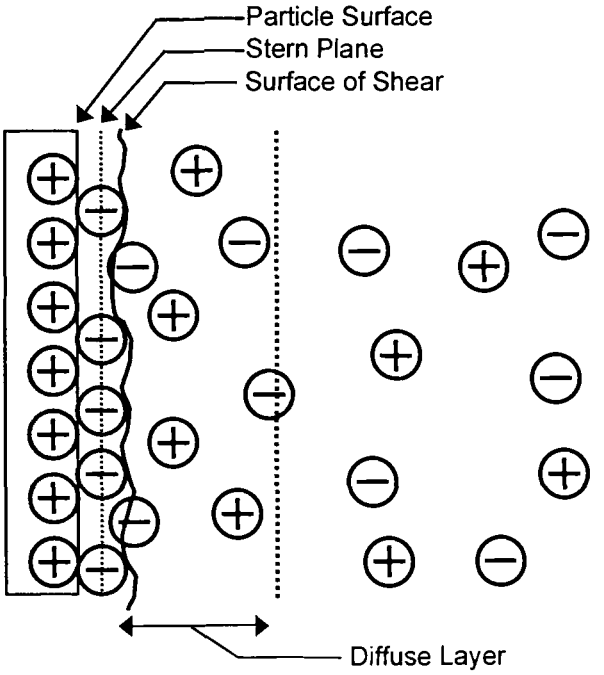

Figure 2.6. Stern model of the electric double layer.

The layer of liquid, which is immediately adjacent to a solid surface (particle), will move with the same velocity as the particle. At some distance then there is a relative motion established between this immobilized layer of liquid and the liquid comprising the bulk. This boundary is known as the surface of shear. According to the Stern model the surface of shear occurs well within the double layer, and the zeta potential, ζ, is defined as the potential at that surface, Figure 2.7.

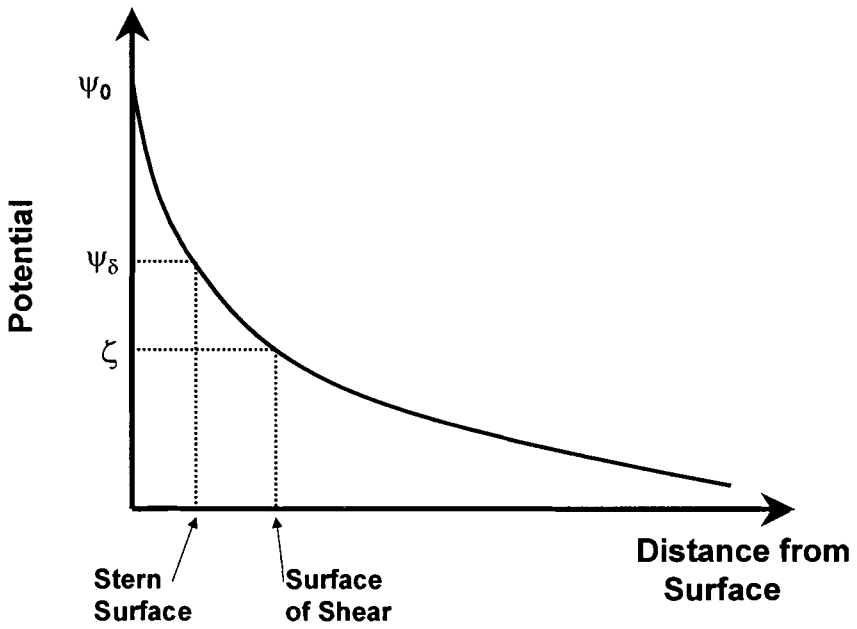

Figure 2.7. The relative magnitudes of various double layer potentials.

The zeta potential is then seen to be different from the potential at the Stern surface, ψ_δ, and also from the potential existing at the actual particle surface, ψ_0.

2.2.3.2. Determination of Zeta Potential from the Electrophoretic Mobility

As mentioned previously, it is the electrophoretic mobility of the suspended particles that can be experimentally measured, and the zeta potential calculated by resorting to theoretical arguments. Zeta potential is related to the electrophoretic mobility by the *Henry equation* [29].

The relationship is given by;

$$u = \frac{2\varepsilon\zeta}{3\eta} f(\kappa a) \tag{2.11}$$

where u = electrophoretic mobility

ζ = zeta potential

ε = dielectric constant

η = viscosity

$f(\kappa a)$ = Henry's function

Henry's function depends on the shape of the particle undergoing the motion, and hence also depends on the ionic environment. For spherical particles a is the radius of the particles. The units of κ are reciprocal length, and κ^{-1} is a measure of the thickness of the double layer, called the Debye length.

The dimensionless number κa effectively measures the ratio of particle radius to the double layer thickness. In the application of *Henry's equation* for the determination of zeta potential there are two limiting cases. For small values of κa the Henry function approaches 1, and this is also known as the Hückel approximation. The Hückel approximation is applicable when the ionic concentration approaches zero, as in virtually non-conductive media. At the other limit for large values of κa the Henry function approaches a value of 1.5, and this is also known as the Smoluchowski approximation. This approximation applies when the ionic concentration is high enough to significantly

compress the double layer. The situations applying to both limiting approximations are illustrated in Figure 2.8.

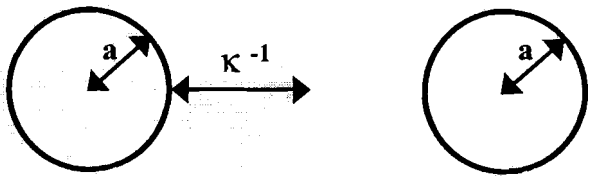

Smoluchowski Approximation

Hückel Approximation

Figure 2.8. Limiting cases for the Henry function.

More exact values for the Henry function can be used when information on the particle size is known, since the value of the Debye length may be calculated once the concentration of ionic species is known. Representative values of $f(\kappa a)$ are given in Table 2.4, an can be used to replace the limiting values imposed by the aforementioned approximations [30].

κa	f(κa)
0	1.000
1	1.027
2	1.066
3	1.101
4	1.133
5	1.160
10	1.239
25	1.370
100	1.460
∞	1.50

Table 2.4. Values of the Henry function for various values of the dimensionless number *κa*.

2.2.3.3. Techniques for Measuring Electrophoretic Mobility

The classical method of measuring the velocity of the suspended particles under the influence of an applied electric field is known as micro-electrophoresis. This earlier method involves the direct observation of individual particles with a light microscope, and the subsequent timing of their movement across a known distance. For practical reasons the system of interest must be in the form of a reasonably stable dispersion, and be of a particle size that is observable by light microscopy (> ≅ 200 nm). Other

disadvantages of micro-electrophoresis is the difficulty in making measurements on poorly scattering particles, along with the need for repeat experiments to ensure statistically sound results. The introduction of light scattering techniques for the measurement of particle velocities has expanded the application range of electrophoretic measurements. The technique used in this work is known as Laser Doppler Electrophoresis.

The walls of the capillary cell, used for electrophoretic measurements, will also carry a surface charge. Under the influence of an applied electric field this surface charge will cause the liquid (dispersing medium) to flow along the cell walls. This phenomenon, as described at the beginning of this section, is called electroosmosis. Therefore, in the measurement of the electrophoretic mobility of the suspended particles, this flow will be superimposed on the particle velocity and needs to be accounted for. However, by using a closed cell this flow along the capillary walls must be compensated by a reverse flow down the center of the capillary. At some point in the cell there will be a position in which the electroosmotic flow is zero, and the measured particle velocity is the true electrophoretic mobility. This position in the cell is called the stationary layer, and is depicted in Figure 2.9.

In Laser Doppler Electrophoresis a pair of mutually coherent laser beams are aligned and made to cross at the stationary layer in the cell. The velocity measurement is obtained by the Doppler effect, in which light scattered from a moving particle experiences a frequency shift that is related to the particle velocity.

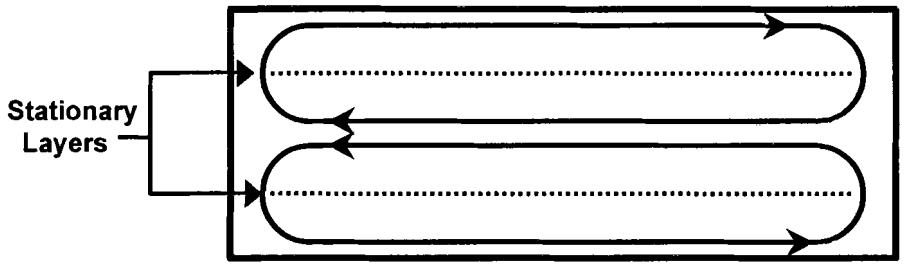

Figure 2.9. Formation of stationary layers in an electrophoretic capillary cell.

The scattered light from this crossing region is detected by a photomultiplier that is directed along one of the laser beams (the reference beam). The use of an attenuated reference beam for the measurement is known as a heterodyne measurement, and this is the detection mode used in this work. The heterodyne optics configuration is illustrated in Figure 2.10. For this optical layout the scattered light from the particles in the measurement zone is mixed with attenuated light from the reference beam. The intersection of these two beams occurs at a low angle (12.7° in this system), which increases the resolution, as the effect of Brownian motion is reduced at forward scattering angles. As the intersection angle is increased the effect of Brownian motion is to "smear" out the velocity spectrum, making it difficult to resolve mixtures of particles with different velocities.

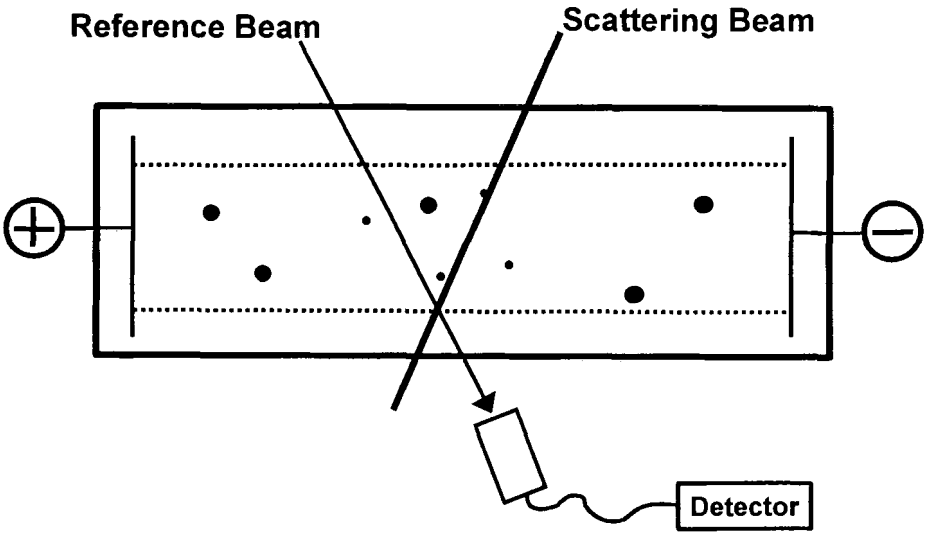

Figure 2.10. Heterodyne optics configuration.

As compared to the traditional microscopic observation for the determination of particle mobilities, Laser Doppler Electrophoresis offers many advantages. Some of the important advantages are:

- Measurement times in seconds rather than 10 – 30 minutes
- Measurement of smaller particles, 5 – 10 nm limit instead of a minimum of 200 nm
- Measurement of zeta potential distributions
- Statistically better measurements due to the extremely large number of particles measured.

CHAPTER 3. DEVELOPMENT OF AN INFRARED TECHNIQUE FOR MONITORING ADSORPTION ONTO MINERAL PIGMENTS IN AN AQUEOUS ENVIRONMENT

3.1. Introduction

In this chapter an *in situ* infrared technique is described which allows the detection of adsorbed surface species on metal oxide particles in an aqueous environment. The technique involves first formulating a "coating" comprised of high surface area, silica particles and a polymeric binder in a suitable solvent. The resulting coating is applied to the surface of an internal reflection element (IRE) and mounted in a flow-through Attenuated Total Reflection (ATR) apparatus. The technique is demonstrated using a ZnSe element coated with fumed silica particles in a polyethylene (PE) matrix. Access of the silica surface in the matrix to adsorbates is evaluated by comparing the gas-phase reaction of silanes on silica/PE coated CsI windows in transmission with silica/PE coated ZnSe in an ATR evacuable cell. It is shown that the PE weakly perturbs about 25% of the surface hydroxyl groups, and that all surface groups are available for reaction with silanes. The silica/PE system is indefinitely stable in an aqueous environment and has advantages of at least two orders higher sensitivity, and a wider spectral range over studies using oxidized silicon wafers. The usefulness of this technique for studying adsorption from water-based systems onto metal oxide surfaces is demonstrated with the reaction of succinic anhydride on an aminosilanized silica surface. This reaction sequence demonstrates how the attachment chemistry between a pigment particle and water soluble species can be monitored *in situ*.

3.2. Background and Literature Review

Surface modified metal oxide particles have numerous applications in colloid and interface science related technologies [31]. One of the principle tools used to interrogate the surface chemistry and surface reactions on metal oxide particles is infrared spectroscopy [32,33]. Typically, the metal oxide particles have high surface areas (25 – 400 m^2/g) which affords easy detection of bands due to surface groups as well as characteristic bands identifying the nature of the adsorbed species. While there have been numerous *in situ* infrared studies of gaseous reactions and those conducted from non-aqueous solutions, very few infrared studies have been reported for aqueous based adsorption on metal oxide particles. Surface studies in water are difficult because water is a strong absorber of infrared light.

The most common approach to overcome the strong absorption of infrared radiation by water is to use attenuated total reflection (ATR) spectroscopy. The finite penetration of the evanescent wave into the aqueous solution is such that spectral transparency is obtained over much of the infrared region. Furthermore, by working at dilute concentrations the spectral contributions due to excess adsorbate in solution are small in comparison to the spectral features due to adsorbed species [34]. However, the use of ATR for surface studies requires that the internal reflection element (IRE) be used for the surface/water interface. Unless the surface of interest is available as an IRE [23,24,35,36], the IRE must be modified in some way to mimic the desired metal oxide surface.

Adsorption onto silica has been one of the most widely studied systems by ATR methods. A common approach is to establish a silica layer by preparing an oxide layer

directly on a silicon IRE [37-39]. This technique has the advantage of preparing an oxide surface that is stable in an aqueous environment, and one that is amenable to orientation studies using polarized light [38]. However, the bands due to adsorbed species are usually weak in intensity, owing to the low surface area of the oxidized IRE. Typically only the most intense bands of the adsorbate are detected. Furthermore the spectral range of a silicon IRE is limited to the region above 1550 cm^{-1}, and many characteristic bands lie below this cutoff. Sputtering a thin film of silicon onto a ZnSe IRE can circumvent this limitation by taking advantage of the expanded spectral range of ZnSe [22]. This technique has proven beneficial in accessing the spectral window between 1550 and 1100 cm^{-1}.

On the other hand, transmission IR studies on silica particles typically probe three orders of magnitude more surface area than an oxidized silicon IRE and can access the entire IR spectral region [40]. Given these advantages, the use or development of methods to anchor high surface area silica particles to ATR crystals is highly desirable. One simple method is to directly deposit the high surface area metal oxide particles from a suspension onto a ZnSe IRE. This technique has been used to prepare water stable, high surface area, TiO_2 layers for the study of surface reactions in water [41]. The technique simply involves forming a suspension of suitable concentration of the metal oxide particles in a solvent. After thoroughly mixing and sonicating to achieve maximum dispersion, a small amount of the suspension is deposited on the surface of the IRE. After drying, and depending on the surface energetics of the system, a stable hydrated gel layer of the metal oxide can be formed. This deposition technique has also been used with colloidal silica particles on a cylindrical ZnSe IRE in non-aqueous solutions [42].

However, attempts to prepare high surface-area silica substrates in this manner, that are stable in water have proven unsuccessful. The silica layer is removed from the crystal when placed in contact with flowing water. An alternative method is to prepare a metal oxide layer via sol-gel techniques. Silica films deposited by sol-gel techniques have the advantage of allowing control over the film thickness, porosity, and chemical composition. These systems have proven to exhibit much greater sensitivity for the detection of trace analytes in water, as compared to an uncoated waveguide [43]. The problems associated with sol-gel techniques include the time-intensive preparation of the sol, the aging and controlled drying conditions, and the associated adhesion and cracking of the final gel layers [44]. Based on these limitations it is clear that a universal technique for anchoring any colloidal particle to the surface of an IRE would expand the applicability of surface reaction studies by aqueous phase ATR spectroscopy. Given the importance of metal based oxides in aqueous colloidal dispersions (paints and coatings), and the heightened activity of biological adsorption processes (i.e., silica is used as a substrate in microarray biochip technology [45]), there is a clear need to develop a general infrared technique that can be used to follow adsorption from aqueous solutions on metal oxide particles.

In this chapter we present a new technique for preparing high surface area particulate layers on a ZnSe IRE for subsequent studies of adsorption from aqueous solutions. Due to the aforementioned difficulties in studying aqueous phase surface reactions on colloidal silica layers via ATR spectroscopy, this metal oxide is the focus of this chapter. The technique involves using a binder, polyethylene (PE), to anchor the colloidal silica particles to the IRE surface. PE is used because it has few bands (C-H

modes) in the mid-IR region, and therefore is a good window material. A deuterated polyethylene (d-PE) can be substituted if access to the C-H modes is required. The resulting "coating" of silica particles and binder is extremely stable in water, and allows reaction with the silica surface to be investigated. To determine the accessibility of the silica surface in this composite structure, we examine the gas-phase reaction of hexamethyldisilazane (HMDS) with silica. Comparison is made between results obtained for the gas phase adsorption of HMDS measured for transmission studies for both pure silica films and silica/PE films supported on a CsI window, as well as gas-phase ATR measurements of the silica/PE films deposited onto a ZnSe IRE. The suitability of this technique for aqueous-phase adsorption studies is then investigated by the reaction of succinic anhydride with an aminosilane treated silica surface.

3.3. Experimental Method

3.3.1. Materials

The fumed silica used in this study was Aerosil 380 (Degussa) with a measured specific surface area of 375 m^2/g, as determined by BET nitrogen adsorption. The polyethylene (PE) was obtained from Aldrich and has a weight-average molecular weight of 4000, with a polydispersity (M_w/M_n) of 2.3. Hexamethyldisilazane (HMDS) and succinic anhydride were used as received from Aldrich. The aminosilane, (3-Aminopropyl)dimethylethoxysilane (APDMES) was purchased from United Chemical Technologies. HMDS and APDMES were transferred to gas bulbs and degassed using standard freeze-thaw methods.

3.3.2. Silica/PE Coating Preparation

The pigment volume concentration (PVC) is defined in the paints and coatings industry as the ratio of the pigment volume to the total volume of the pigment and binder. Paints are formulated at low PVC values, where the polymeric binder fills the interstitial voids between the pigment particles in the dried layer. This gives the paint weatherability and mechanical strength. At the other extreme, paper coatings are formulated at high PVC values, where there is not enough binder present to fill the interstitial voids. Therefore air voids are present in the final dried coating layer, and these contribute to the scattering of the incident light, which enhances the gloss and opacity of the coating. For this application the silica/PE coating is formulated at the highest possible PVC. This approach yields a silica-based coating with the least amount of binder present, which remains stable when in contact with a flowing stream of water.

For the materials in this study we use a mass ratio of silica to PE of approximately 4:1. Figure 3.1 illustrates the preparation of the silica/PE coatings. Typically, 10 mg of polyethylene is completely dissolved in 3 ml of toluene, heated to 105° C and thoroughly mixed. To this 40 mg of the fumed silica is added and mixed vigorously for 30 minutes. A 100 μl aliquot of this dispersion is withdrawn and deposited onto a CsI support for transmission measurements, or 200 μl is deposited onto both sides of a ZnSe IRE for ATR measurements. The solvent is then allowed to evaporate at ambient conditions. Solvent evaporation causes shrinkage of the coating layer, which produces individual islands of coating on the underlying substrate. Figure 3.2 depicts a typical coating layer, after solvent evaporation, deposited on a ZnSe IRE. The individual islands are roughly

20 μm in size, and are separated by approximately 5 μm cracks. Using a stylus profilometer these islands of coating are found to be about 5 μm in thickness.

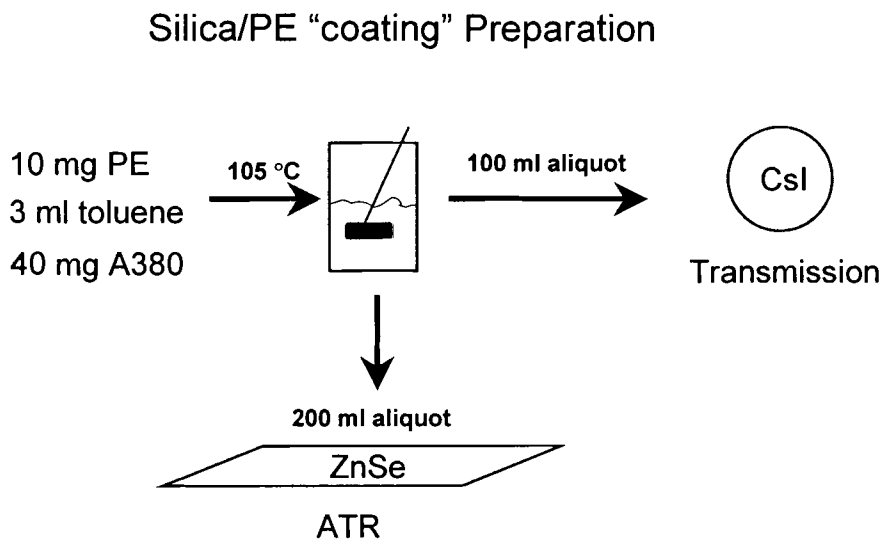

Figure 3.1. Preparation and deposition parameters for the silica/PE coating.

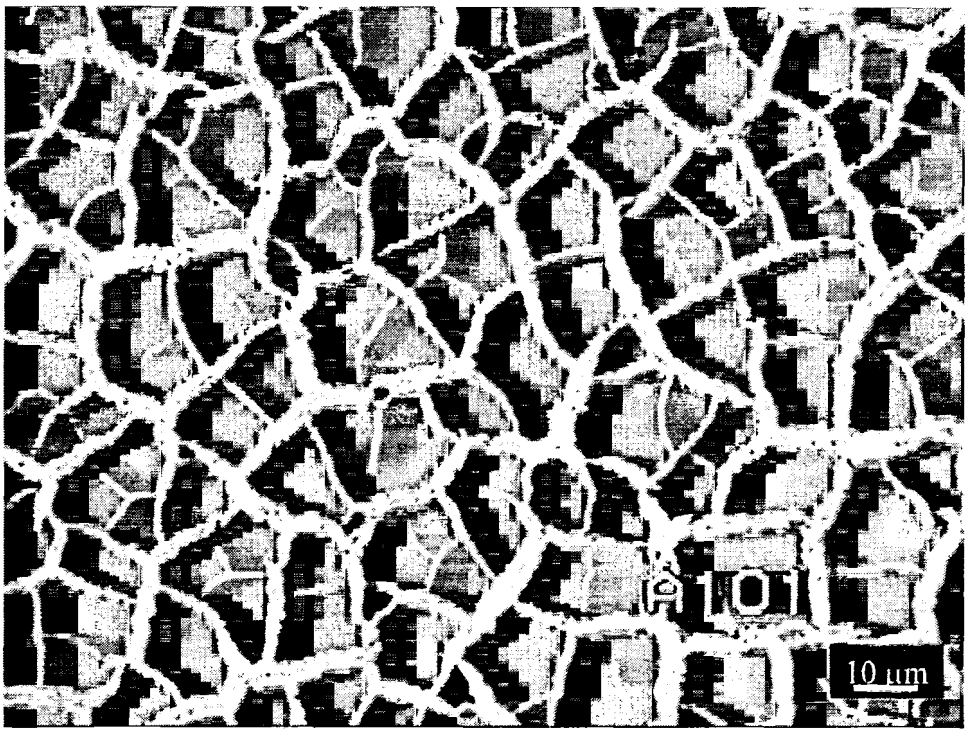

Figure 3.2. Optical image of silica/PE coating deposited onto a ZnSe IRE.

3.3.3. Experimental Setup

Transmission IR experiments were carried out with the *in situ* variable temperature infrared cell shown in Figure 3.3 [40]. A CsI window was used to support the pure silica films and the silica/PE coatings. The pure silica sample was spread onto the window as a thin film, using a glass slide and minimal pressure. The sample (plus support) is inserted into the furnace region of the cell. The experiments here were carried out at room temperature, however the quartz cell is able to withstand temperatures up to 1200° C. The ends of the cell were sealed off with CsI windows using an epoxy resin.

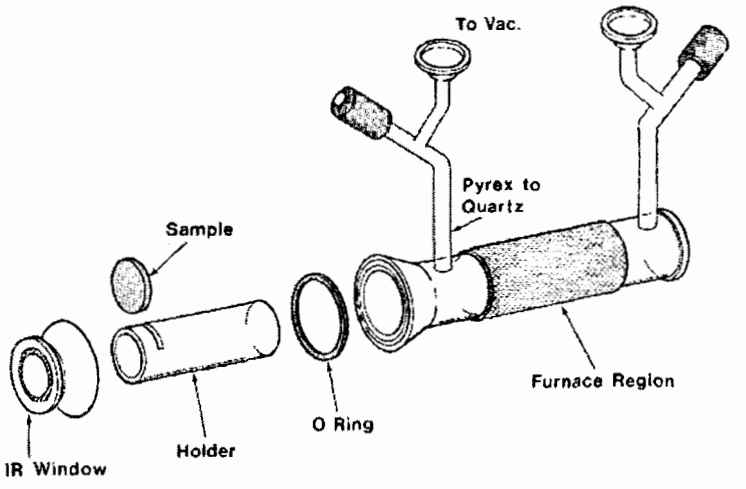

Figure 3.3. *In situ* infrared cell for transmission experiments.

Gas phase adsorption studies by ATR were performed with the in-house designed cell shown in Figure 3.4. The cell consists of a two piece quartz chamber with epoxied NaCl windows on the ends of the chamber. The IRE is mounted in a metal holder that rests on a self-compensating metal base, and is held in position in the chamber with a spring clip, Figure 3.5. This setup allows easy alignment of the cell on top of a twin, parallel mirror reflection attachment from Harrick. The entire chamber is connected to a standard vacuum line.

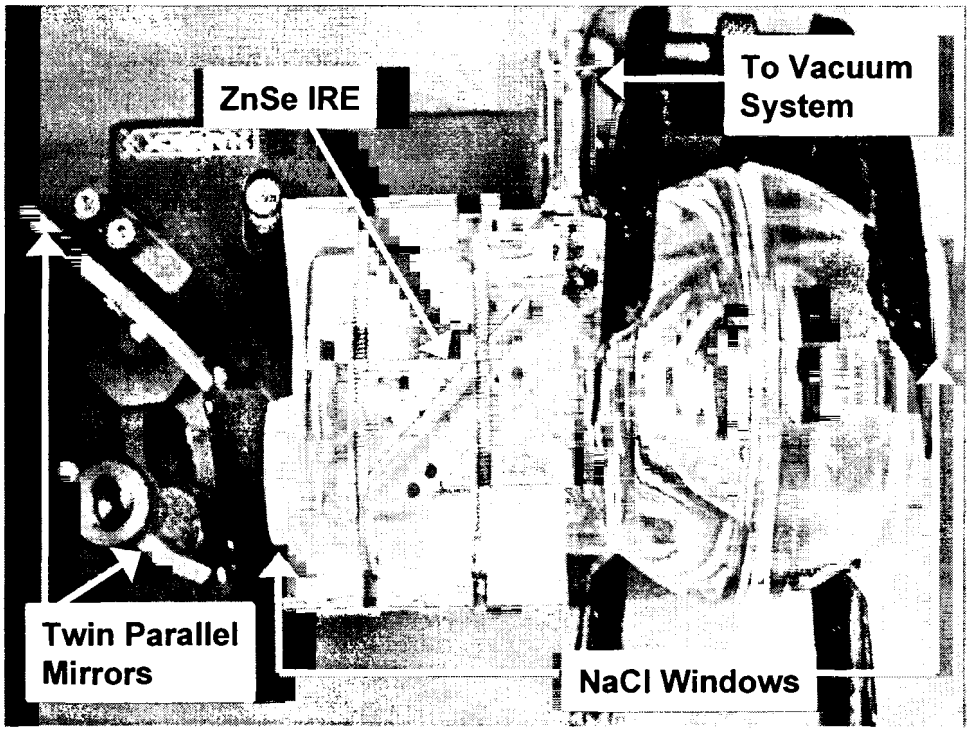

Figure 3.4. ATR cell designed for gas-phase adsorption studies.

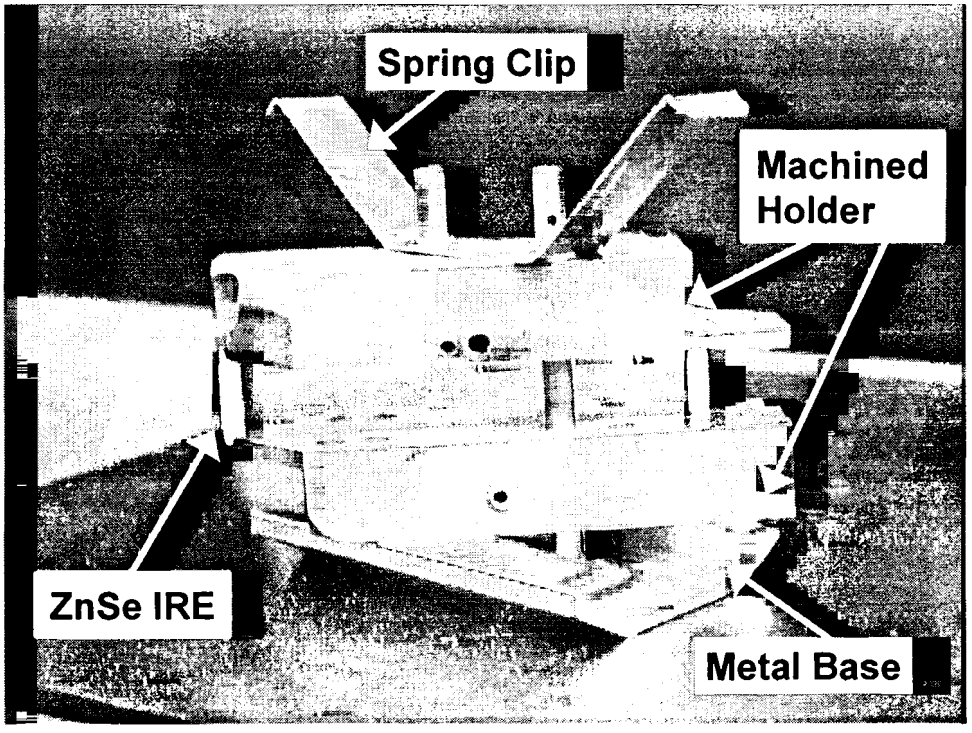

Figure 3.5. ZnSe IRE in the machined insert for the ATR gas cell.

The aqueous phase experiments were carried out using a standard ATR liquid flow cell arrangement from Harrick. A peristaltic pump was used to flow the liquid solution across the silica/PE surface during the aqueous phase experiments. A schematic of the liquid cell experimental setup is shown in Figure 3.6. The cell consists of two stainless steel halves, with a recessed flow cavity on both sides. The coated IRE is clamped between the two halves and a water-tight seal is established with the use of viton o-rings. The aqueous solution is continuously stirred and pumped through the cell by means of the teflon tubing. The entire cell is mounted on a twin, parallel mirror reflection attachment from Harrick, and placed in the infrared beam, Figure 3.7.

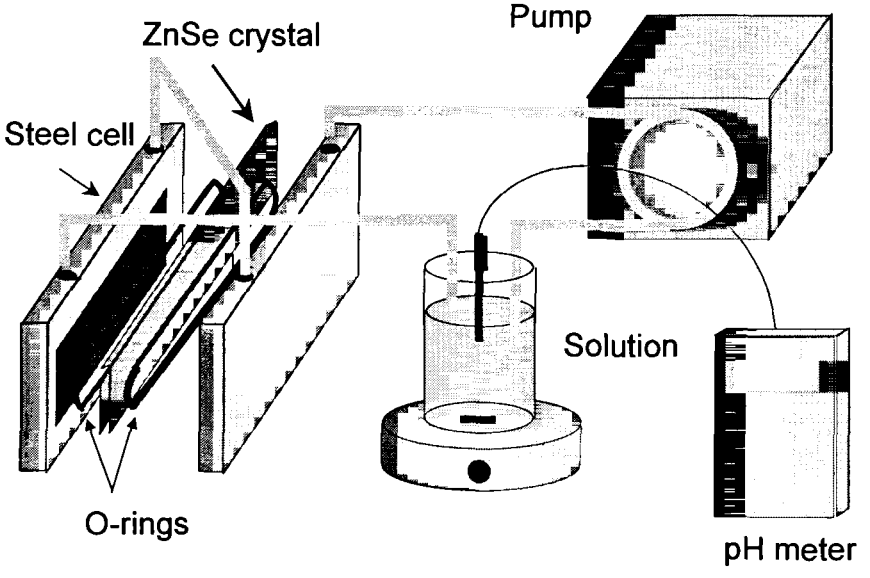

Figure 3.6. Experimental setup for aqueous-phase adsorption studies.

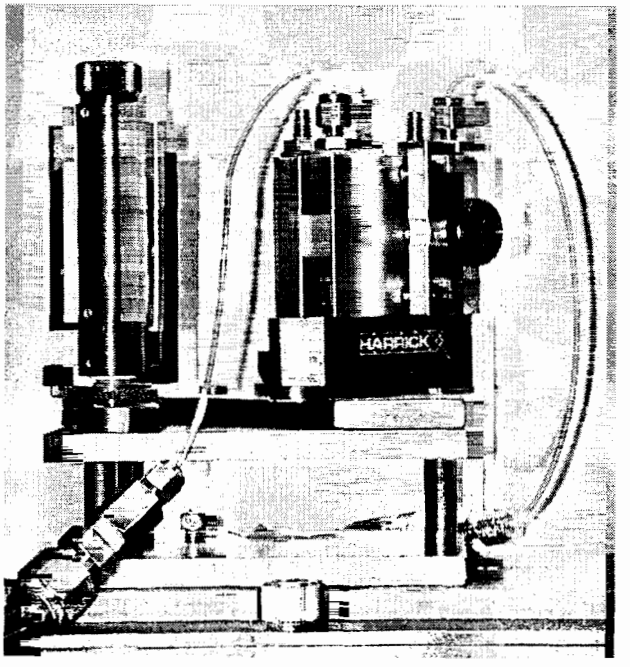

Figure 3.7. ATR liquid cell mounted on twin, parallel mirror reflection attachment.

3.4. Experimental Results

3.4.1. Transmission Spectra of Silica and Silica/PE Films

The thin film transmission spectra of silica (spectrum A) and of the silica embedded in the PE matrix (spectrum B), both dispersed on a CsI window and evacuated at room temperature, are shown in Figure 3.8. The strong absorption bands appearing at 1090 cm^{-1} and 810 cm^{-1} are the Si–O bulk modes of silica, and the peak at 3747 cm^{-1} is assigned to the isolated surface Si_sO–H groups [40]. In spectrum B the C–H modes of the polyethylene appear at 2917, 2850, and 1464 cm^{-1}.

The isolated hydroxyl groups are the principal adsorption sites on silica. The 3747 cm^{-1} surface band shifts to 3690 cm^{-1} when dispersed in CCl_4 or cyclohexane [46],

3590 cm^{-1} when dispersed in toluene, 3350 cm^{-1} in alcohols and 2700 cm^{-1} with amines [47]. This shift represents weak physisorption between the hydroxyl groups on silica and CCl_4 and cyclohexane, a slightly stronger interaction with the aromatic ring of toluene, and hydrogen bonding with alcohols and amines. From a comparison of the relative intensity of the band at 3747 cm^{-1} for the spectra in Figure 3.8 it is concluded that most of the isolated SiOH groups are not perturbed by the presence of the PE binder.

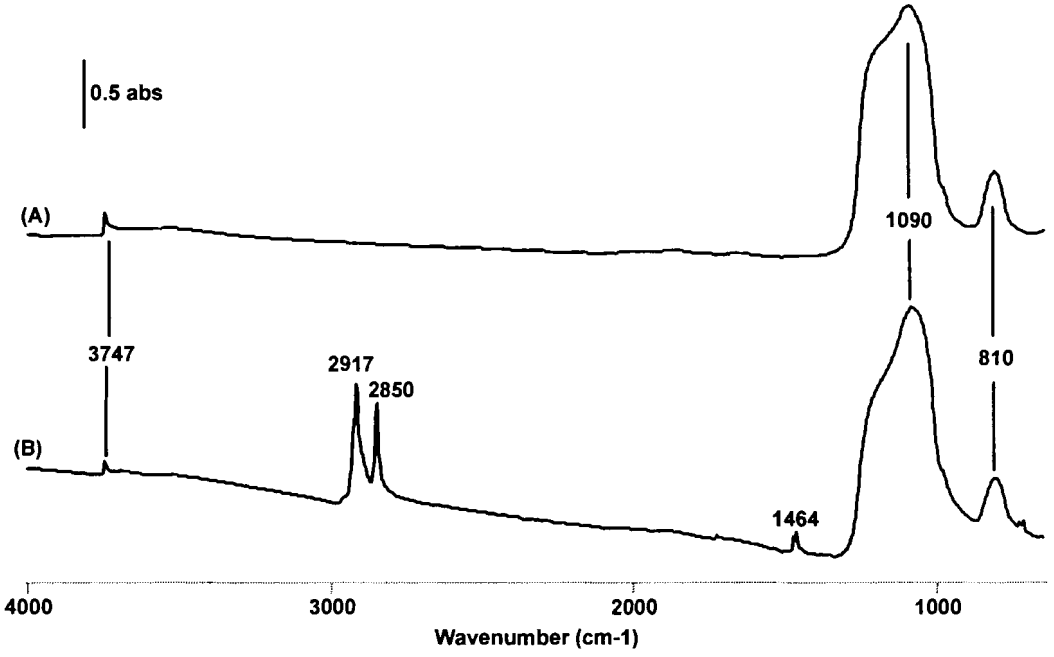

Figure 3.8. (A) IR transmission spectrum of a thin film of silica spread onto a CsI window. (B) IR transmission spectrum of a silica/PE coating deposited onto a CsI window.

An expanded view of the high frequency region of Figure 3.8 is shown in Figure 3.9. For the spectrum of the silica/PE coating shown in curve B of Figure 3.9, there is an additional weak feature centered at 3690 cm^{-1}. The assignment of this band is attributed to a weak van der Waals interaction between a portion of the surface OH groups of the silica and the PE binder (Si–OH·····PE) that is on the same order of strength as that obtained for weakly physisorbed CCl_4 or cyclohexane.

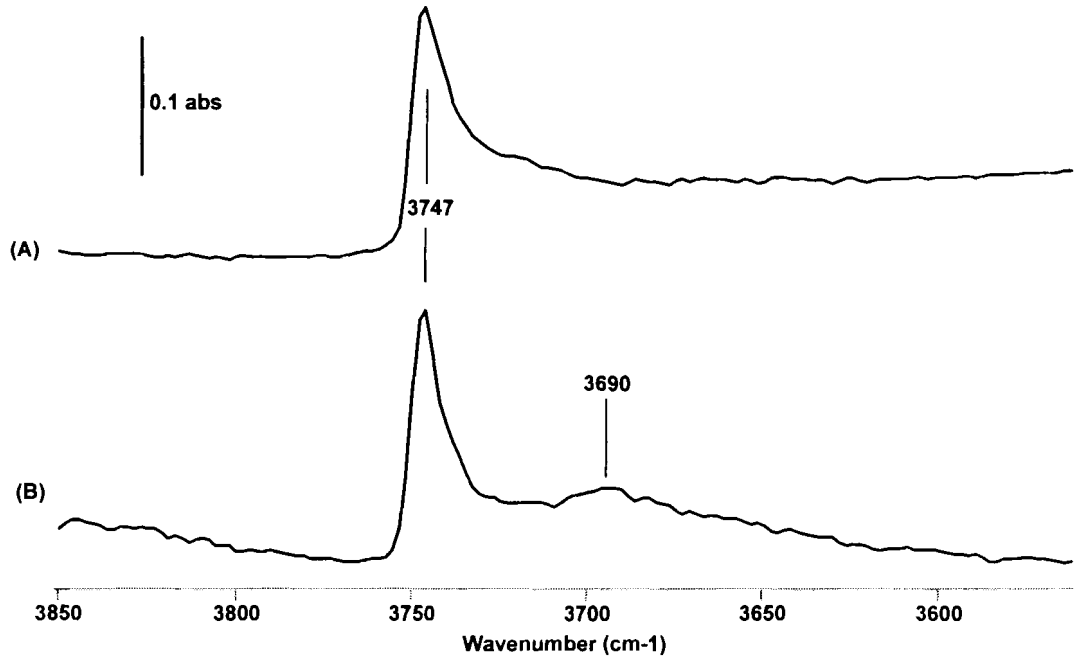

Figure 3.9. (A) Expanded view of high frequency region of spectrum A in Figure 3.8. (B) Expanded view of high frequency region of spectrum B in Figure 3.8.

By taking the ratio of the 3747 cm^{-1} integrated peak area (SiO–H) to that of the 810 cm^{-1} integrated peak area (Si–O bulk mode) we can evaluate the extent of interaction of the PE binder with the surface hydroxyl groups of the silica. For the spectrum of silica, this ratio

is calculated to be 0.0587, while the silica/PE spectrum gives a calculated value of 0.0427. This result shows that approximately 73% of the total available isolated surface hydroxyl groups are unaffected by the presence of the PE binder. From this data we conclude that the fumed silica particles are then just basically "spot-welded" together with the polyethylene as depicted in Figure 3.10.

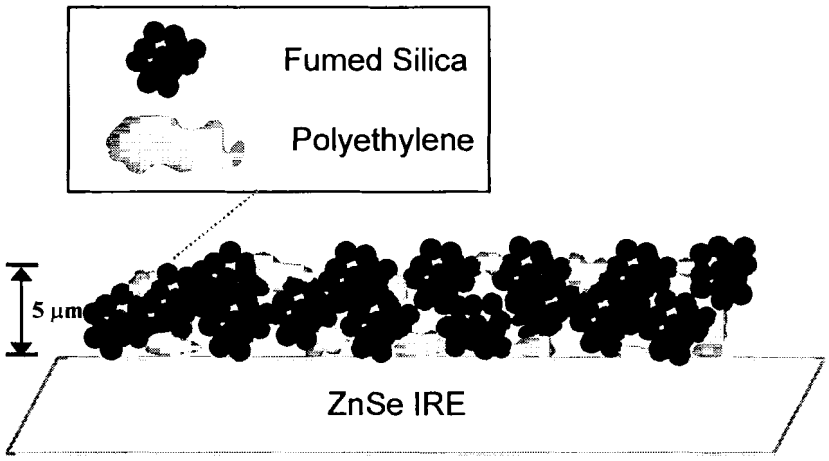

Figure 3.10. Schematic of the dried silica/PE coating deposited onto a ZnSe IRE.

3.4.2. Gas Phase Reaction with the Probe Molecule HMDS

The gas phase reaction of HMDS was studied in order to ascertain the suitability of the silica/PE films for IR adsorption experiments, and to determine the accessibility of the hydroxyl groups perturbed by the PE binder. Transmission experiments of the adsorption of gaseous HMDS on the silica particles embedded in the PE matrix were

compared to the results obtained using thin films of silica dispersed on a CsI window, and also to ATR experiments using a silica/PE film on a ZnSe IRE. HMDS reacts with all isolated SiOH groups (band at 3747 cm^{-1}) at room temperature [48] according to the following reaction;

(3.1) $$2SiOH + (CH_3)_3SiNHSi(CH_3)_3 \rightarrow 2\ Si{-}O{-}Si(CH_3)_3 + NH_3$$

Similar spectral features are obtained for the difference spectra for HMDS adsorbed on silica (Figure 3.11, spectrum A) and on the silica/PE coating (Figure 3.11, spectrum B) recorded in transmission, as well as the ATR spectrum of the silica/PE coating (Figure 3.11, spectrum C). The difference spectra in Figure 3.11 are all referenced against a background of either the pure silica (spectrum A) or the silica/PE coating (spectrum B and spectrum C). Although we plot difference spectra, analysis of the single beam spectra before and after HMDS exposure shows that the decrease in the bands at 3747 cm^{-1} represents 100% reaction with the isolated surface hydroxyl groups. The appearance of a lower intensity of the negative band at 3747 cm^{-1} in the ATR spectrum is due to the wavelength penetration depth dependence of the evanescent wave [19]. Both spectrums B and C show a negative absorption band at 3690 cm^{-1}, and this shows that the surface hydroxyl groups, which were initially perturbed by the PE binder, are able to participate in the reaction with HMDS. The assignments of the other bands have been reported in the literature [48].

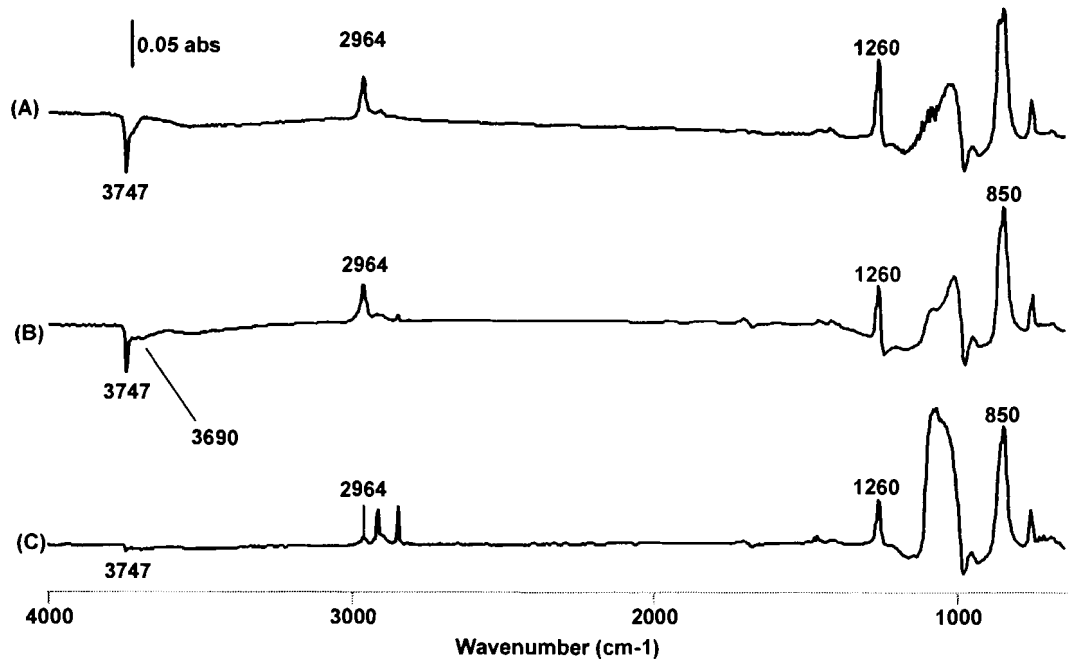

Figure 3.11. Difference spectra after exposure to HMDS for 10 minutes, followed by evacuation for 5 minutes. (A) Fumed silica on a CsI window in transmission mode. (B) Silica/PE coating on a CsI window in transmission mode. (C) Silica/PE coating on a ZnSe IRE in ATR mode.

The presence of a band in the 1060 cm^{-1} region is indicative of chemisorption of the HMDS with the silica surface through the formation of Si_s–O–Si linkages. The slight difference in shape of the band at 1060 cm^{-1} in the transmission spectra (spectrum A and B) as compared to the ATR spectrum (spectrum C) is due to the effect of penetration depth. Slight changes in the refractive index of the region containing the strong Si–O–Si bulk modes will have an effect on the band intensity in ATR spectra. All other positive bands are various C–H modes. The similarity of the spectra in Figure 3.11 show that the

presence of the polyethylene binder does not hinder the detection of bands due to adsorbed species, or their reaction with the surface hydroxyl groups for either transmission or ATR studies.

3.4.3. Gas Phase Reaction of APDMES Treated Silica

The main purpose of using the PE as a matrix in the ATR experiments is to provide a means for anchoring the silica particles to the crystal in order to prevent their removal in a flowing stream of water. We have found no loss of intensity in the bands due to silica when a silica/PE coating on a ZnSe crystal is mounted in an ATR flow through cell and subjected to several hours of flowing water at a rate of 10 ml/min. To demonstrate the suitability of this arrangement for adsorption studies from aqueous solution we examine the reaction of succinic acid with an aminosilanized silica surface.

The anticipated reaction scheme is shown in Figure 3.12. The reaction of the APDMES with the silica/PE structure was conducted in the gas phase using the same procedures outlined for the HMDS reaction. The aminosilane reacts with the isolated surface hydroxyl groups of silica, forming a covalent Si–O–Si attachment, and giving off ethanol as a byproduct.

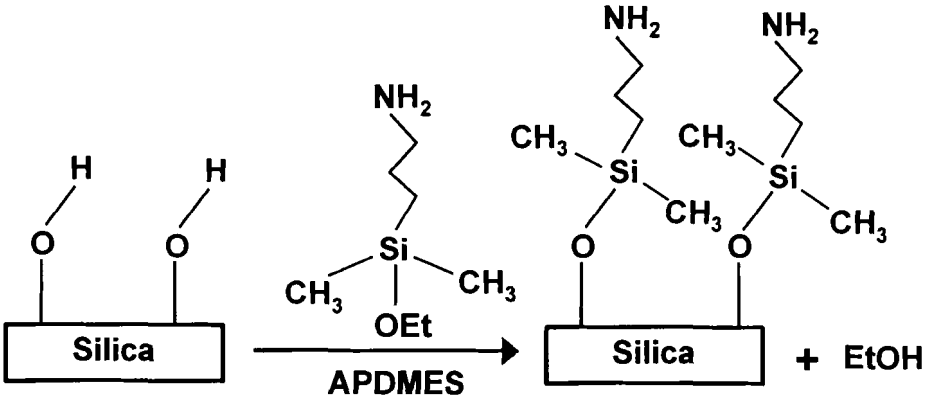

Figure 3.12. Anticipated (ideal) reaction scheme for the attachment of APDMES to the silica surface.

The spectrum obtained after reaction of the silica/PE coating with the APDMES is shown in Figure 3.13, and is similar to that recently reported in the literature [49]. In brief, the negative SiOH bands at 3747 and 973 cm^{-1}, the absence of the strong Si–O–C modes at 1118 cm^{-1} for the gaseous molecule (not shown), and the appearance of an Si–O–Si band at 1050 cm^{-1} is clear evidence of a surface Si–O–Si bond formed from a reaction of a surface SiOH group with the ethoxy group of the APDMES. Furthermore, the amine group is not freely dangling from the surface, as indicated in the ideal scheme of Figure 3.12, but instead hydrogen bonded to surface SiOH groups. The N–H bending mode appears at 1596 cm^{-1} instead of 1622 cm^{-1} for the free amine.

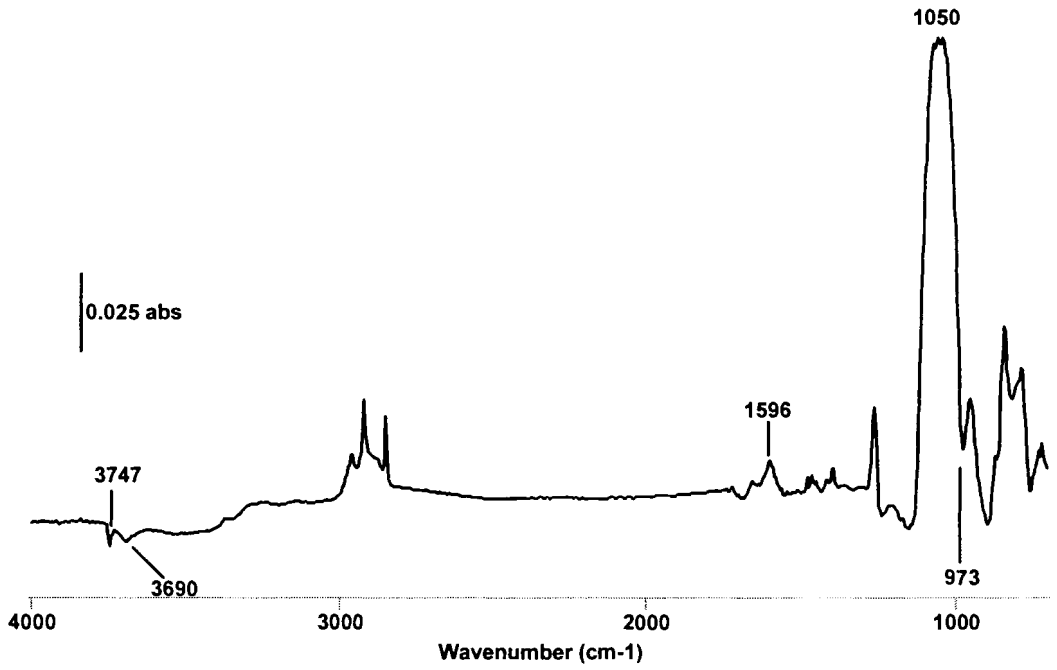

Figure 3.13. ATR gas-phase difference spectrum of the silica/PE coating after exposure to APDMES vapor for 10 minutes, followed by evacuation for 5 minutes.

Thus, a more realistic picture for the adsorbed APDMES is shown in Figure 3.14. While the APDMES reaction was performed directly on the silica/PE ATR film, it is noted that this treatment could have been performed *ex situ* on the silica particles, and then dispersed in the PE solution. In this way surface modified metal oxide particles could be prepared under more severe reaction conditions (high reaction temperatures, organic solvents, etc) than could be tolerated by the PE binder. For example, in our case the silica powder could be pretreated with APDMES in the gas phase at 200° C, then dispersed in the PE coating for later aqueous based adsorption measurements.

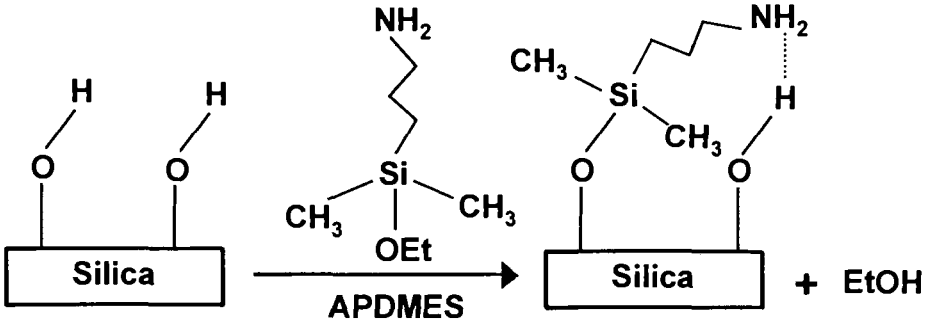

Figure 3.14. Observed reaction scheme for the gas-phase attachment of APDMES to the silica/PE coating.

3.4.4. Aqueous Phase Reaction of Succinic Acid with the APDMES Treated Silica

The final confirmatory test of the PE binder technique is the ability to monitor adsorption from aqueous solution. For this experiment the APDMES treated silica/PE coating is exposed to a solution of succinic acid. Reaction of the dicarboxylic acid with the aminosilane treated silica occurs through the formation of amide linkages. The ideal reaction scheme is illustrated in Figure 3.15. Succinic anhydride is the starting material, and this quickly hydrolyses to succinic acid when placed in water.

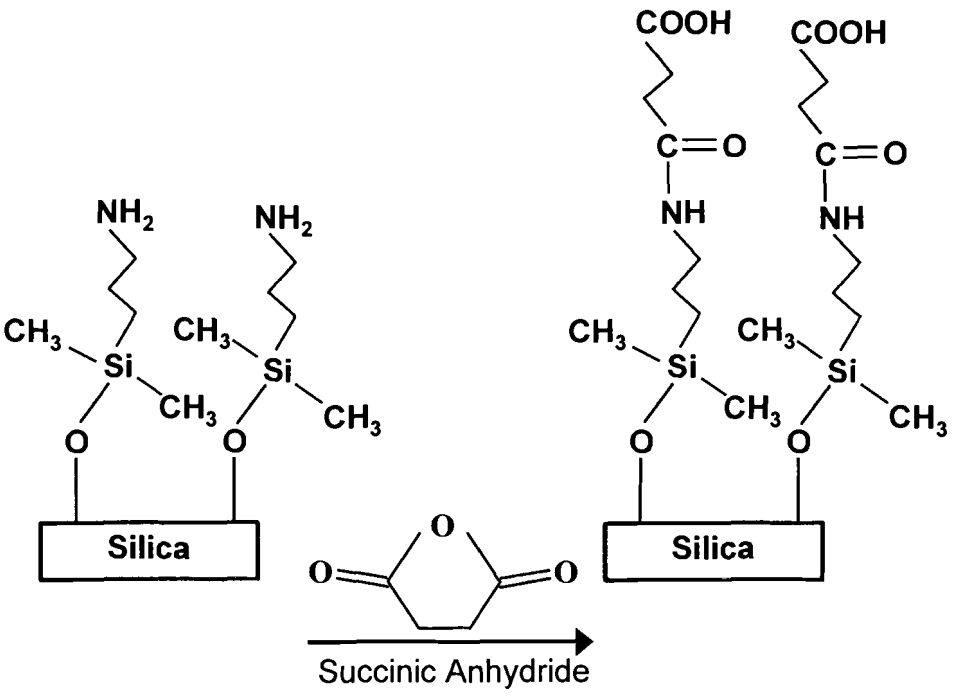

Figure 3.15. Ideal reaction scheme for the attachment of succinic anhydride to the APDMES treated silica surface.

To aid in the assignment of the bands due to the surface adsorbed species, a series of solution phase experiments were first undertaken in the absence of the silica/PE coating. The difference spectra in Figure 3.16 are the results after subtraction of pure water from the solution spectra. Spectrum A is the result of a 6 x 10^{-2} molar solution of succinic anhydride. The succinic anhydride hydrolyses to a dicarboxylic acid and the bands at 1780 and 1720 cm^{-1} are due to the carbonyl group, while the band at 1408 cm^{-1} has been assigned to the deformation frequency of a methylene group adjacent to a carbonyl group [50]. Spectrum B is the result of a 1:1 mixture of APDMES and succinic acid. The formation of an amide linkage is indicated by the appearance of the amide I band at 1640 cm^{-1} and the amide II band at 1555 cm^{-1}. This is also accompanied by a

decrease in the 1720 and 1780 cm^{-1} bands due to the decrease in the amount of free carbonyl groups of the acid. The positive band at 1258 cm^{-1} has been previously assigned to the Si–CH_3 bending mode of the APDMES. A growth in the band in the 1400 cm^{-1} region, along with a shift towards lower frequencies, indicates that this band is a combination of the methylene deformation mode of the diacid, and the amide linkage. Spectrum C is the result of adding an excess of the aminosilane to the succinic acid, this solution contained an APDMES to acid ratio of 1.4:1. All traces of the free carboxylic acid have disappeared, and this is accompanied by an increase in the amount of amide linkages. The contribution of the amide linkage to the 1400 cm^{-1} band is seen by an increase in the absolute intensity, accompanied by a further shift towards lower frequency.

Figure 3.17 shows the results of two experiments where a 10^{-3} molar solution of succinic acid is allowed to flow over the APDMES treated silica/PE coating. The spectra in Figure 3.17 are referenced against the silica/PE coating in pure water and differ from the spectra obtained at high solution concentrations and in the absence of the silica/PE layer (Figure 3.16, spectra B and C) by the absence of the strong amide I band. The absence of the amide I band in the spectra of Figure 3.17 is due to masking by the water-bending mode at 1638 cm^{-1}. The deposition of the silica/PE coating causes an increase in the refractive index of the interfacial region, as compared to the solution systems of Figure 3.16. The result is an increase in the depth of penetration of the evanescent wave. The water-bending mode for the ZnSe/solution system of Figure 3.16 has an absorbance of 1.3, whereas for the silica/PE system the absorbance is increased to 1.9.

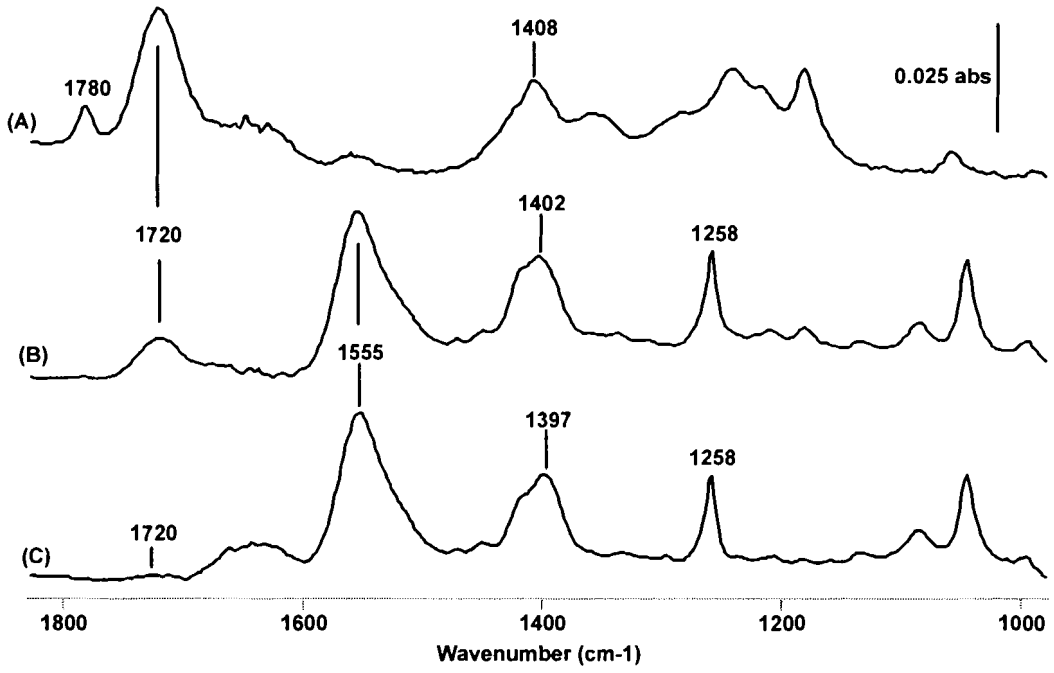

Figure 3.16. ATR aqueous solution spectra. (A) 6 x 10^{-2} molar succinic acid solution. (B) 1:1 mixture of APDMES and succinic acid. (C) 1.4:1 mixture of APDMES and succinic acid.

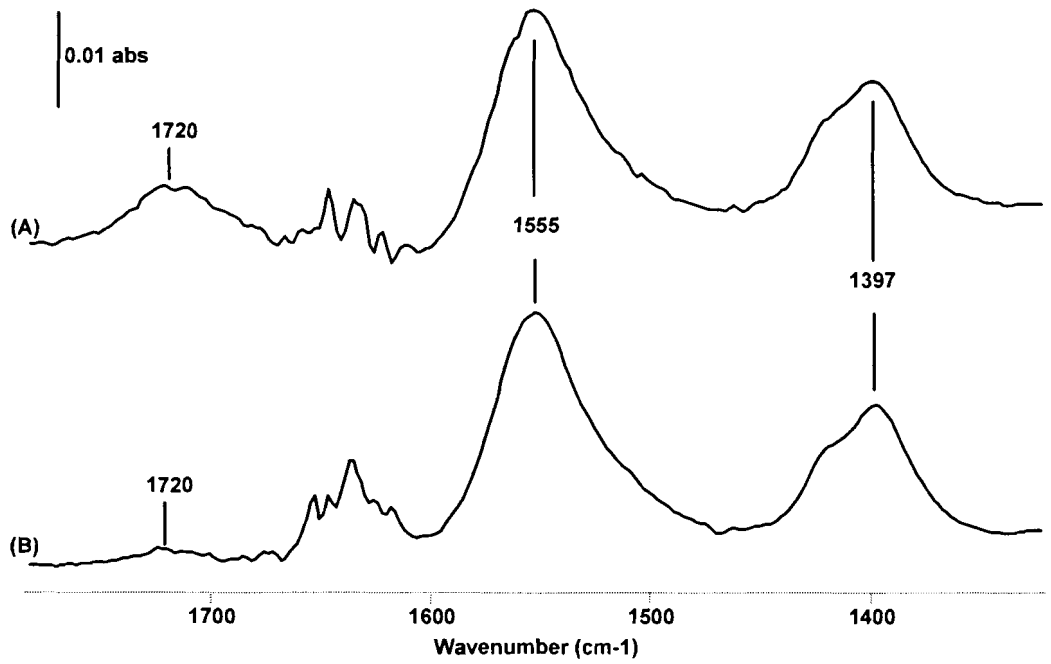

Figure 3.17. ATR difference spectra after exposure of the APDMES treated silica/PE coating to a 10^{-3} molar solution of succinic acid. (A) 50% APDMES surface coverage. (B) Full APDMES surface coverage.

The spectra in Figure 3.17 appeared immediately with contact of the succinic acid and did not change with time, indicating that the reaction proceeded rapidly. In spectrum A (Figure 3.17), the appearance of the amide II band at 1555 cm^{-1} indicates reaction of the succinic acid with the amine group of the APDMES. There is also evidence of free carboxylic acid, as indicated by the band at 1720 cm^{-1}. However, in comparing spectrum B to spectrum A, we find the 1720 cm^{-1} band due to the free acid is much weaker in intensity, while the absolute intensity of the amide II band has increased. The difference between the samples is that the amount of initially attached APDMES on silica used in the experiment to generate spectrum B was twice that for the silica/PE sample in spectrum A.

These results clearly indicate that the experimental conditions associated with the gas phase reaction of APDMES with the silica surface have a profound effect on the structure of the functionalized surface. Specifically, it is shown that the initial APDMES surface density has an effect on the number of acid functionalities dangling out from the surface. At the higher APDMES surface density there are a greater percentage of diacid molecules reacting difunctionally to form amide linkages with two adosrbed APDMES species. A more realistic picture of the reaction of succinic acid with the APDMES treated silica is shown in Figure 3.18. The relative number of free carboxylic groups is important because these sites are used to attach amino-terminated oligonucliotides. Thus, a variation in carboxylic acid groups will translate to a variation in the number of attached oligonucliotide probe molecules.

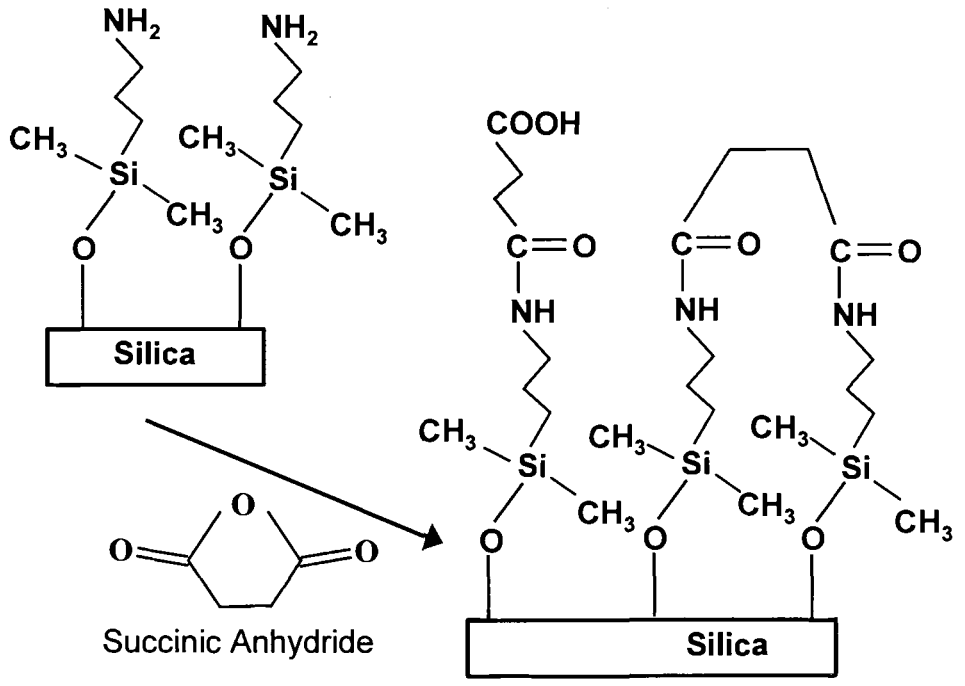

Figure 3.18. Observed reaction scheme for the attachment of succinic acid to the APDMES treated silica surface.

3.5. Summary

The results presented here clearly demonstrate the ability of this technique to follow the surface chemical reactions occurring from aqueous solutions on the surface of silica particles. These results would not be possible without the higher surface area and extended range advantages of using silica powders over traditional methods using oxidized silicon wafers.

While it has been demonstrated how this technique can be used to study adsorption on silica particles, it is noted that it also can be used for infrared adsorption studies onto any small particulate matter. It is also noted that this initial study has focused on relatively small molecule adsorption studies. At this time it is not known if

the presence of the polyethylene binder will impede the access of larger molecules such as polymers, surfactants, and polyelectrolytes. On a final note, the PE binder can be used to temperatures of 50° C, which is sufficient for most aqueous based processes. Slightly higher temperatures are possible with the use of higher molecular weight PE.

CHAPTER 4. THE IMPORTANCE OF ADSORBED CATIONIC SURFACTANT STRUCTURE IN DICTATING THE SUBSEQUENT INTERACTION OF ANIONIC SURFACTANTS AND POLYELECTROLYTES WITH PIGMENT SURFACES

4.1. Introduction

In the last chapter a novel technique was introduced which allows the detection of adsorbed surface species on the surface of colloidal pigment particles in an aqueous environment. The use of a polymeric binder was shown not to impede the adsorption of small molecules. This chapter makes use of the colloidal deposition technique in order monitor the adsorption of larger molecules (surfactants and polyelectrolytes). Since surfactants consist of large hydrophobic tails, which could interact with the binder, the omission of the binder was deemed paramount. The choice of TiO_2 pigments allowed this technique to be used, since the TiO_2 particles form a dense, water stable film without the use of a binder.

The adsorption dynamics of the cationic surfactant cetyltrimethylammonium bromide ($C_{16}TAB$) at the TiO_2 – water interface is investigated using Fourier transform infrared – attenuated total reflection spectroscopy (FTIR-ATR). Specifically, the response of the adsorbed $C_{16}TAB$ to the anionic surfactant sodium dodecyl sulfate (SDS) is used to discern the structure of the adsorbed $C_{16}TAB$ at the hemimicelle concentration (HMC). In this low concentration regime $C_{16}TAB$ is shown adsorb as isolated clusters

with a "defective" bilayer structure. However, these bilayer structures can be effectively transformed into monolayer structures through the interaction with the non-adsorbing polyelectrolyte sodium polyacrylate (NaPA). It is shown that the structure of the adsorbed C_{16}TAB layer, and not the amount of adsorbed surfactant, dictates the subsequent adsorption of anionic species on negatively charged TiO_2 particles.

4.2. Background and Literature Review

The adsorption of surfactants at the solid – liquid interface plays an important role in such areas of industry as ore flotation, paper manufacturing, petroleum recovery, and pharmaceutical production [51]. In addition to these more traditional sectors, surfactants are emerging as powerful contributors in areas such as electronic printing, microelectronics, advanced battery technology, and biotechnology [52]. Although the properties of surfactants, and their associated aggregation behavior (micelle formation) in bulk solutions are reasonably well understood [53,54], the self-assembly of surfactants at the solid-liquid interface is still a much developing area. The surfactant microstructures formed at the solid-liquid interface by adsorption from low surfactant concentration solutions (<< CMC) is to be distinguished from the process of bulk micelles adsorbing from solution onto a solid surface.

In the low concentration region, the adsorption of ionic surfactants onto oppositely charged mineral surfaces occurs primarily through adsorption of individual surfactant ions through attractive electrostatic forces. It is generally accepted that at a defined surfactant concentration, the adsorbed ions begin to associate through hydrophobic interactions of the surfactant tails into surface aggregates. This surfactant

concentration is termed the hemimicelle concentration (HMC), and occurs at much lower concentrations than the corresponding bulk critical micelle concentration (CMC). This associative behavior has been referred to as cooperative adsorption, in which the molecules tend to adsorb in clusters and give rise to S-shaped adsorption isotherms [55]. The onset of formation of a hemimicellar structure has been used to explain the rapid rise in the S-shaped isotherm as well [56,57]. A hemimicelle is described as a localized patch of adsorbed surfactant, due to the self-assembly of surfactant molecules at the interface. Later an alternative structure termed the admicelle was introduced to describe surface aggregates that consist of localized clusters of surfactant molecules with a bilayer structure [58]. An illustrative picture of these surface structures, as previously reported in the literature [59], is given in Figure 4.1.

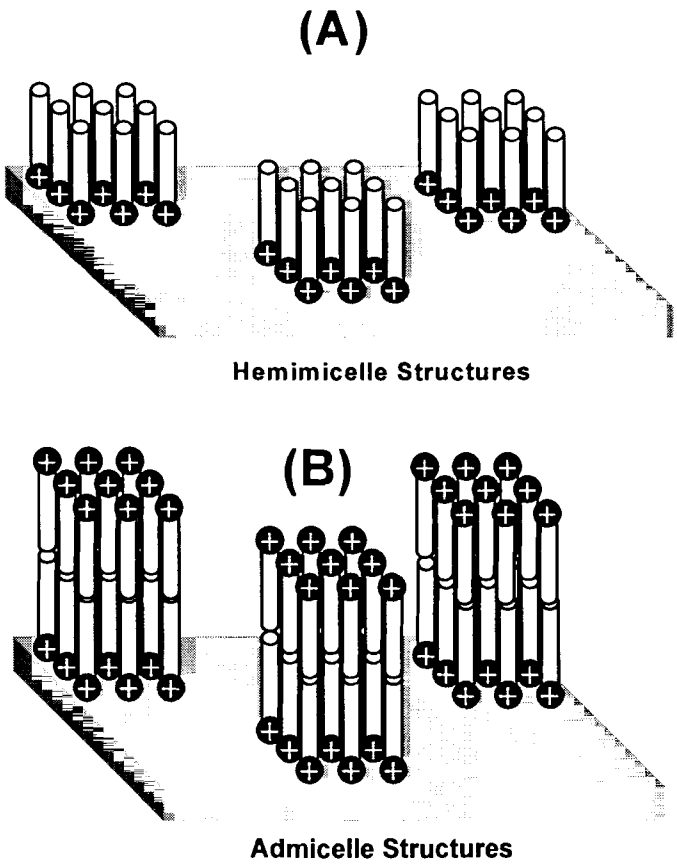

Figure 4.1. Idealized structures of surfactant aggregates adsorbed at the solid-liquid interface. (A) Hemimicelle structures. (B) Admicelle structures.

Theoretical investigations have been undertaken in order to shed light on the possible microstructures formed at the solid-aqueous surfactant solution interface. An early patchwise adsorption model was presented which predicted that bilayer surface aggregates could form without first the formation of monolayer aggregates [60]. Later a theoretical treatment of the monolayer/bilayer transition was presented which concluded that both structures could be present at the same time, depending on the heterogeneity of the adsorbent surface [59]. A model of ionic surfactant adsorption onto polar charged surfaces was proposed in which individual surfactant ions act as anchors, to which isolated spherical aggregates form as a result of hydrophobic interactions [61,62]. This work was later extended to include not only electrostatically adsorbed surfactant ions as anchors, but also covalently attached alkyl chains [63]. Recent theoretical work, based on the molecular thermodynamics of the self-assembly of surfactants at solid-liquid interfaces, has shown that several types of adsorbed surfactant microstructures are possible [64,65]. This model predicts the critical surfactant concentration for the formation of surface aggregates (HMC), along with their associated morphology, by taking into account the equilibrium free-energy for the formation of a given microstructure. The microstructures considered include monolayer coverage, spherical and cylindrical surface aggregates, composite structures such as monolayers covered by hemispheres, hemicylinders, and bilayers. The strength of this model is that it incorporates both the molecular properties of the surfactant and the properties of the solid surface, and can therefore be applied to specific surfactant/solid systems. One of these systems in which the model predictions have been specifically applied to is the

adsorption of the cationic surfactant alkyl trimethylammonium bromide (C_nTAB) onto the hydrophilic surfaces of mica and silica [64].

The adsorption of C_nTAB at the metal oxide-aqueous surfactant solution interface has been one of the most widely studied surfactant/solid systems. The adsorption of C_nTAB onto the hydrophilic surfaces of silica [66], alumina [67], and titania [68] has been experimentally studied using conventional depletion techniques. Adsorption of C_nTAB onto the TiO_2 surface was postulated to occur as a bilayer, based on a measured saturation adsorption density corresponding to 1.4 vertically oriented monolayers [68]. However, experimental evidence of the surfactant structures at the onset of hydrophobic association, such as at the hemimicelle concentration, were not discussed.

Atomic force microscopy (AFM) has been applied to the study of C_nTAB adsorbed to the hydrophilic surface of mica [69-73]. At high surfactant concentrations (twice the bulk CMC), AFM images of the interface revealed a variety of adsorbed microstructures [69]. In the absence of added electrolytes flat sheets were observed, which transformed into cylindrical structures with the addition of a salt. At concentrations below the bulk CMC, adsorption occurs through formation of sparse patches of surfactant molecules on the surface [70,71,73]. By measuring the width of the surfactant layers, it was found that both monolayers and bilayers are adsorbed at the mica interface [72]. Increasing the surfactant concentration promoted the formation of cylindrical surfactant aggregates on the surface [70]. In these studies the solution conditions (pH, electrolyte conc.) play an important role in the final adsorbed surfactant structure.

The adsorption of C_nTAB at the hydrophilic silica surface has been recently explored using Fourier transform infrared attenuated total reflection (ATR) spectroscopy [37,38,74]. In addition to providing equilibrium (surface excess) and kinetic properties of the adsorption process, the structure of the self-assembled surfactant layer can also be monitored by employing IR polarization techniques. A kinetic study of cetyltrimethylammonium bromide ($C_{16}TAB$) adsorbing to a silica surface, at a bulk concentration below the CMC, indicated that the adsorbed surfactant becomes more oriented in a direction normal to the surface as the adsorption process progresses in time [38]. Upon desorbing the $C_{16}TAB$ from the surface by the use of an anionic polyelectrolyte, the remaining surfactant on the surface retained a highly ordered configuration. The conclusion was that the residual surfactant was present in isolated clusters of highly ordered molecules. However, no indication as to the microstructure of these highly ordered aggregates was proposed.

By combining ATR polarization measurements with contact angle and zeta potential measurements, the structural transitions of adsorbed dodecyltrimethylammonium bromide ($C_{12}TAB$) at the silica surface were investigated as a function of surfactant concentration [74]. The experimental observations indicate that at low $C_{12}TAB$ concentrations the surfactant adsorbs randomly, with no associated structure. As the surfactant concentration is increased the presence of hemimicelles on the surface is observed. Increasing the concentration further results in the formation of spherical aggregates on the surface, with no evidence of the intermediate formation of bilayers.

As can be ascertained by this brief review of the literature, the adsorption of the cationic surfactant alkyl trimethylammonium bromide (C_nTAB) onto the hydrophilic surfaces of mineral oxides can produce a wide variety of experimentally observed, and theoretically predicted surface structures. The underlying central concept, commonly agreed upon by the various investigators, is the occurrence of hydrophobic interactions at a certain critical surfactant concentration, which lead to the formation of surface aggregates. The onset of these hydrophobic interactions is generally accepted to occur at the surfactant concentration at which the slope of the adsorption isotherm abruptly increases, commonly referred to as the hemimicelle concentration (HMC).

An understanding of the structure of these surface aggregates, for specific surfactant/solid systems, is especially important for the paints and coatings industry. These systems primarily consist of mineral pigments and synthetic binders (latex) dispersed in an aqueous medium, along with a wide variety of functional additives. Surfactants and/or polymers are used to influence the degree of flocculation of the aqueous pigment suspensions, and surfactants are necessarily present to stabilize the synthetic latex. The structure of surfactant aggregates at the mineral surface has been shown to influence the stability of mineral suspensions [75,76]. Also, due to the interactions between the various components, it has been shown that the order of addition in the preparation of coatings can have a dramatic effect on the rheological properties of the system [77]. These rheological effects are then carried over to influence the final performance properties of the applied, and dried, coating layer.

In this chapter the adsorption dynamics of the cationic surfactant cetyltrimethylammonium bromide (C_{16}TAB) onto the negatively charged surface of TiO_2 is investigated. TiO_2 is the premier white pigment used in paints and coatings, owing to its superior whiteness and hiding power [78]. The equilibrium properties of this surfactant/oxide system have been reported in the literature [68] for the rutile phase of TiO_2. By combining dynamic adsorption data from ATR spectroscopic measurements with information on the electrophoretic mobility, it is shown how the structure of a C_{16}TAB layer adsorbed onto a solid, particulate TiO_2 surface is determined without the use of IR polarization techniques. The protocol involves the use of anionic probe molecules to uncover the underlying C_{16}TAB structure. The probes used in this study are the anionic surfactant sodium dodecyl sulfate (SDS) and the anionic polyelectrolyte sodium polyacrylate (NaPA). This chapter is concerned with the structure of the adsorbed C_{16}TAB at the point where hydrophobic interactions between adsorbed surfactant ions begin to cause surface aggregation, namely the hemimicelle concentration (HMC).

4.3. Experimental Details

4.3.1. TiO_2 Substrate Preparation

Due to the desire to monitor the adsorption of surfactants and polyelectrolytes onto the TiO_2 surface, an alternative means of anchoring the titania to the surface of a ZnSe internal reflection element was needed. The use of a polyethylene binder, as outlined in Chapter 3, restricts the sensitivity of monitoring the adsorption of molecules with long hydrocarbon portions (i.e. surfactants, polymers), since the polyethylene binder

contains the similar methylene backbone, and absorbs infrared radiation in the same region. Therefore a technique was needed in which a pure titania surface could be deposited onto the ZnSe IRE, and also be indefinitely stable in an aqueous environment. Two different routes were taken; the first involves the controlled hydrolysis and condensation of a titanium alkoxide (sol-gel technique), while the second involves the direct deposition of colloidal TiO_2 particles.

4.3.1.1. Sol-Gel Preparation of TiO_2 Substrate

The sol-gel technique involves the polymerization of organometallic compounds such as alkoxides to produce a gel with a continuous network. The basic principle is to form a solution of the elements of the desired compound in an organic solvent, polymerize the solution to form a gel, and dry and fire this gel to displace the organic components and form a final inorganic oxide. These reactions are generally rapid and exothermic and can lead to premature gellation, which tends to produce an opaque film that is prone to shrinking and cracking upon drying. This can be overcome by adding a chelating organic ligand into the solution to control the hydrolysis rate.

The preparation of TiO_2 gels were obtained through hydrolysis and polycondensation of $Ti(OBu)_4$ in an n-butanol–acetic acid–water solution [79]. The n-butanol acts as the solvent while the acid is used as a ligand to control the rate of hydrolysis. The hydrolysis and polycondensation of the titanium(IV) butoxide can be represented by the following set of reactions.

Hydrolysis:

(4.1) $M(OR)_n + H_2O \rightarrow M(OR)_{n-1}(OH) + ROH$

Condensation:

(4.2) $M(OR)_{n-1}(OH) + M(OR)_{n-1}(OH) \rightarrow M_2O(OR)_{2n-2} + H2O$

The procedure involves first adding glacial acetic acid to the pure $Ti(OBu)_4$. An exothermic reaction indicates substitution of OBu groups by bidentate CH_3COO groups, and the formation of a new soluble species $Ti(OBu)_x(Ac)_y$. After acidification hydrolysis is performed by adding a water-butanol solution under vigorous stirring. Gellation occurs after a certain period of time, which strongly depends on the respective concentrations of titanium, acetic acid, and water. Evidence in the literature suggests that transparent monolithic gels are obtained with the following experimental conditions: $[Ti] \approx 0.8$ mol/l, $[CH_3COOH]/[Ti] \approx 1.5$, and $[H_2O]/[Ti] \approx 4$. Therefore this is the experimental recipe that was followed during this work. With these conditions it was found that a continuous gel, that spanned the entire reaction volume, was formed after 30 minutes.

In order to ascertain the structure of the final product an infrared analysis of the powder obtained from the reaction was performed. The powder was dispersed in a KBr matrix and compressed into a self-supporting disc for analysis. The infrared spectrum of this powder is shown in Figure 4.2. The band assignments have been reported in the literature [79], and will be briefly discussed. The two bands at 1555 and 1450 cm^{-1} are an indication of chelating acetate groups, while the small band at 1718 cm^{-1} is attributed to free acetic acid. The three bands at 1125, 1095, and 1029 cm^{-1} are due to OR groups

linked to titanium. The three bands in the 2800 – 3000 cm^{-1} region are due to various C–H modes. The broad absorption band in the low frequency region should be caused by the formation of a Ti–O–Ti network. This result clearly shows the presence of the chelating acetate groups, which remain in the gel network even after drying.

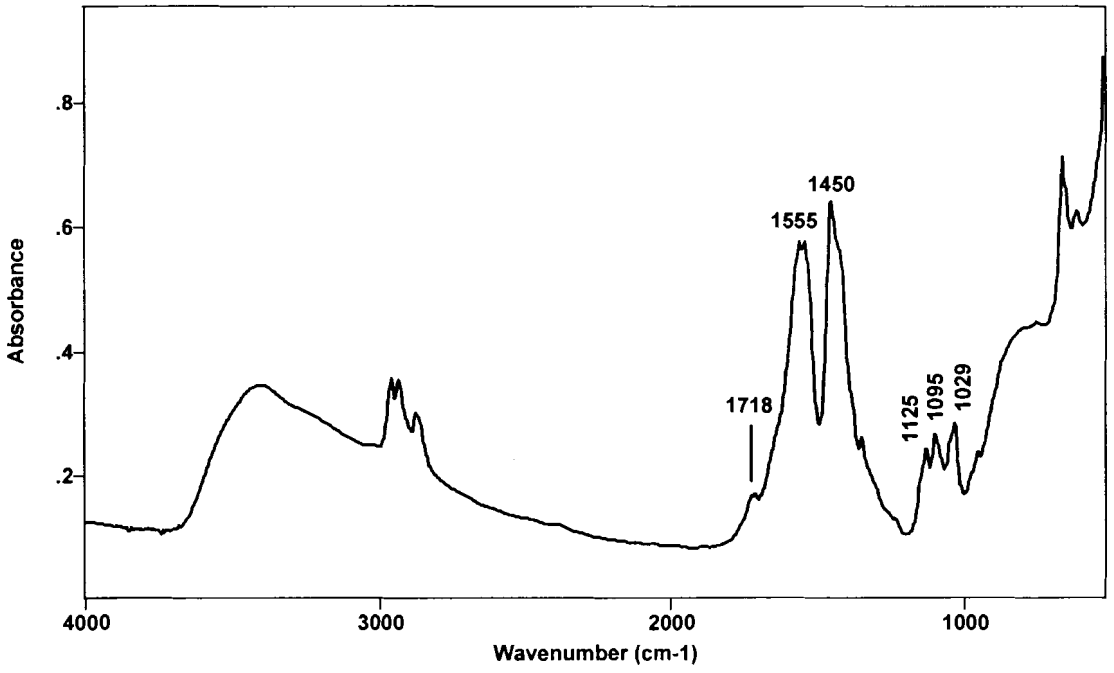

Figure 4.2. IR spectrum of sol-gel product after room temperature drying.

In order to remove these groups, and to form a pure titania product, the gel must be calcined at elevated temperatures. A thermal analysis of the gel product was performed, and it was found that a temperature of 450° C was needed to completely remove the organic components, and subsequently form a crystalline TiO_2 product. The Raman spectrum of the final product is shown in Figure 4.3, and clearly shows the presence of TiO_2 in its anatase crystalline form. However, in order to form a titania layer

on the surface of a ZnSe IRE, the reaction mixture must be allowed to gel on the surface of the IRE. This also necessitates the firing of the gel at a temperature of 450° C while on the ZnSe substrate. The useful temperature of ZnSe in air is 300° C [19]. Above this temperature it has been found that ZnSe will sublime. It has also been found difficult to dry and age the titania gels so that they form a continuous inorganic film on the substrate. Figure 4.4 illustrates a dried TiO_2 layer which has been deposited onto the surface of a ZnSe IRE. Drying of the film can be seen to cause shrinkage and the associated cracking of the film.

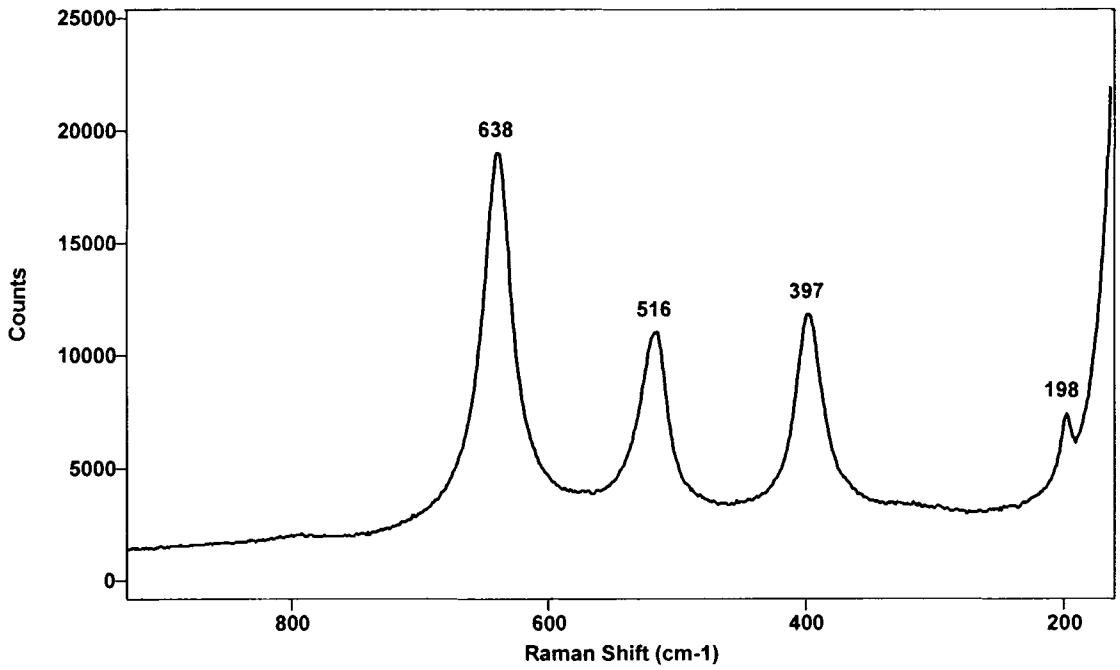

Figure 4.3. Raman spectrum of TiO_2 sol-gel after firing at 450° C.

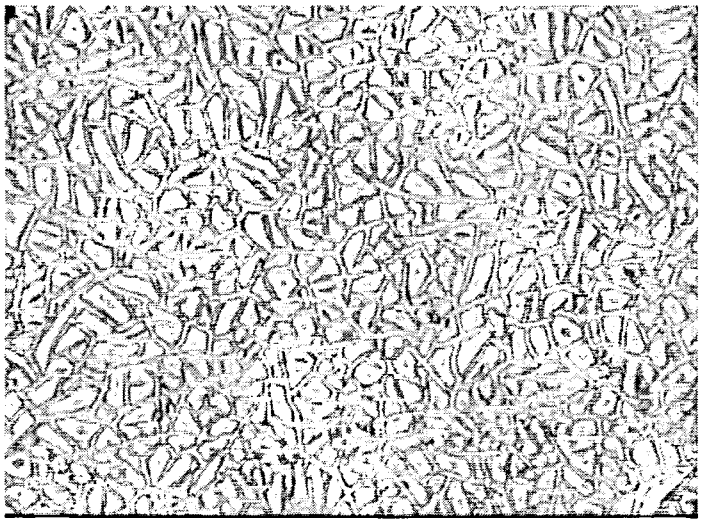

Figure 4.4. TiO_2 sol-gel film deposited onto a ZnSe IRE after firing.

Although there are infrared transmitting materials that can withstand the high temperature needed to form the TiO_2 layer (i.e. silicon, germanium), they do not possess the wide spectral window of ZnSe. In lieu of the fact that crystalline TiO_2 films can be prepared by this sol-gel technique, it was deemed unsatisfactory to compromise the wider spectral advantages of ZnSe for a more temperature stable material. Therefore the colloidal deposition route to the formation of TiO_2 films was undertaken.

4.3.1.2. Preparation of TiO_2 Films by Colloidal Deposition

The colloidal deposition method involves the dispersion of colloidal particles in a liquid to form a sol, and then the destabilization of the sol to produce a gel. This technique has been successfully used to prepare stable titania layers on the surface of internal reflection elements through the hydrolysis of titanium(IV) chloride [80-83]. The procedure involves hydrolysis of titanium(IV) chloride at 0° C, followed by dialysis to a pH of 2.6. The titania gel layers are formed by overnight room-temperature evaporation of 100 μl of the sol on the horizontal surface of a ZnSe internal reflection element (IRE). A much simpler procedure has been demonstrated in the literature for the preparation of water-stable TiO_2 gel layers. By starting with a commercially available fumed titania (Degussa, P25), stable gel layers were formed, on the surface of ZnSe, through deposition of a suspension of the particles in water [41]. This last procedure is the synthesis route undertaken in this work.

The fumed titanium dioxide (P25) powder was obtained from Degussa, and is 85% anatase and 15% rutile. The manufacturer's product information states a specific surface area of 50 m^2/g and an isoelectric point (IEP) at pH 6.5, which agrees well with an IEP at pH 6.6 as determined by electrophoretic mobility measurements. The TiO_2 was used without further purification.

The ZnSe internal reflection element (IRE) was obtained from Harrick, and has dimensions of 50x10x2 mm, with 45° beveled faces. The procedure for depositing the TiO_2 layer onto the IRE for the subsequent adsorption studies was as follows. A dispersion of P25 in methanol was first made with 30 mg of the oxide in 25 ml of the alcohol. The dispersion was sonicated for 30 minutes to minimize agglomeration. A 200

μl aliquot of the dispersion was then deposited onto one side of the IRE, and the alcohol allowed to evaporate at room temperature. The uniformity and thickness of the applied TiO_2 film was evaluated using an atomic force microscope (AFM). The AFM results reveal a film thickness of approximately 500 nm, with a surface roughness of about 80 Å. The surface of the TiO_2 film is shown in the electron micrograph of Figure 4.5. A relatively uniform surface is seen, with the presence of some drying induced surface cracks.

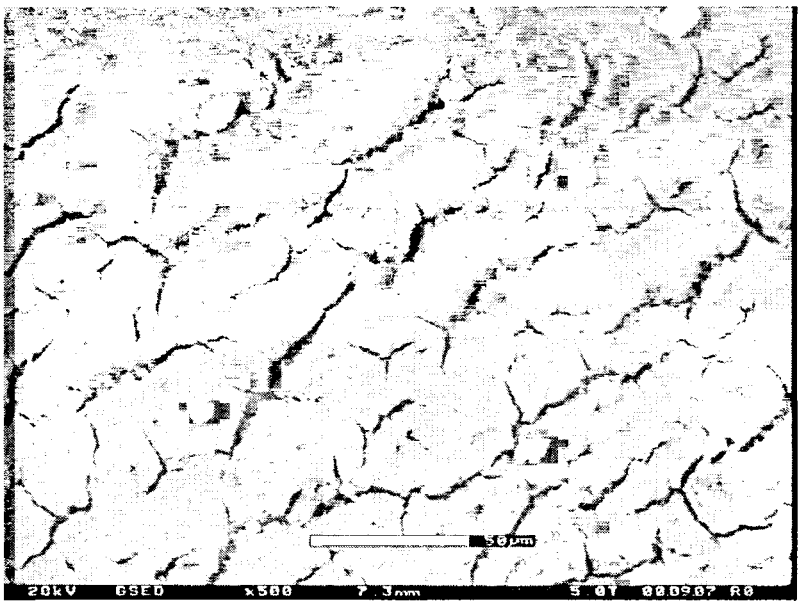

Figure 4.5. Electron micrograph of the deposited P25 titania layer.

Methanol was chosen as the deposition solvent, in place of water, because it wets the ZnSe surface completely, resulting in a thin uniform TiO_2 film that is stable when in contact with a flowing stream of water. The effect of using methanol as a deposition medium, with regards to the surface properties of TiO_2, was checked by both IR and

electokinetic measurements. After deposition from methanol, and the removal of methanol by evaporation, the oxide particles were measured for their electrophoretic mobility. It was found that the methanol treatment does not alter the surface charging, when compared to the oxide particles which were not contacted by methanol. The TiO_2 particles were also analyzed via IR, and showed no evidence of methoxy modes on the surface. Therefore it is concluded that the deposition process from methanol does not alter the surface chemistry of the oxide particles.

4.3.2. Adsorbates

The cationic surfactants alkyltrimethylammonium bromide (C_nTAB), with n = 12,14 and 16, anionic surfactant sodium dodecyl sulfate (SDS), and anionic polyelectrolyte sodium polyacrylate (NaPA) were all obtained from Aldrich. The NaPA has a weight average molecular weight of 1200, and was used as received. Surface tension measurements were used to determine the purity, and also to verify the critical micelle concentration (CMC) of the various surfactants. The Du Nouy ring method was employed, using a Sigma 70 surface tension analyzer from KSV Instruments. An empirical relationship exists for the alkyltrimethylammonium bromide surfactants which allows a rough determination of the CMC [84]. This is represented by the following equation.

$$\log C_{CMC} = A - BN \tag{4.3}$$

In this relationship A is a constant for a particular ionic headgroup at a given temperature, B is another constant, and N is equal to the number of carbon atoms in the hydrophobic chain. At a temperature of 25° C the two constants have been evaluated and found to be, $A = 1.7$ and $B = 0.30$ for alkyltrimethylammonium bromide surfactants [85].

The surface tension vs. log concentration plot for the C_nTAB surfactants is shown in Figure 4.6. There is no indication of surface – active impurities, and each surfactant yields a CMC consistent with the empirical values (shown as the dashed lines). Even though no impurities were found in the cationic surfactants, they were nevertheless purified by doubly recrystallizing from an acetone/ethanol mixture [86].

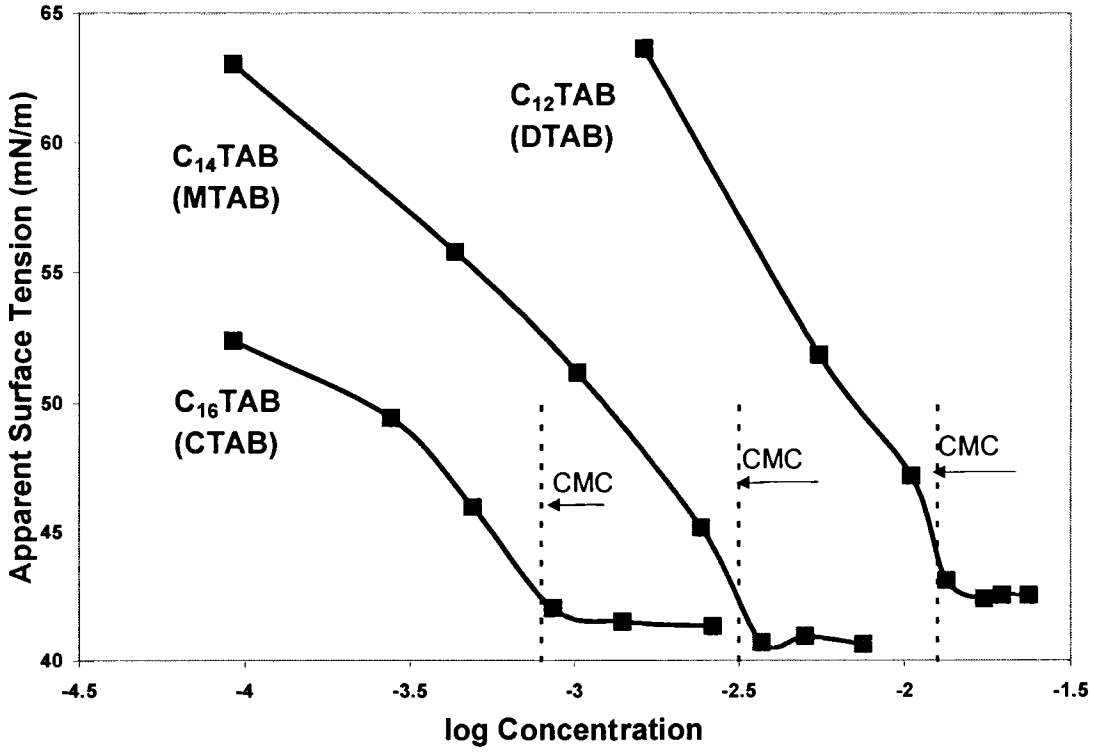

Figure 4.6. Surface tension plots of the alkyltrimethylammonium bromide surfactants.

The surface tension plot for SDS however exhibited a pre-CMC minimum. This minimum is known to be due to the presence of dodecanol as an impurity [87,88]. Therefore the SDS was purified by repeated recrystallization from ethanol according to the following procedure. Warm ethanol is added to the SDS until all of the surfactant dissolves. At this point the solution is allowed to cool very slowly to room temperature. The precipitate which is formed is then filtered off under vacuum and rinsed with copious amounts of ethanol. When the SDS has dried the entire procedure is repeated. The removal of the dodecanol impurity is confirmed by the marked improvement in the surface tension plot, Figure 4.7, which shows no evidence of the pre – CMC minimum after two recrystallization cycles.

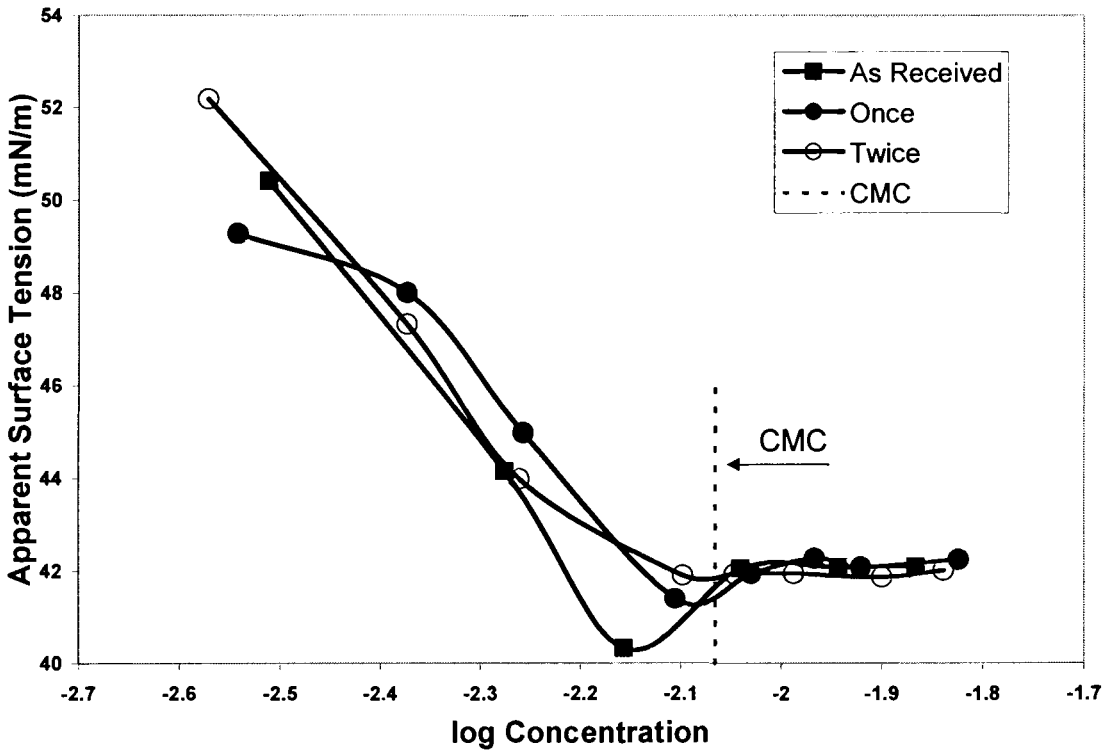

Figure 4.7. Surface tension plot of the anionic surfactant SDS as received, recrystallized once, and recrystallized twice from ethanol.

4.3.3. Experimental Procedure

Electrophoretic mobility was measured on a Malvern Zetasizer 3000. A TiO_2 stock solution containing 50 mg of the oxide in 100 ml of water was used as the starting dispersion. A 250 µl aliquot of the stock solution was then diluted to a total volume of 100 ml with the corresponding surfactant solutions at varying surfactant concentrations. The pH was adjusted with NaOH. The ATR adsorption experiments were carried out using a standard ATR liquid flow cell arrangement from Harrick (see Chapter 3 for details). A peristaltic pump was used to flow the aqueous solutions through the cell and across the TiO_2 film surface. All IR spectra were recorded on a Bomem MB-Series FTIR, equipped with a liquid N_2 cooled MCT detector. Typically 100 scans were co-added at a resolution of 4 cm^{-1}, except for the initial adsorption stage where only 10 scans were used.

4.3.4. Experimental Adsorption Calibration

An experimental calibration was performed in order to quantify the amount of adsorbed surfactant (molecules/nm^2) at the TiO_2 – aqueous solution interface. The molar absorptivity of each of the adsorbing species, along with the TiO_2, was determined by dispersing known quantities in a KBr pellet, and recording transmission spectra. Next a series of ATR adsorption experiments were performed in which the amount of adsorbed surfactant per unit area of TiO_2 was varied. This was accomplished by either modifying the amount of deposited TiO_2, or by changing the solution conditions (pH, adsorption time, ionic strength, etc.). Once the *in situ* ATR spectrum of the adsorbing species was obtained, the solution was immediately purged from the flow cell and the TiO_2 film (with

adsorbed surfactant) was allowed to dry. The ZnSe IRE (with the TiO_2/surfactant film attached) was then mounted in a magnetic holder and a transmission spectrum of the system obtained. The amount of adsorbed surfactant per unit area of TiO_2 was then calculated by comparing the band intensities in the transmission spectrum of the ZnSe ATR crystal with the previously obtained molar absorptivity values using KBr pellets. The calibration plot based on the symmetric CH_2 vibrational mode of $C_{16}TAB$ is shown in Figure 4.8. Once calibrated this method allows us to quantitatively determine the surface density of the adsorbed surfactants directly from the *in situ* ATR spectra.

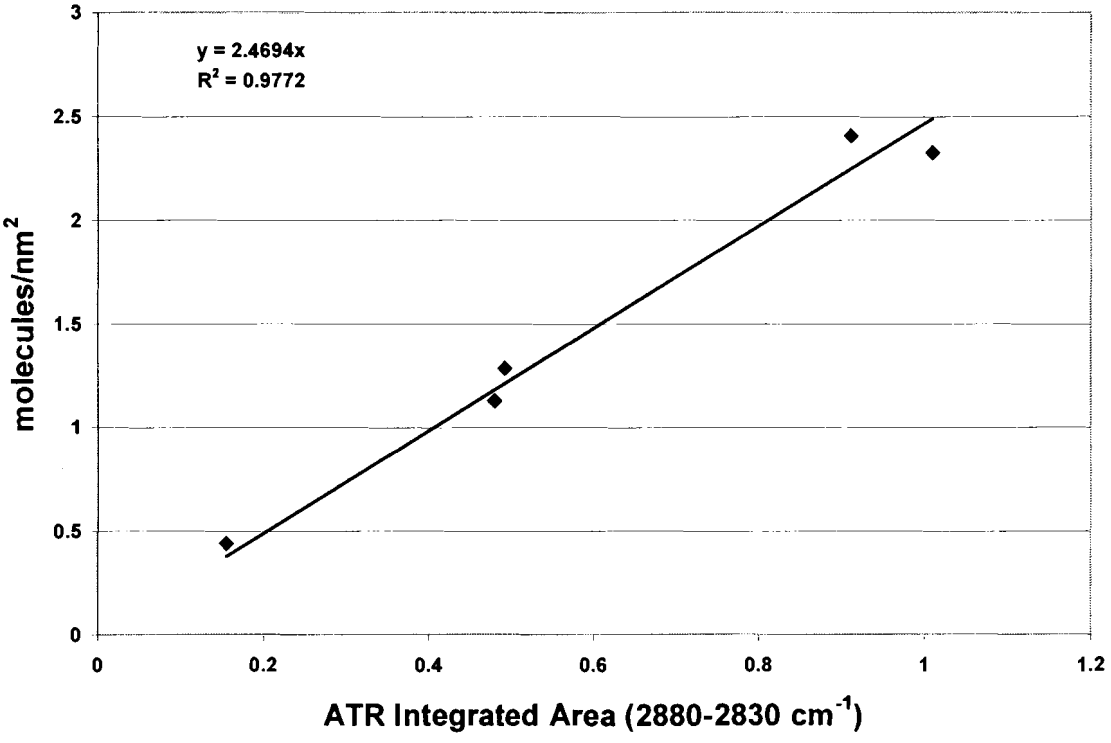

Figure 4.8. Calibration plot for the determination of surface excess of adsorbed surfactants based on the *in situ* ATR adsorption spectra.

4.4. Experimental Results

4.4.1. *In Situ* Adsorption Measurements

The primary advantage of using *in situ* ATR spectroscopy for the measurement of adsorption phenomena is that the analysis can be carried out in the presence of the solution phase. This means that there is no requirement to separate the solid adsorbent from the solution (i.e. centrifugation) in order to measure the amount of adsorbed species on the surface (surface excess). The sensitivity and selectivity of IR spectroscopy allows the determination of multi-component adsorption to be studied based on the differences in the molecular structure of the various components in the solution phase. Also, for self-assembling systems such as surfactants, monitoring the shifts in frequency of the IR bands due to the hydrocarbon tails allows a qualitative determination of the degree of "ordering" in the system. In this chapter the interest is in determining the structure of the cationic surfactant cetyltrimethylammonium bromide (C_{16}TAB), at a solution concentration corresponding to the onset of hydrophobic association, occurring on the TiO_2 surface, and how the structure of this adsorbed surfactant dictates the subsequent interactions with anionic species in solution. The anionic species studied include the anionic surfactant sodium dodecyl sulfate (SDS) and the anionic polyelectrolyte sodium polyacrylate (NaPA).

The differences in the molecular structure of these various species lead to characteristic bands (Figure 4.9) that can be used to distinguish between the various adsorbed species on TiO_2. Spectrum A of Figure 4.9 shows two strong bands appearing at 2924 cm^{-1} and 2853 cm^{-1} which correspond to the asymmetric and symmetric stretching frequencies of the CH_2 modes of the C_{16}TAB (C16) and SDS (C12) surfactant

hydrocarbon tails. The CH_2 stretching modes are generally the most intense features observed, and are therefore frequently used in ATR spectroscopy because of the low surface area of internal reflection elements. The widths and frequencies of these vibrational modes are sensitive to the *gauche/trans* conformer ratio of the surfactant tails. A shift from higher frequencies to lower frequencies, accompanied also by a decrease in the band width, is an indication of a transition from a "disordered" system (*gauche* conformers) to a more highly "ordered" system (*trans* conformation) [89]. The use of a high surface area, deposited TiO_2 particulate film allows also the detection of the weaker head-group absorption bands of the surfactants. The total amount of adsorbed surfactant, whether C_{16}TAB or SDS, can be determined by monitoring the changes in the intensity of the CH_2 modes. However, in order to distinguish between the amount of adsorbed C_{16}TAB and adsorbed SDS, we use the bands due to the polar head-groups of the two surfactants. The head-group of C_{16}TAB consists of a trimethylammonium group, and this structure gives rise to the distinctive IR spectrum shown in spectrum B of Figure 4.9. The band at 1467 cm^{-1} (CH_2 scissor mode) is common to both C_{16}TAB and SDS, while the two bands at 1479 cm^{-1} and 1490 cm^{-1} are assigned to the vibrational mode of the CH_3–N^+ group [90], and are therefore unique to C_{16}TAB. The head-group of SDS consists of a sulfate group and gives rise to the bands shown in spectrum C of Figure 4.9. The lower frequency band at 1058 cm^{-1} is assigned to the asymmetric stretch of the S–O group, while the symmetric stretch gives a doublet with bands appearing at 1206 cm^{-1} and 1238 cm^{-1} [90]. The characteristic infrared bands of the polyelectrolyte (NaPA) are illustrated in spectrum D of Figure 4.9. With ionization of the salt of a carboxylic acid, resonance structures are possible between the two C–O bands. The result is that the

characteristic carbonyl absorption band ($\approx$ 1720 cm^{-1}) vanishes and is replaced by two bands of lower frequency. The bands at 1552 cm^{-1} and 1405 cm^{-1} in spectrum D correspond to the asymmetric and symmetric stretch of the C–O group respectively [50].

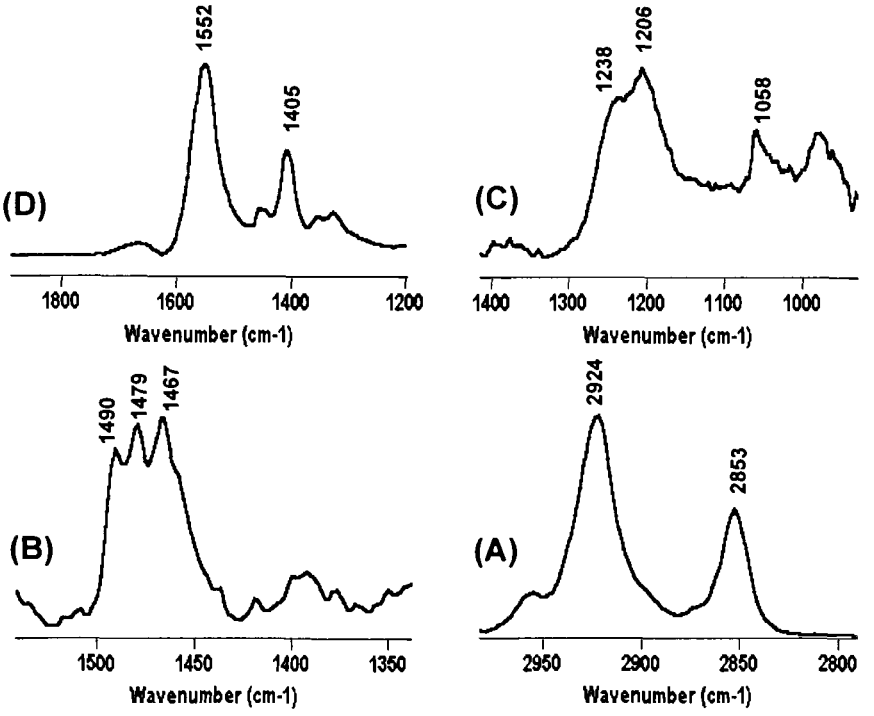

Figure 4.9. Characteristic mid-IR spectral regions used to identify adsorbed species. (A) C–H stretching region of C_{16}TAB or SDS methylene tails. (B) C_{16}TAB head-group region. (C) SDS head-group region. (D) C–O stretching region of NaPA.

4.4.2. $C_{16}TAB$ Adsorption onto TiO_2

The adsorption of ionic surfactants onto the charged surfaces of metal oxides is pH dependent. The isoelectric point (IEP) of the P25 particles was measured at pH 6.6, and this corresponds well with values of the IEP reported in the literature for the anatase form of TiO_2 [91]. Therefore, adsorption of the cationic surfactant $C_{16}TAB$ onto the surface of TiO_2 should occur readily at pH values greater than that of the IEP, where the titania surface has an overall net negative surface charge. It was observed that no $C_{16}TAB$ adsorption occurred at pH values below 6.6, while the adsorption density of $C_{16}TAB$ increased as the pH was raised above the IEP. Since in this chapter we are primarily concerned with the influence of the adsorbed cationic surfactant structure at low bulk concentrations, and not with the influence of the solution environment (pH, ionic strength, etc.), all experiments were carried out at pH 10.3. At this pH the overall surface charge of the TiO_2 is negative, and increases the amount of adsorbed $C_{16}TAB$.

In Figure 4.10 the equilibrium zeta potential values are plotted as a function of the bulk $C_{16}TAB$ concentration for TiO_2 at pH 10.3. The result is the typical S-shaped adsorption isotherm for the adsorption of an ionic surfactant onto a charged surface of opposite sign [57]. In region I the adsorption occurs primarily by ion-exchange, showing little or no dependence on the logarithmic $C_{16}TAB$ concentration. At a bulk surfactant concentration of around 0.01 mM there is a dramatic increase in the amount of adsorbed surfactant. This corresponds to the onset of region II, where it is generally accepted that the marked increase in adsorption is a result of interactions between the hydrophobic chains of the surfactant. This same $C_{16}TAB$ concentration has been found to correspond to the onset of hydrophobic interactions when adsorbed to the surface of rutile at pH 10.5

[68]. In region II the adsorption of the cationic surfactant first causes a neutralization of the TiO_2 surface charge, then at higher concentrations the sign of the surface charge is reversed. By the end of region II the solid surface has acquired a charge of the same sign as the adsorbing surfactant. Region III occurs in the vicinity of the CMC of the surfactant. Adsorption is dramatically reduced since the adsorbing surfactant ions must overcome a strong electrostatic repulsion between the positively charged ions and the now positively charged solid surface.

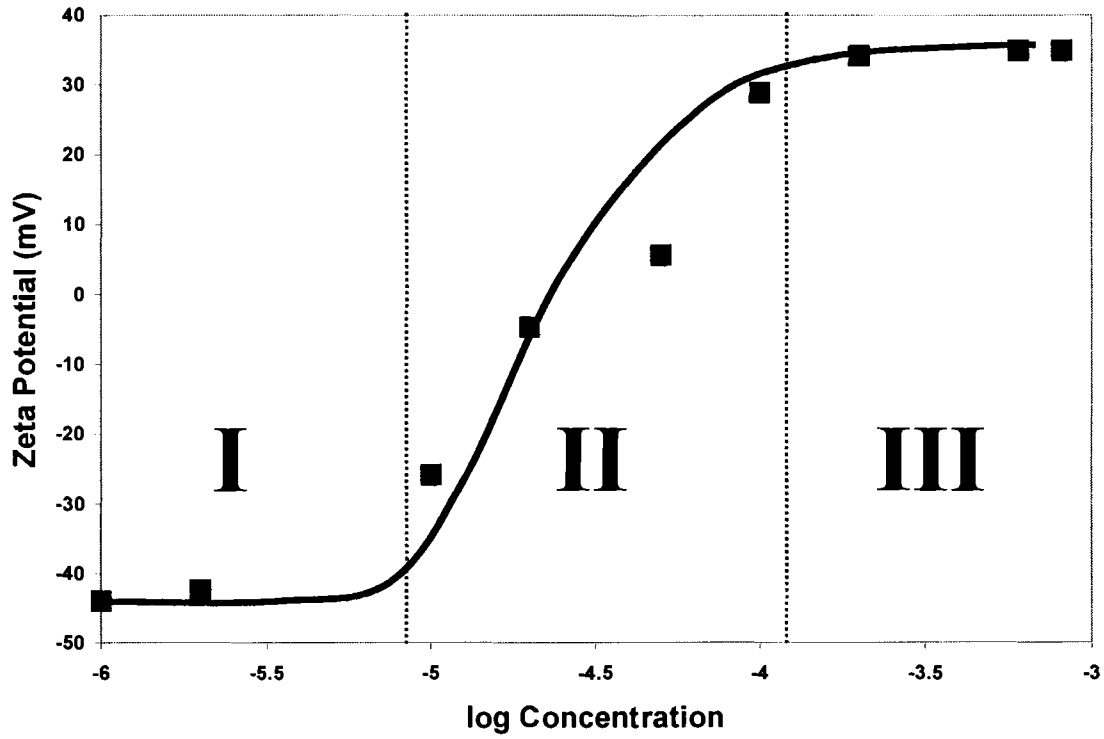

Figure 4.10. Zeta potential vs. concentration profile for $C_{16}TAB$ adsorbed to TiO_2 particles at pH 10.3.

In the remaining discussion we will be concerned with the structure of the adsorbed surfactant at the onset of region II (indicated by the dashed vertical line, C_{CTAB} = 0.01 mM), where hydrophobic association of the surfactant tails begin to play a role in the adsorption process, and surface aggregates begin to form.

The dynamics of $C_{16}TAB$ adsorbing to the surface of a TiO_2 colloidal film, from a bulk solution concentration of 0.01 mM and pH 10.3, is shown in Figure 4.11. The amount of adsorbed $C_{16}TAB$ on the surface is followed by monitoring the change in intensity of a characteristic IR band due to the surfactant. In the case of a one-component system ($C_{16}TAB$ only), the IR band at 2853 cm^{-1} (symmetric stretch of the CH_2 mode) is used to follow the adsorption process. It should be mentioned that by working at such dilute concentrations the spectral contributions due to excess adsorbate in solution are negligible in comparison to the spectral features due to adsorbed species. In other words, in the absence of any specific adsorption at the solid-solution interface, the contribution of the $C_{16}TAB$ in the bulk is less than 1% of that due to adsorbed $C_{16}TAB$. It can be seen from Figure 4.11 that there is an initial, rapid adsorption of the surfactant in the first 10 minutes, followed by a gradual decrease in the slope that plateaus after about 60 minutes contact. Although we only show the results up to a total contact time of 2 hours, results after 48 hours show only a slight increase ($\approx$ 5%) in the amount of adsorbed surfactant. The slight increase is presumably due to a slow rearrangement of the adsorbed surfactant tails, which then allows more surfactant ions to adsorb to the surface. Referring again to the adsorption isotherm in Figure 4.10, it can be seen that at a $C_{16}TAB$ concentration of 0.01 mM the overall surface charge is still negative. Therefore the adsorption density (0.4 molecules/nm^2) at this low concentration corresponds to much less than a full

monolayer, and is in agreement with the results of C_{16}TAB adsorbed to the surface of rutile [68].

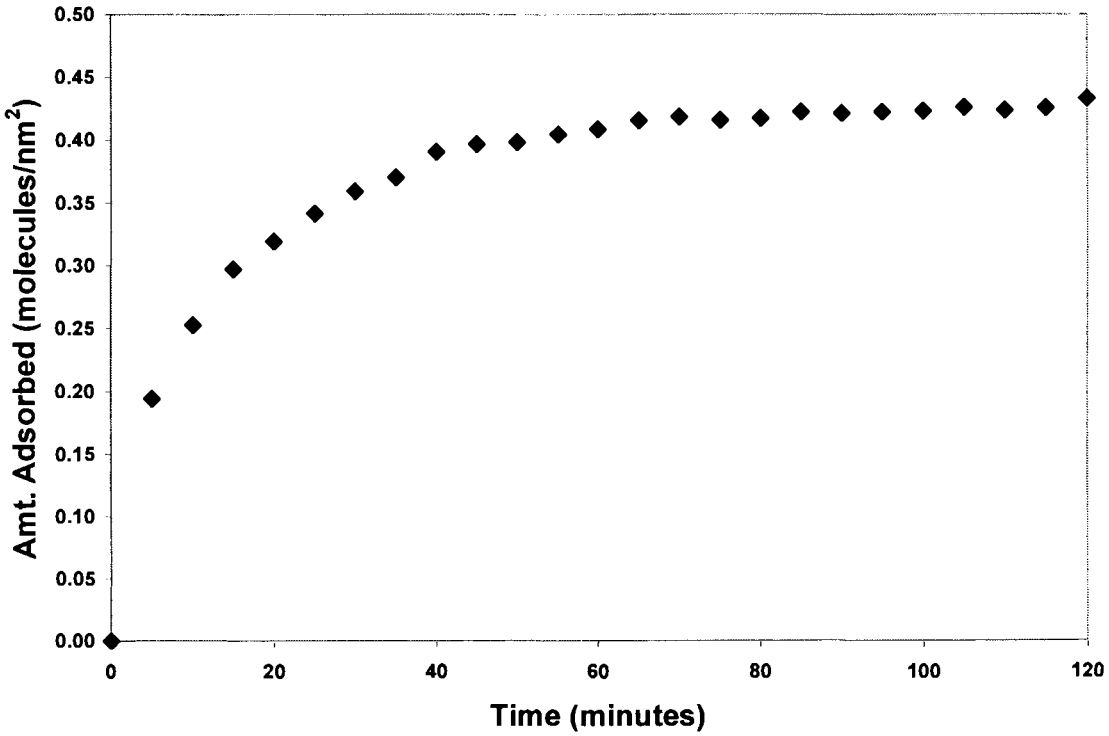

Figure 4.11. Dynamics of C_{16}TAB adsorbing to TiO_2 surface. [C_{16}TAB] = 0.01 mM, pH = 10.3.

4.4.3. Interaction of the Pre-Adsorbed $C_{16}TAB$ Layer with the Anionic Surfactant SDS

Mixed surfactant systems containing both cationic and anionic species have a limited composition dependent region in which to investigate. The ion-pairing ability and the subsequent precipitation of the complex dictate this region [90]. *In situ* ATR measurements using a liquid flow cell, however allow us to investigate the adsorption phenomena of these mixed surfactant systems at an interface by using a sequential addition procedure. Each surfactant solution, at the same pH, is allowed to interact with the solid surface in the absence of the other surfactant in solution. A small spacer volume, equal to the interior volume of the flow cell, of water at the same pH is introduced between the different surfactant solutions in order to minimize any mixing and ion-pairing. A controlled desorption experiment was performed to confirm that no $C_{16}TAB$ is removed from the surface during the short time period (< 5 sec.) in which the spacer volume is introduced to the cell.

The results of this sequential addition procedure for the $C_{16}TAB$/SDS system are illustrated in Figure 4.12. Again, a 0.01 mM $C_{16}TAB$ solution (pH 10.3) is allowed to adsorb at the TiO_2-solution interface for two hours, then a 0.05 mM SDS solution (pH 10.3) is introduced and allowed to interact with the pre-adsorbed $C_{16}TAB$ layer for two hours. The filled symbols in Figure 4.12 represent the amount of adsorbed surfactant as calculated from the integrated intensity of the CH_2 symmetric vibrational mode. Experimental evidence has shown that the anionic surfactant SDS does not adsorb to the surface of TiO_2 at pH 10.3, due to the large repulsive, electrostatic barrier between the negatively charged surfactant and the negatively charged TiO_2. However, in the presence

of pre-adsorbed $C_{16}TAB$ there is an immediate and rapid adsorption of the SDS. By monitoring the vibrational modes of the $C_{16}TAB$ head-group we can also determine that the amount of adsorbed $C_{16}TAB$ does not change upon addition of the SDS.

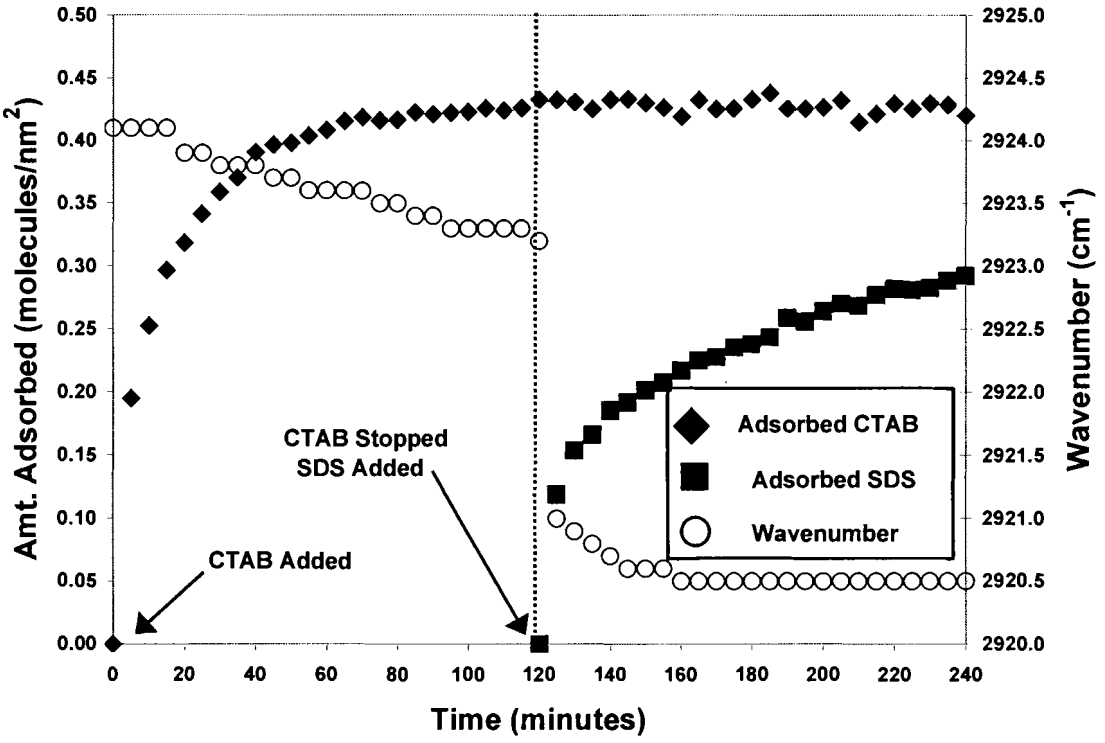

Figure 4.12. Adsorption dynamics for the sequential addition of $C_{16}TAB$ followed by SDS. [$C_{16}TAB$] = 0.01 mM, [SDS] = 0.05 mM, pH = 10.3.

Upon addition of the SDS to the pre-adsorbed $C_{16}TAB$ there is also an immediate shift of the CH_2 modes towards lower frequency. The frequency of the asymmetric CH_2 stretching mode is depicted by the open symbols in Figure 4.12, and the corresponding scale is shown on the right side of the plot. The frequency and width of the CH_2 stretching modes are sensitive to the state of order, or packing, of the hydrocarbon tails of the surfactants. It can be seen that the initial adsorption of $C_{16}TAB$ to the bare titania

surface results in a slight shift (≈ 0.5 cm^{-1}) of the methylene stretching mode. This corresponds well with previous work on the adsorption of $C_{16}TAB$ to the silica surface, which showed an increase in the ordering of the surfactant tails as a function of adsorption time [38]. At this point it should be noted that both $C_{16}TAB$ and SDS have a natural vibrational frequency of 2924 cm^{-1} when in the solution phase at concentrations below their respective CMC's, or when initially adsorbed to a bare TiO_2 surface (SDS adsorbed to a TiO_2 surface at pH 3.5). Therefore the large shift in frequency, about 4 cm^{-1}, indicates that some type of ordered structure of both $C_{16}TAB$ and SDS is instantaneously being formed at the surface. Support of an ordered structure comes from IR spectra of LB films of octadecyldimethylamine oxide ($C_{18}DAO$) on gold-evaporated slides, where a downward shift of 5 – 7 cm^{-1} of the CH_2 stretching modes was obtained upon the accumulation of the second layer [92]. This observation indicating that the hydrocarbon chains are becoming more ordered and perpendicular to the substrate surface as a bilayer structure is being formed.

For the $C_{16}TAB$/SDS mixed surfactant system, however, we must consider what the initial adsorbed $C_{16}TAB$ structure on the surface is, which would lead to such a response upon the addition of the anionic surfactant SDS. Since SDS has been shown not to adsorb to TiO_2 surface sites at pH 10.3, and we observe a very rapid adsorption of SDS to the pre-adsorbed $C_{16}TAB$ layer, there must be isolated areas of positive charge for which the negatively charged SDS ions can interact. Therefore the experimental evidence suggests that the $C_{16}TAB$ initially adsorbs to the surface of TiO_2 as isolated islands with a "defective" bilayer structure, as illustrated in drawing A of Figure 4.13. This structure would agree with the electrokinetic measurements that indicate that at a

C_{16}TAB concentration of 0.01 mM the overall surface charge is still negative. The positive C_{16}TAB head-groups extending into solution serve as anchors for the negative SDS head-groups. In addition to the favorable electrostatic interactions between the oppositely charged head-groups, there is a favorable hydrophobically driven interaction that would allow the hydrocarbon tails of the SDS molecules to escape the aqueous environment and intercalate with the pre-adsorbed C_{16}TAB tails. These favorable interactions would lead to a highly packed surfactant system on the surface (drawing B of Figure 4.13), consistent with the large downward shift in frequency of the CH_2 stretching modes.

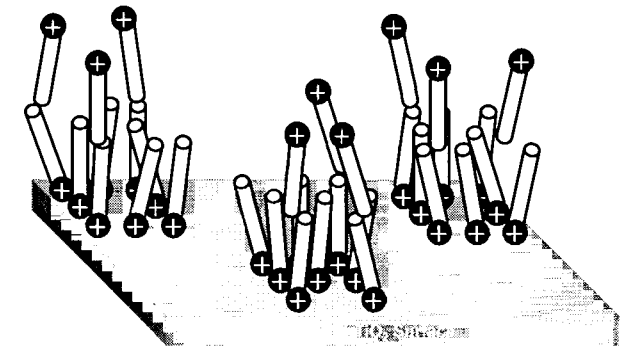

(A) "As Formed" C_{16}TAB Structure

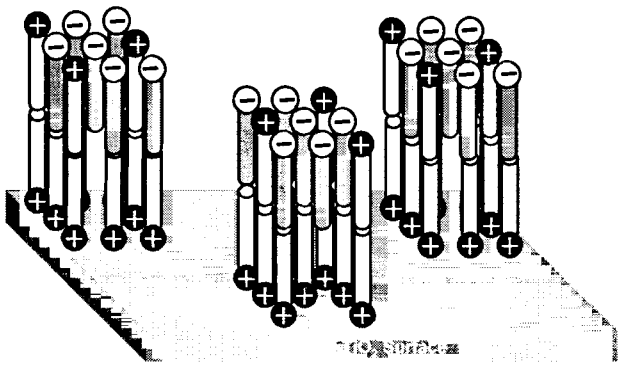

(B) After SDS Addition

Figure 4.13. Proposed surfactant structures at the TiO_2 – surfactant solution interface. (A) Before SDS addition. (B) After SDS addition.

4.4.4. Interaction of the Pre-Adsorbed C_{16}TAB Layer with the Anionic Polyelectrolyte Sodium Polyacrylate (NaPA)

The response of the pre-adsorbed C_{16}TAB layer to a 60 ppm NaPA solution is shown in Figure 4.14. The observed interaction of the anionic polyelectrolyte is completely opposite to that observed with the anionic surfactant. First, there is no adsorption of the NaPA, which is confirmed by the absence of an IR band in the

1550 cm^{-1} region of the spectrum ($-COO^-$ mode of the NaPA). Second, the amount of adsorbed $C_{16}TAB$ does not remain constant, but decreases with exposure time to the NaPA. The amount of $C_{16}TAB$ which is desorbed from the surface does not continually increase with exposure time, but plateaus off after approximately 25% removal. By monitoting the frequency of the CH_2 modes it can be seen that removal of a portion of the adsorbed $C_{16}TAB$ layer by the NaPA causes no change in the packing of the adsorbed surfactant, in contrast to the instantaneous ordering observed with SDS.

Considering the previous argument that was made concerning the "defective" bilayer structure of the adsorbed $C_{16}TAB$, these results would seem to suggest that the NaPA is interacting and complexing with the $C_{16}TAB$ molecules which comprise the bilayer portion of the surface aggregate. Unlike the anionic surfactant SDS, which has a long hydrophobic tail, the anionic polyelectrolyte has an affinity for the aqueous phase. The attractive electrostatic interaction between the polar $C_{16}TAB$ head-groups and the negatively charged polyelectrolyte can overcome the weaker hydrophobic forces holding the $C_{16}TAB$ bilayer to the surface, resulting in desorption of the $C_{16}TAB$ from the surface. This interaction scheme is depicted in Figure 4.15.

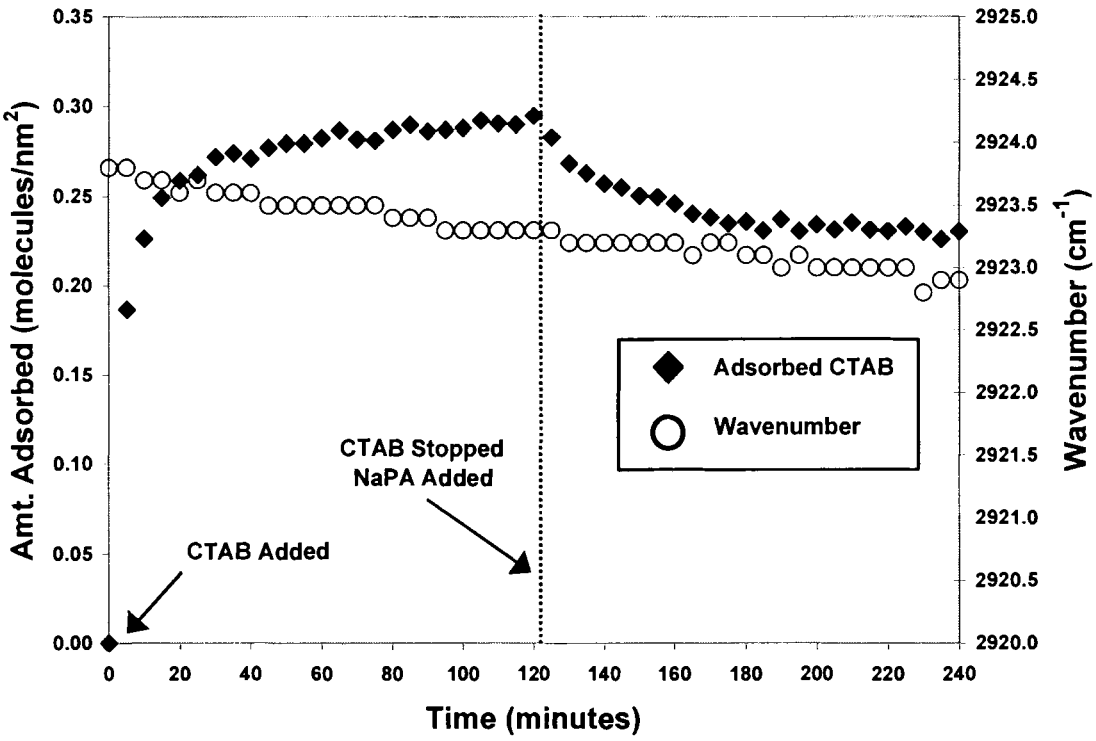

Figure 4.14. Adsorption dynamics for the sequential addition of C_{16}TAB followed by NaPA. [C_{16}TAB] = 0.01 mM, [NaPA] = 60 ppm, pH = 10.3.

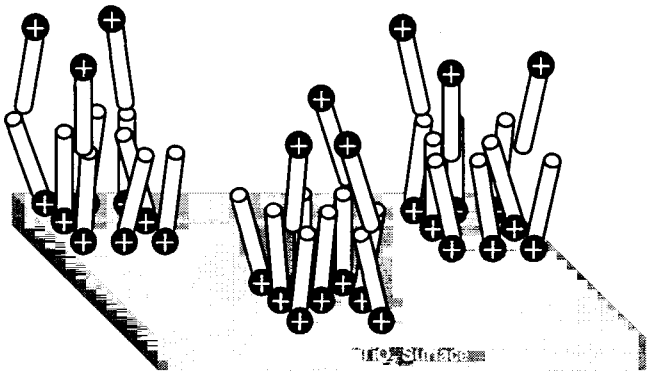

(A) "As Formed" C_{16}TAB Structure

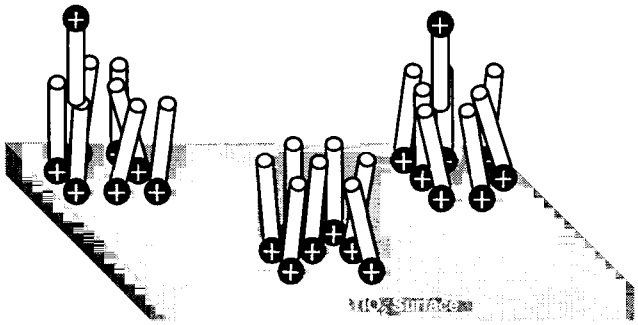

(B) After NaPA Addition

Figure 4.15. Proposed C_{16}TAB structures at the TiO_2 – surfactant solution interface. (A) Before NaPA addition. (B) After NaPA addition.

4.4.5. Sequential Addition of NaPA followed by SDS to a Pre-Adsorbed $C_{16}TAB$ Layer

At this point the qualitative picture that has been drawn assumes that the rapid adsorption of SDS, and the subsequent highly ordered structures that are formed on the surface, is due to interactions with the bilayer portion of the pre-adsorbed $C_{16}TAB$. Also, that this "defective" bilayer portion is what is being removed by the addition of the anionic polyelectrolyte sodium polyacrylate (NaPA). For this to be the case, then the addition of SDS to the remaining $C_{16}TAB$ on the TiO_2 surface (monolayer) should illicit a different response to that when the SDS is added to the "as formed" $C_{16}TAB$ layer (bilayer). The results of this experiment are illustrated in Figure 4.16. Again, the $C_{16}TAB$ (0.01 mM, pH 10.3) is allowed to adsorb to the TiO_2 surface for two hours. This is followed by exposure of the adsorbed $C_{16}TAB$ layer to a 60 ppm NaPA solution, also at pH 10.3, for two hours. Finally a 0.05 mM SDS solution (pH 10.3) is introduced and allowed to interact for another two hours.

The results clearly show that the adsorption of the SDS to the pre-adsorbed $C_{16}TAB$ layer has been severely diminished by the removal of the bilayer portion by the NaPA. There is a slight adsorption of the SDS, which quickly plateaus after only 10 minutes of contact time. This is to be compared to the result presented in Figure 4.12, where the SDS concentration at the surface is continually increasing even after two hours of contact. There is still an abrupt shift in the frequency of the CH_2 stretching mode, indicating that the entire bilayer portion of the pre-adsorbed $C_{16}TAB$ has not been completely removed. However, the degree of ordering is still less than that depicted in

Figure 4.12. The frequency of the asymmetric CH_2 mode is measured at 2919.7 cm^{-1} ($C_{16}TAB$ + SDS) as compared to 2921.3 cm^{-1} ($C_{16}TAB$ + NaPA + SDS).

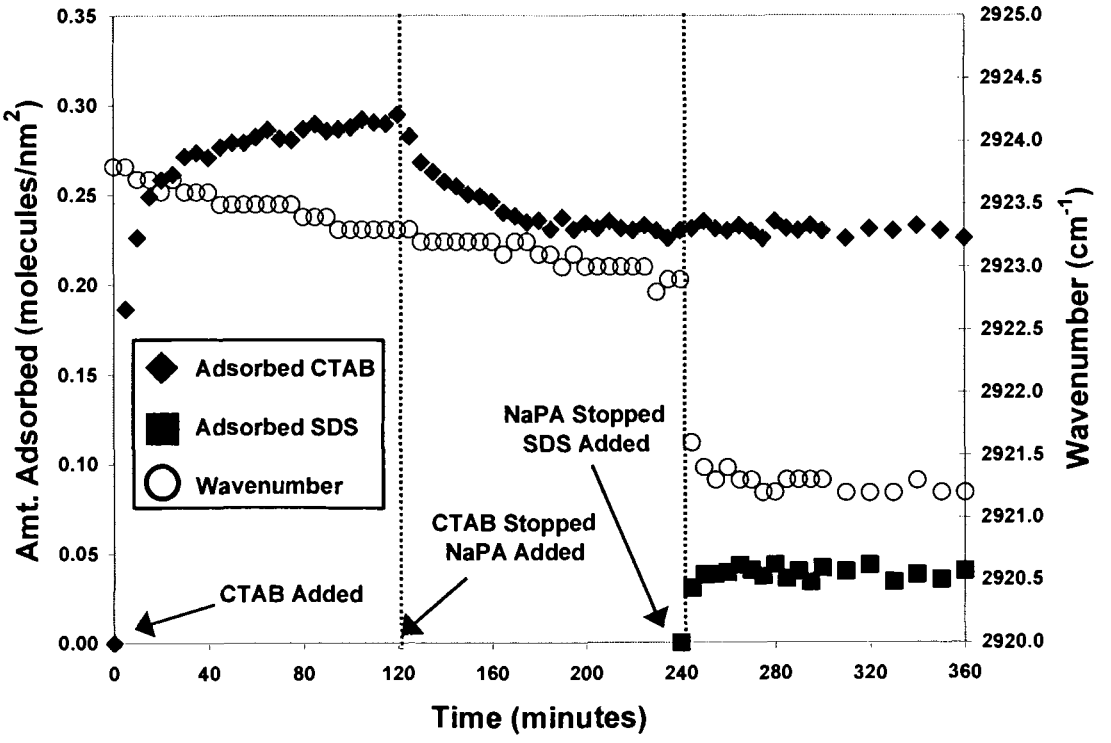

Figure 4.16. Adsorption dynamics for the sequential addition of $C_{16}TAB$ followed by NaPA, followed by SDS. [$C_{16}TAB$] = 0.01 mM, [NaPA] = 60 ppm, [SDS] = 0.05 mM, pH = 10.3.

The one variable that remains to be addressed is the initial surface coverage of $C_{16}TAB$ on the TiO_2 surface before the SDS solution is introduced. Comparing the results in Figure 4.12 ($C_{16}TAB$ then SDS) to those obtained in Figure 4.16 ($C_{16}TAB$ then NaPA then SDS), it can be seen that the amount of pre-adsorbed $C_{16}TAB$ in both cases is different. This could be a possible reason for the different SDS adsorption responses. In

order to address this situation another experiment was performed in which the $C_{16}TAB$ was allowed to adsorb at the TiO_2 surface for only 15 minutes. At this point the SDS solution was introduced and allowed to interact with the adsorbed $C_{16}TAB$. In doing this we ensure that the initial amount of adsorbed $C_{16}TAB$ on the surface is the same as that in Figure 4.16, after partial desorption by the NaPA. The response is shown in Figure 4.17. With the same amount of adsorbed $C_{16}TAB$ on the surface, the "as formed" $C_{16}TAB$ structure (bilayer) shows a dramatic ability to adsorb the SDS, and form highly ordered surface structures. While the $C_{16}TAB$ structure modified by the NaPA (monolayer) shows only a slight affinity for the SDS. These results seem to confirm our picture that the SDS interacts with the "defective" bilayer portion of the pre-adsorbed $C_{16}TAB$ layer. By removing this portion of the $C_{16}TAB$ layer, we effectively reduce the subsequent incorporation of SDS into the surfactant surface layer.

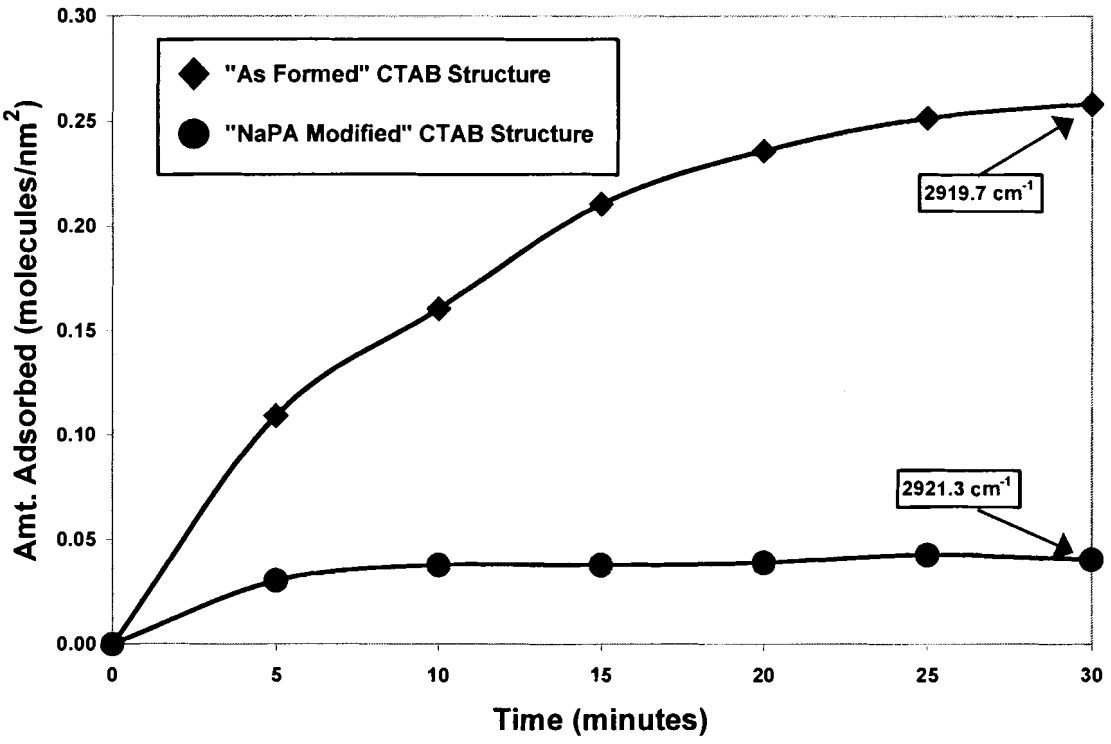

Figure 4.17. Comparison of SDS adsorption response to different pre-adsorbed $C_{16}TAB$ surface structures.

4.5. Summary

At low bulk concentrations (<< CMC) the cationic surfactant cetyltrimethylammonium bromide ($C_{16}TAB$) has been shown to adsorb to the surface of TiO_2 as isolated islands with a "defective" bilayer structure (admicelle). In situ FTIR-ATR spectroscopy has been used to uncover this adsorbed surfactant structure through the use of anionic probe molecules. The sequential adsorption of the anionic surfactant sodium dodecyl sulfate (SDS) to a pre-adsorbed $C_{16}TAB$ layer has been shown to form highly ordered surfactant surface structures. The adsorption response of SDS is highly dependent on the "structure" of the adsorbed $C_{16}TAB$ layer, and not on the amount of

adsorbed C_{16}TAB. The use of the anionic polyelectrolyte sodium polyacrylate (NaPA) has been shown to effectively "tune" the interfacial properties of the adsorbed C_{16}TAB layer by interacting and removing the bilayer portion, effectively producing a hemimicelle structure. Removal of the C_{16}TAB bilayer greatly diminishes the interaction of the adsorbed C_{16}TAB with the anionic surfactant SDS.

CHAPTER 5. FORMATION OF A THIN TiO_2 LAYER ON THE SURFACES OF SILICA AND KAOLIN THROUGH ATOMIC LAYER DEPOSITION

5.1. Introduction

The surface chemistry of pigments impacts their performance in multi-component coating systems, as was discussed in Chapter 1. Also the particle size and shape of the pigments influences such properties as the rheology of the coating and the particle packing behavior in the final dried state. In order to separate the influence of surface chemistry and particle morphology we are interested in studying pigments which have the same morphology, but different surface chemistries. In this chapter Atomic layer deposition (ALD) is used to deposit a TiO_2 layer onto the surfaces of both a silica and kaolin pigment. The reactive vapors of $TiCl_4$ and H_2O are used in a cyclic reaction sequence to grow the titania layer. Fourier transform infrared spectroscopy is used to monitor the cycle-to-cycle changes, *in situ*, during the deposition. Raman spectroscopy is used to determine the morphology of the deposited TiO_2 layer. The formation of Si–O–Ti surface bonds, through the reaction with the silica surface silanols, is detected and shows that three complete reaction cycles are necessary to fully cover the silica surface. Detection of a covalent surface bond to the kaolin is difficult due to the intensity and number of kaolin lattice vibrations in the low frequency region. Differences in the structure of adsorbed water were therefore used to monitor the extent of titania surface coverage on the kaolin. Again it is found that three complete reaction cycles are necessary to fully cover the kaolin surface. The behavior of the modified kaolin in water

is determined through measurement of its electrophoretic mobility and its dispersion stability.

5.2. Background and Literature Review

Kaolin finds widespread use as a paper coating pigment, especially for wood-containing papers, and particularly for the lightweight-coated grades (magazines, periodicals, catalogs). The sheet-like atomic structure of kaolin, resulting from the alternating alumina and silica sheets, produces a flat, plate-like particle shape with a high aspect ratio (ratio of diameter to thickness). Therefore the advantage of these plate-like pigment particles is that maximum fiber coverage can be achieved with the least amount of applied coating [1]. Kaolin particles carry a net negative charge on their planar surfaces, primarily due to isomorphous substitution [93]. At the plate edges the sheet-like atomic structure is disrupted and the broken bonds are accommodated as –OH groups [94]. The charging of the silica and alumina sites at the edges is therefore pH dependent, owing to protonation and deprotonation reactions [27]. The edges of the kaolin platelets have been estimated to occupy about 10% of the entire kaolin surface area [95]. This dual charging characteristic of kaolin particles can lead to aggregation when dispersed in water; the positively charged edge of a platelet is attracted to the negatively charged face of another platelet [96]. These aggregation mechanisms can lead to increased slurry viscosity and the formation of a structured network. At the high shear rates (10^6 s^{-1}) encountered in modern blade coating applications, these aggregated structures can lead to shear thickening behavior and blade defects [96].

Typically 100% kaolin coatings are unable to meet the required brightness and opacity targets for the final coated paper. In these cases, the introduction of a "brightening" or "whitening" pigment into the formulation is necessary. Titanium dioxide (TiO_2) is frequently added to kaolin-based coatings to achieve the desired level of opacity and brightness. The high refractive index of TiO_2 (2.56 for anatase and 2.74 for rutile) gives this pigment a high opacifying power [4]. The introduction of small amounts of TiO_2 into a coating enables a thinner applied coating for the fibrous basepaper, and is therefore particularly well suited for the production of lightweight-coated (LWC) paper grades. The major disadvantage of TiO_2 as a paper coating pigment is its relatively high cost, as compared to the kaolin and $CaCO_3$ pigments. Therefore the approach is to optimize the use of the other coating constituents (e.g. kaolin), and then to add TiO_2 to achieve the desired end-use properties [4].

An alternative means of introducing TiO_2 into coating formulations is the creation of novel pigment structures based on a low refractive index core material (e.g. silica) coated with a thin shell of titania [3]. A theoretical investigation of the optical properties of these synthetic pigments, which was based on Mie theory, has shown them to be less efficient light scatterers as compared to pure rutile [4]. However, experimental results have proven that the hiding power of these core-shell pigments is comparable to commercial rutile pigments [3]. Many different techniques have been used to attach a titania surface coating to a silica base material. The majority of the syntheses have been carried out in solution using techniques such as incipient wetness impregnation [97], sol-gel methods [98], and deposition using titanium-alkoxides [99,100]. The growth of TiO_2 thin films on silica has also been accomplished using atomic layer deposition (ALD) with

the cyclic reaction of $TiCl_4$ and H_2O vapors [101,102]. By using a gas-phase deposition process one can avoid the use of organic solvents, and also more easily control the deposition parameters.

While the synthesis of titania-coated silica pigments has been the most widely studied, the use of silica in paper coating formulations is quite negligible as compared to the use of kaolin. Silica is the most widely used pigment for the preparation of ink-jet printing papers. The high surface area and highly porous nature of amorphous silica are ideal for the required fast setting of water-based ink-jet inks [1]. Kaolin however is used in the most quantity as compared to all other paper-coating pigments, especially for the commercial production of publication grade papers. The goal of the work in this chapter is not to propose a new method of modifying kaolin on a large scale, but to understand the role of surface chemistry on the suspension behavior.

The ALD method of TiO_2 deposition using the reactive vapors of $TiCl_4$ and H_2O is employed to synthesize both silica and kaolin-based titania pigments. The characterization of the titania deposition is accomplished using vibrational spectroscopic techniques (FTIR and Raman). Performance of the modified kaolin in a water based coating is assessed by means of its electrophoretic mobility, and also its sedimentation behavior.

5.3. Experimental Details

5.3.1. Materials

The kaolin used is a commercial grade paper-coating pigment from Imerys (Astraplate). The kaolin was taken from the production process before the addition of

any dispersing agents. The kaolin was washed thoroughly with de-ionized water and heated in a furnace at 300° C for 24 hours prior to use. The reference pigments were both obtained from Degussa, and consisted of fumed silica (Aerosil 380) and fumed titania (P25). The P25 is primarily anatase with traces of rutile, as shown by Raman analysis. Titanium (IV) chloride ($TiCl_4$) was obtained from Aldrich and used without further purification.

5.3.2. Experimental Methods

The pigment particles (kaolin and silica) were spread as thin, dry films onto a CsI support and placed in an evacuable gas cell for infrared analysis. The thin film technique and the gas cell have been described previously in Chapter 3. The pigments were evacuated at either room temperature (silica), or elevated temperatures (kaolin), for a minimum of one hour before introduction of the reactive vapors. The IR spectra were collected on a Bomem MB-Series FTIR spectrometer equipped with a liquid nitrogen cooled MCT detector. Typically 100 scans were co-added at a resolution of 4 cm^{-1}. With a few noted exceptions the infrared spectra are reported as difference spectra, and therefore positive absorption bands are due to species formed on the pigment surface and negative bands indicate removal of species (bonds) from the surface.

Electrophoretic mobilities of the various samples were measured with a Malvern Zetasizer 3000 system. Stock solutions of the pigments were prepared by dispersing the kaolin (10 mg) or the TiO_2 (2 mg) in 500 ml of a 10^{-3} M NaCl solution. The background electrolyte solution was used to keep the ionic strength constant while the pH was

adjusted with HCl and NaOH. Five measurements at each pH, for each sample, were averaged to determine the corresponding electrophoretic mobility.

Raman spectra were obtained using a Renishaw 1000 spectrometer. The powdered samples were formed into dense films onto the surface of glass slides. Sample excitation was accomplished with a 785 nm Diode laser. Laser power at the sample is typically 30 mW. The 180° scattered light was collected and focused onto a charged coupled device (CCD) for detection.

5.4. Experimental Results

5.4.1. Deposition Sequence and Pretreatment Protocol

The cyclic reactions of $TiCl_4$ and H_2O with a fully dehydrated metal oxide surface can be described by the following reactions [102].

(5.1) $(-OH)_n + TiCl_4 \rightarrow (-O-)_nTiCl_{4-n} + nHCl$

(5.2) $(-O-)_nTiCl_{4-n} + (4-n)H_2O \rightarrow (-O-)_nTi(OH)_{4-n} + (4-n)HCl$

(5.3) $(-O-)_nTi(OH)_{4-n} + TiCl_4 \rightarrow (-O-)_n(TiO)_{4-n}TiCl_{4-n} + nHCl$

In this idealized depiction the $TiCl_4$ reacts with the surface hydroxyl groups to form a covalently attached $TiCl_x$ group. The second step, addition of water vapor, hydrolyses these groups to form new –OH groups at the surface. The formation of these new –OH groups, along with condensation of the added H_2O, allows the reaction sequence to be continued. Subsequent doses of $TiCl_4$ continue the propagation of a TiO_2 network, as shown in the third step. The pretreatment (dehydration and/or

dehydroxylation) of the metal oxide is of considerable importance in determining the nature of the attached groups, since this will dictate the type of surface hydroxyl groups and adsorbed water available for reaction. For silica, evacuation at room temperature is sufficient to remove all adsorbed water, while evacuation at 400° C will remove all hydrogen bonded hydroxyl groups [103].

The surface chemistry of kaolin is not as straightforward as that of silica. It has been estimated that 90% of the kaolin surface is comprised of the inert basal planes (faces), with the remaining surface being the edges of the disrupted layer structure [95]. The edges may contain three possible hydroxyl groups for the direct reaction of the first dose of $TiCl_4$ [94]. For the reaction on the kaolin faces, with no surface hydroxyl groups, the reaction proceeds by a controlled surface polymerization with a thin adsorbed water layer. Therefore removal of the surface adsorbed water, prior to the first addition of $TiCl_4$, is necessary for direct covalent attachment through the edge sites.

The thin film absorbance spectra of silica and kaolin, evacuated at 22° C, are shown in Figure 5.1. The band at 3747 cm^{-1} in the silica spectrum (spectrum A) is due to the isolated surface silanol groups [103]. The sharp bands in the 3600 – 3700 cm^{-1} region of the kaolin spectrum (spectrum B) are due to the internal –OH groups of the layered structure [104]. Dehydroxylation of kaolin, as monitored by the loss of signal intensity of these –OH groups, begins to occur above 420° C [105].

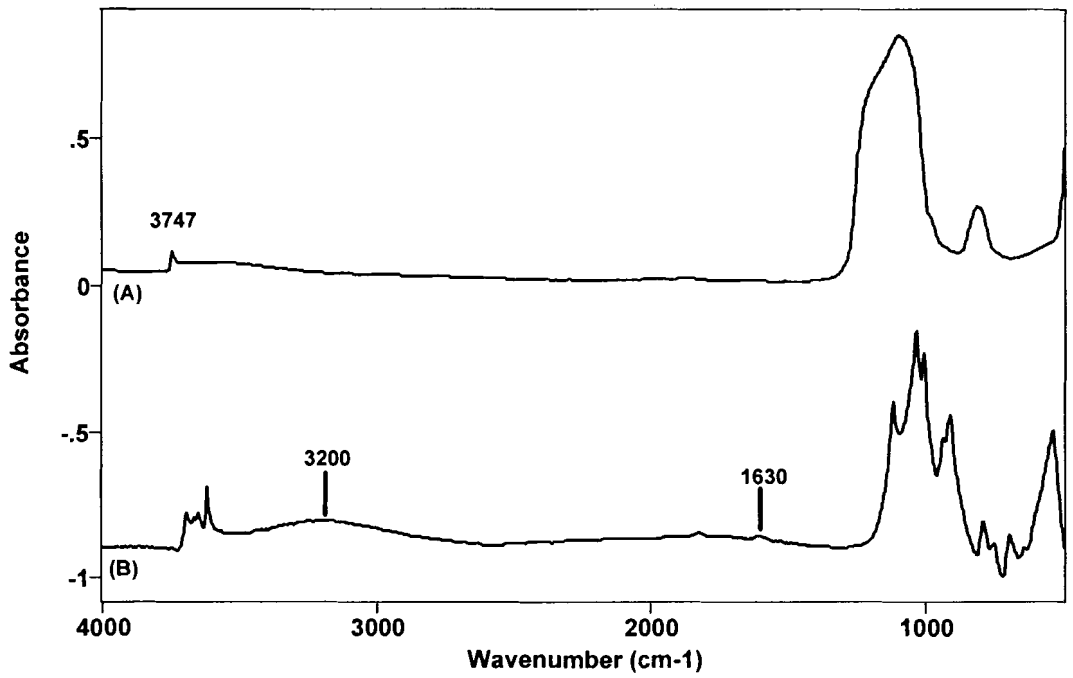

Figure 5.1. Thin film infrared spectra of (A) silica, (B) kaolin, evacuated at 22° C.

While evacuation at room temperature is sufficient in removing the adsorbed water from the silica surface, the spectrum of kaolin (Figure 5.1, spectrum B) shows a broad absorption band at 3200 cm^{-1}, and also a band at 1630 cm^{-1}. These bands are due to the H–O–H stretching and bending modes of the adsorbed water respectively. The quantification of the removal of the adsorbed water from the kaolin surface is accomplished through measurement of the intensity of these two vibrational modes. Evacuation at room temperature (22° C) removes approximately 57% of the total adsorbed water. The adsorbed water remaining after evacuation at room temperature is not completely removed until a temperature of 300° C has been reached. The removal of

this more strongly held water, as a function of evacuation temperature, is depicted by the difference spectra in Figure 5.2.

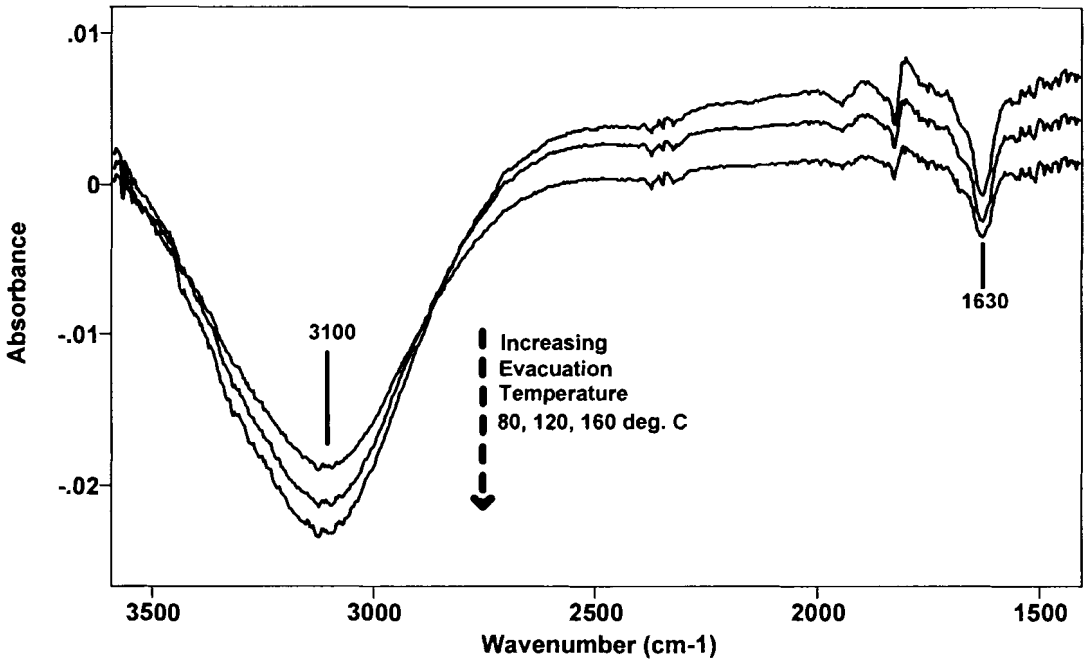

Figure 5.2. Difference spectra illustrating the dehydration of the kaolin surface as a function of evacuation temperature.

The reference spectrum for the spectra in Figure 5.2 is that of the kaolin evacuated at room temperature. The lower frequency of the water-stretching mode at 3100 cm^{-1}, is characteristic of a more strongly associated, or structured, adsorbed water layer. The result of the removal of the remaining adsorbed water on kaolin, as a function of evacuation temperature, is illustrated in Figure 5.3. The remaining 43% of the adsorbed water is not removed until an evacuation temperature of 300° C has been reached. This

result agrees well with the reported value of 280° C needed to remove the tightly held water in ground kaolinite [106]. Therefore the kaolin used in the following syntheses was evacuated at a temperature of 300° C for a minimum of one hour, then cooled to room temperature, prior to the introduction of the reactive vapors. For the silica samples, evacuation at room temperature was sufficient to ensure complete removal of the surface adsorbed water.

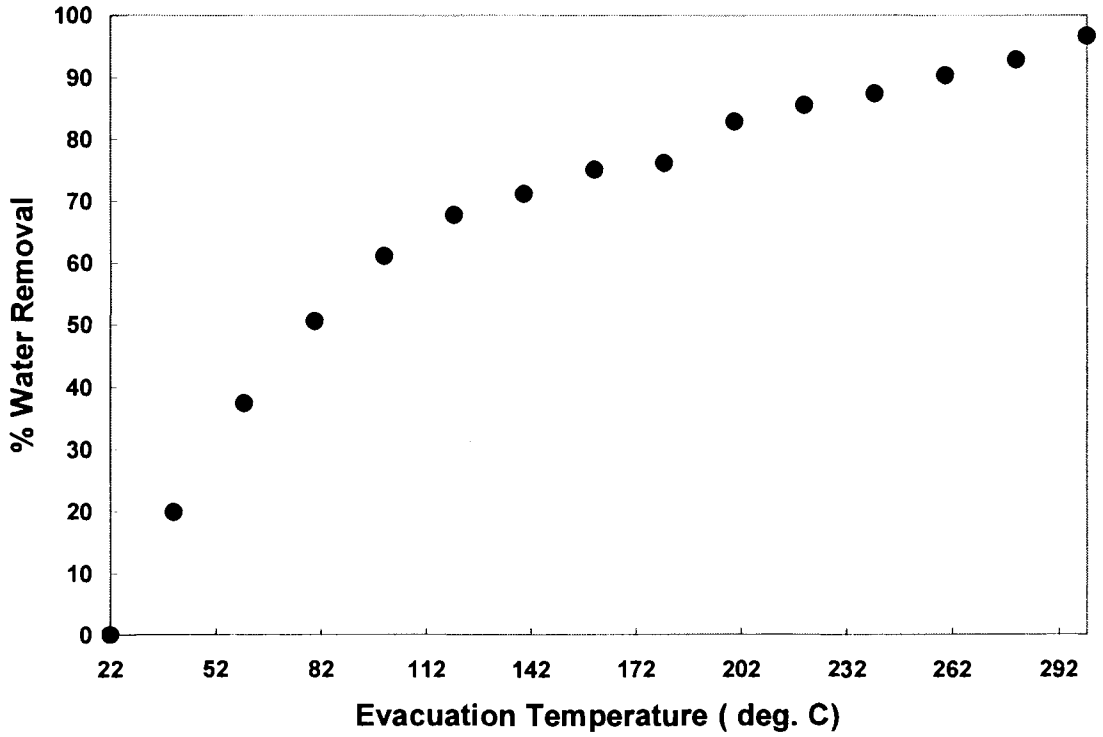

Figure 5.3. Dehydration results of kaolin as a function of evacuation temperature.

5.4.2. Spectroscopic Analysis of TiO_2 Deposition on Silica

The infrared difference spectrum resulting from reaction of $TiCl_4$ with the room temperature evacuated silica is shown as spectrum A in Figure 5.4. The sharp negative band at 3747 cm^{-1} indicates interaction with isolated surface silanols, while the broad negative feature centered at 3520 cm^{-1} indicates a small level of interaction with hydrogen-bonded silanols [107]. The low frequency region shows the appearance of numerous positive bands due to the formation of surface species. $TiCl_4$ has been shown to react both mono and bifunctionally with the silica surface –OH groups, with the relative proportion of each species depending on the pretreatment temperature of the silica [108]. The bands at 1011 and 780 cm^{-1} have been attributed to the antisymmetric and symmetric Si–O–Ti stretching modes of the monodentate $SiOTiCl_3$ species [109,110]. The formation of bands at 920 and 725 cm^{-1} are due to the creation of bidentate $(SiO_2)TiCl_2$ species, as a result of $TiCl_4$ reacting with hydrogen-bonded silanols. The band at 500 cm^{-1} is here assigned to the doubly degenerate mode of the Ti–Cl stretch. The decrease of the Si–OH band, coupled with the appearance of Si–O–Ti modes, is evidence of chemisorption via reaction depicted in Equation 5.1.

The difference spectrum resulting from the addition of H_2O vapor to the $TiCl_4$ treated silica for 5 minutes, followed by evacuation for 10 minutes, is reported as spectrum B in Figure 5.4. Hydrolysis of the $TiCl_x$ surface species results in the removal of the Ti–Cl band at 500 cm^{-1}. The formation of Ti–O–Ti bonds is indicated by the appearance of a broad band near 700 cm^{-1}. Anatase (P25) shows a broad absorption maximum in this region, as shown by spectrum C of Figure 5.4.

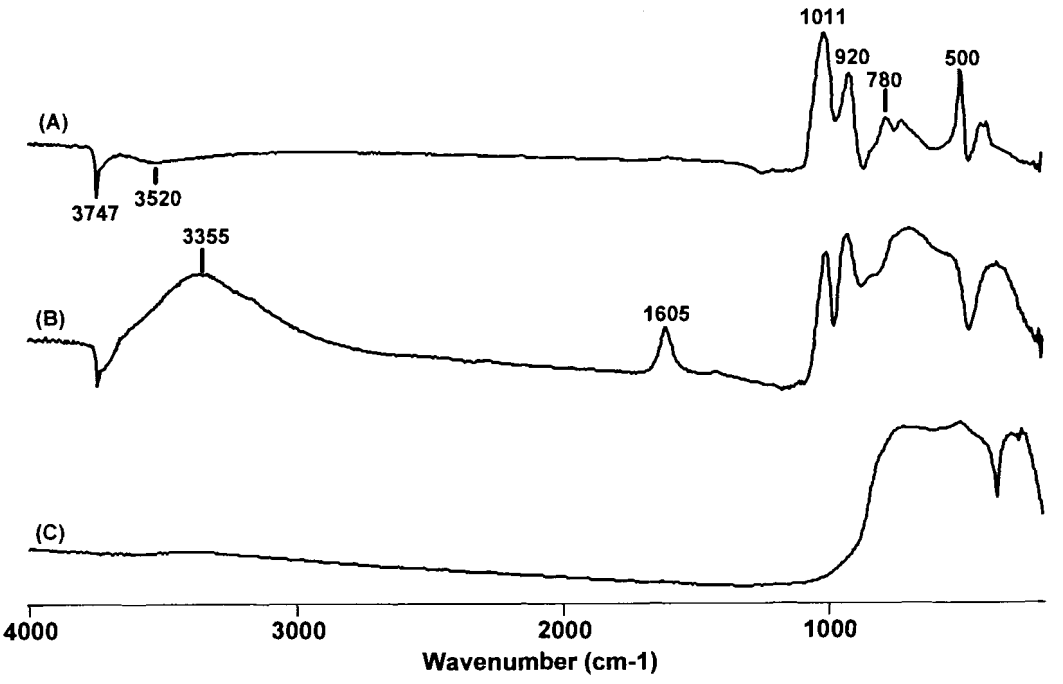

Figure 5.4. Infrared spectra. (A) Difference spectrum after first addition of $TiCl_4$, (B) Difference spectrum after first addition of H_2O. (C) Spectrum of TiO_2.

The results after one $TiCl_4$ dose show that the $TiCl_4$ is reacting with both isolated and H-bonded silanol groups, giving rise to surface attached $TiCl_x$ groups (x = 2, 3). The water vapor reacts with these groups to form a Ti–O–Ti network. Moreover, there appear the strong H–O–H stretching and deformation modes at 3355 and 1605 cm^{-1}. The silica particles are now also behaving like a titanium oxide as shown by the prevalence of adsorbed water. The adsorbed water is completely removed by evacuation at room temperature for silica, but not for titania.

The spectra in Figure 5.5 show the results after one, two, and three complete reaction cycles ($TiCl_4 + H_2O$). The increasing slope of the baseline is due to the increase

in refractive index of the silica particles caused by the high refractive index of titania (n_r = 2.5 for anatase), as compared to a refractive index of 1.46 for the silica core. This illustrates the tunability of the refractive index, of the composite particles, as a function of the number of deposition cycles. The infrared bands at 1011 and 920 cm^{-1}, assigned previously to the Si–O–Ti modes are relatively unchanged, as compared to the large increase in the region below 800 cm^{-1} due to the formation of a Ti–O–Ti network. This indicates that the anchoring to the silica surface is nearly complete after one reaction cycle, while the formation of a Ti–O–Ti network continues as Ti–OH surface groups are regenerated after each reaction cycle. We do observe a small amount of reformation of surface silanol groups after each exposure to the water vapor. Direct chlorination of the silica surface during the $TiCl_4$ treatment has been postulated as an explanation. The Si–Cl groups on the surface would produce surface silanols upon interaction with the water vapor. The reformation of surface silanol groups ceases after three complete reaction cycles.

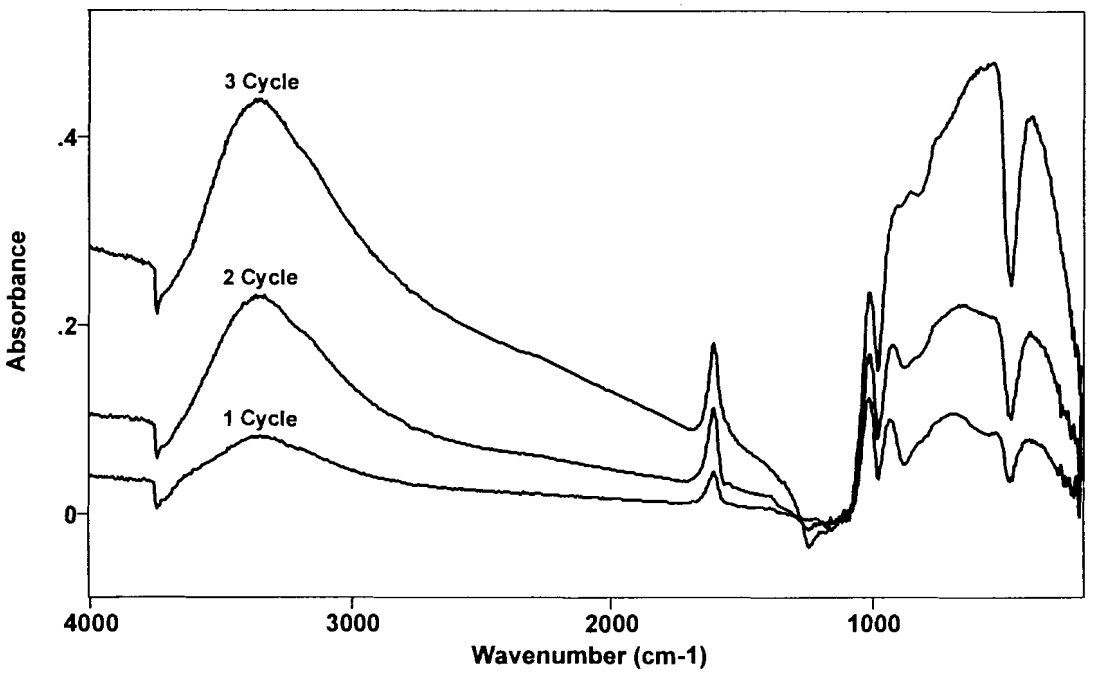

Figure 5.5. Difference spectra resulting after one, two, and three complete $TiCl_4 + H_2O$ reaction cycles.

The low frequency Raman spectrum of the starting fumed silica is shown as spectrum A in Figure 5.6. The bands at 980 and 800 cm^{-1} have been assigned to the Si–OH stretching mode and the Si–O–Si stretching mode respectively, while the bands at 605 and 490 cm^{-1} have been assigned to the D2 and D1 defect modes of tri- and tetracyclosiloxane rings which are produced via the condensation of surface silanol groups [109]. The spectrum after three deposition cycles is shown as spectrum B. The appearance of three broad bands at 600, 430, and 215 cm^{-1} are observed. These cannot be assigned to either the anatase or rutile crystalline forms of TiO_2. They are in the region where the Ti–O–Ti modes are observed, but appear to represent an amorphous TiO_2

form. After calcining to a temperature of 500° C (spectrum C), the well known bands of anatase appear at 635, 520, 403, and 146 cm^{-1}.

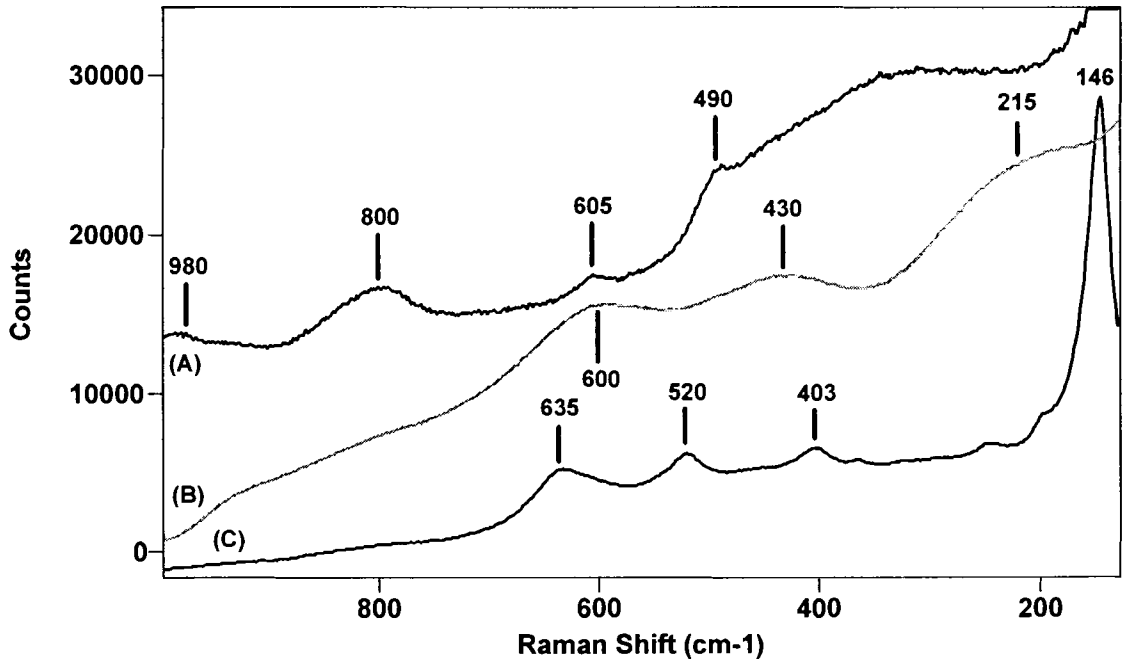

Figure 5.6. Raman spectra. (A) Silica, (B) Silica after three deposition cycles, and (C) Silica after three deposition cycles and calcination at 500° C.

5.4.3. Spectroscopic Analysis of TiO_2 Deposition on Kaolin

As compared to silica (Figure 5.1, spectrum A), the infrared spectrum of kaolin (Figure 5.1, spectrum B) is quite complex in the low frequency region (below 1200 cm^{-1}) due to the multitude of lattice vibrations of this layered alumina-silicate. Assignment of these bands has been attributed to the Si–O out-of-plane stretch at 1109 cm^{-1}, the 810 and 540 – 550 cm^{-1} region to the AlO_6 octahedron stretch, and the 470 cm^{-1} band to the tetrahedral deformation mode [111]. The number and intensity of absorption bands in this region make the detection and assignment of adsorbed surface species difficult, as compared to the results presented for silica in Figure 5.4. Reaction of the surface hydroxyl groups of silica was used to determine the extent of coverage of the deposited titanium oxide, which showed that after three reaction cycles the surface was completely covered. The presence of reactive –OH surface groups on the kaolin edges is small in comparison to the total available surface area of the clay. In addition, the intensity of the vibrational modes due to the internal hydroxyl groups would mask any detection of reaction with these surface –OH groups in the high frequency region. Therefore we make use of the crystalline structure of kaolin, and in particular the difference in the structure of water adsorbed to kaolin versus that due to an amorphous titania, in order to determine the extent of reaction with the kaolin surface.

The difference spectra after 1, 2, 3, 4, and 5 complete reaction cycles on kaolin are shown in Figure 5.7. The similarities between the spectra in Figure 5.7 (kaolin) and Figure 5.5 (silica) are apparent. There is the increase in the amount of adsorbed water as indicated by the growth in the water-stretching band (3000 – 3400 cm^{-1} region) and the water-bending mode (1600 – 1640 cm^{-1} region). The increasing slope of the baseline is

indicative of an increase in refractive index. The overall growth in the absorption in the region below 1000 cm^{-1} is similar to that observed on silica, and indicates the growth of a Ti–O–Ti network. In the low frequency region the appearance of many artifacts, which increasingly get more pronounced with each reaction cycle, correspond directly with the positive absorption bands of the parent kaolin. Therefore the low frequency absorption bands are not due to multiple Ti–O–Ti modes, but are caused by a change in refractive index, superimposed on a large aborbance band of the parent kaolin, and not to bond formation or destruction. We also observe slight negative bands in the 3600 – 3700 cm^{-1} region after each addition of $TiCl_4$, which indicates that the $TiCl_4$ molecules are able to enter the layered structure and react with the internal hydroxyl groups. However, the decrease in these bands is less than 5% of the total absorbance shown in Figure 5.1.

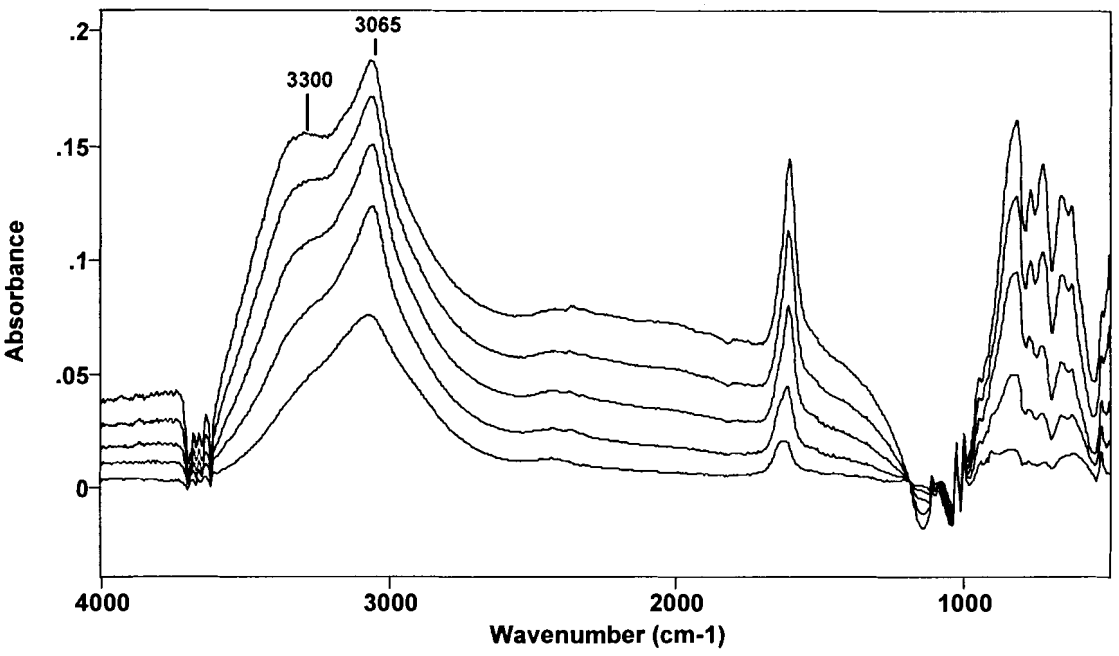

Figure 5.7. Difference spectra after 1, 2, 3, 4, and 5 complete reaction cycles from bottom to top respectively.

As mentioned previously the structure of the adsorbed water is used to determine the extent of the kaolin surface covered by the deposited titania. After the first complete reaction cycle the adsorbed water is in a highly structured configuration, as shown by the relatively low H_2O stretching mode at 3065 cm^{-1}, and the correspondingly high H_2O bending mode at 1630 cm^{-1}. There is also the appearance of a slight shoulder at 3300 cm^{-1}. We know from the dehydration behavior of the kaolin that the adsorbed water remaining after evacuation at room temperature is strongly associated with the kaolin surface, showing a stretching frequency near 3100 cm^{-1}. From the titania deposition onto the fumed silica (Figure 5.5), we observed the adsorbed water associated with the amorphous titania to show a H_2O stretching mode at 3300 cm^{-1}, along with the H_2O

bending mode at 1605 cm^{-1}. The kaolin was pretreated by evacuating at 300° C, followed by cooling to room temperature. The subsequent reaction steps were all carried out at room temperature. The first reaction cycle therefore results in the majority of the added water being adsorbed by the kaolin surface (3065 cm^{-1} band), with a small portion associated with a region of deposited titania (3300 cm^{-1} band). After successive reaction cycles the amount of adsorbed water associated with the deposited titania increases (3300 cm^{-1} band), while that associated with vacant kaolin surface sites decreases (3065 cm^{-1} band) after three complete cycles. This result is more easily recognized by looking at the behavior of the H_2O bending mode. Figure 5.8 reveals the shift in this band as a function of the number of reaction cycles.

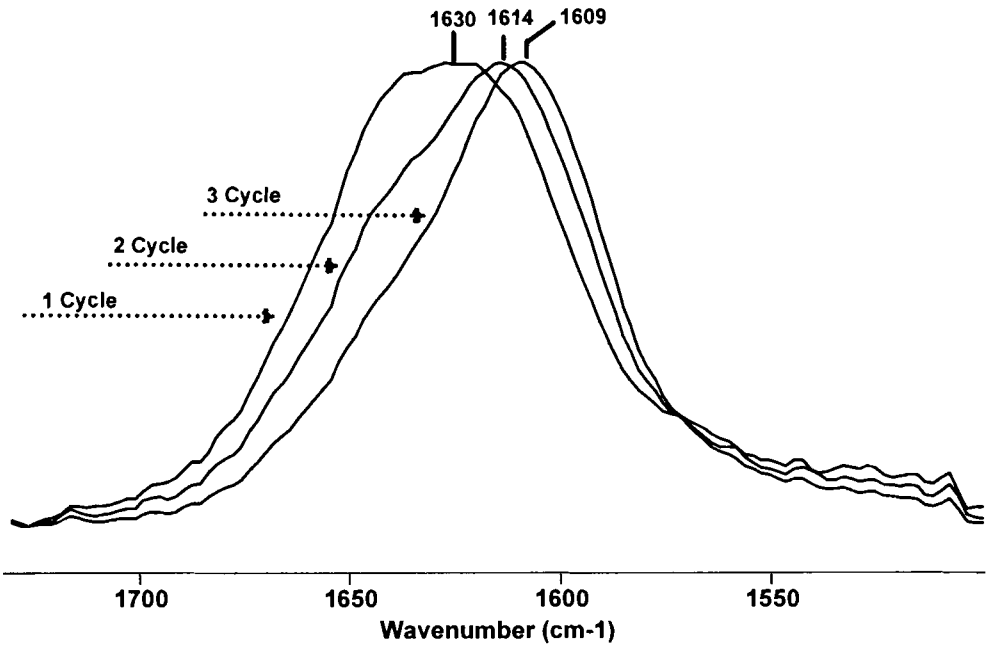

Figure 5.8. Shift in H_2O bending mode as function of number of reaction cycles.

The first deposition results in a bending mode associated with water adsorbed to the kaolin surface (broad band at 1630 cm^{-1}). After two reaction cycles the maximum has shifted to 1614 cm^{-1}, with a slight shoulder apparent at 1630 cm^{-1}. After the third cycle the H_2O bending mode has narrowed and shifted to 1609 cm^{-1}. The behavior of the adsorbed water therefore moves from one associated with a kaolin-like surface, to one associated with an amorphous titania surface. The behavior in the H_2O stretching region also shows that after three complete reaction cycles the remaining adsorption of water occurs on a titania-like surface. The layer-to-layer changes in this region are shown in Figure 5.9. The spectra are constructed by subtracting the spectrum corresponding to the previous reaction cycle from the spectrum of the current reaction cycle (e.g. cycle 3 – cycle 2). The first observation to be noted is the presence of a highly structured water layer, even after the first complete reaction cycle. This has been alluded to earlier when the $TiCl_4$ was seen to penetrate the inter-lamellar space. The formation of TiO_2 in these spaces causes a slight swelling of the clay, which is seen as a slight increase in the total surface area of kaolin sites. As can be seen, after three complete reaction cycles the kaolin surface has been completely covered, since there is no further adsorbed water associated with the bare kaolin surface (no change of the 3065 cm^{-1} band).

The low frequency Raman spectrum of the starting kaolin is shown as spectrum A in Figure 5.10. The spectrum is dominated by a large laser-induced fluorescent background. The spectrum corresponding to three $TiCl_4$ + H_2O reaction cycles is shown as spectrum B. The Raman spectrum is unchanged from that of the untreated kaolin, with no discernable absorption bands. After calcining to a temperature of 500° C (spectrum C), the characteristic bands of anatase appear at 638, 515, 401, and 146 cm^{-1}. The Raman

results mimic those of the titania deposition on silica, which showed the presence of crystalline TiO_2 only after calcination at a temperature of 500° C.

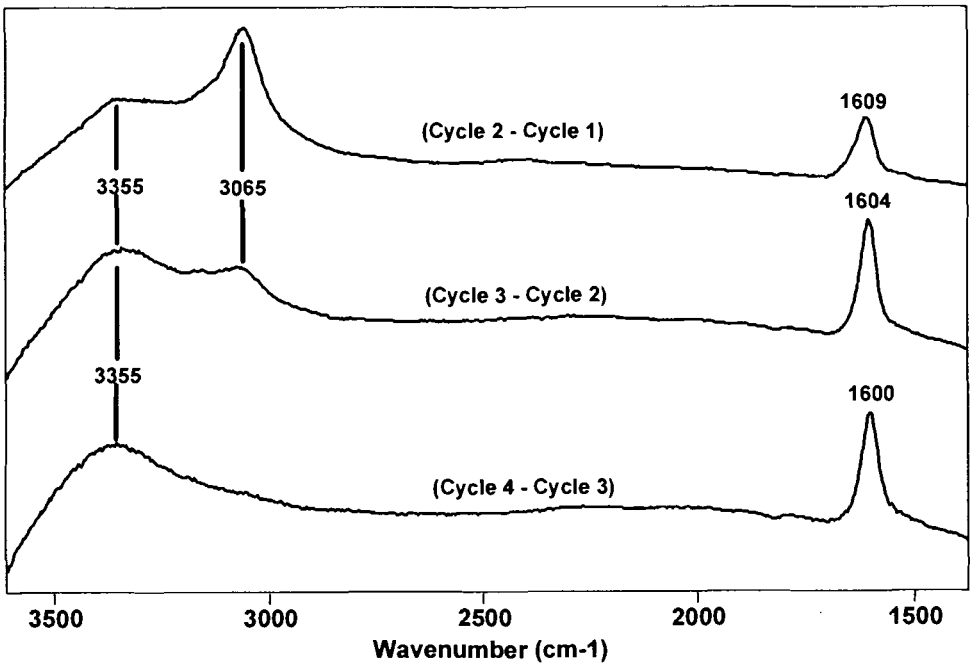

Figure 5.9. Layer-to-layer changes in the water absorption bands.

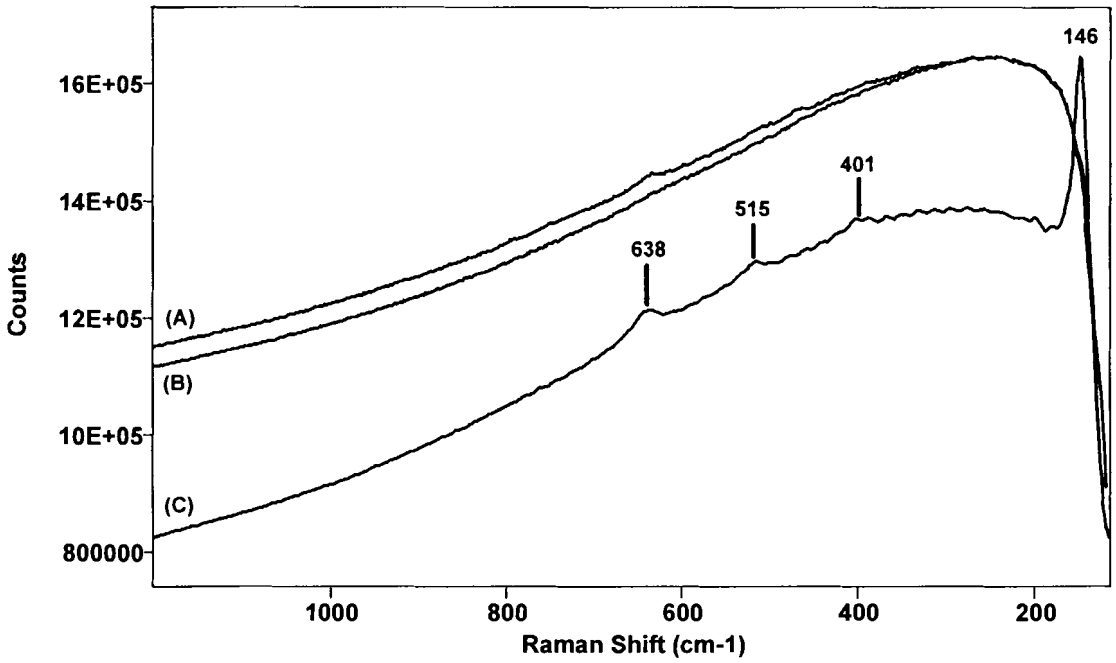

Figure 5.10. Raman spectra of (A) untreated kaolin, (B) kaolin after three reaction cycles, and (C) kaolin after three reaction cycles and calcination at 500° C.

5.4.4. Performance of TiO_2 Coated Kaolin in a Water Based System

Figure 5.11 shows the variation in the electrophoretic mobility with pH for the untreated kaolin, 1 cycle titania-coated kaolin, 3 cycle titania-coated kaolin, and pure titania (P2%). It is seen that the untreated kaolin carries a net negative charge at all pH values investigated. The edges, composed of the disrupted silica and alumina layers, have an isoelectric point in the range of pH 5 – 8, while the faces are negatively charged throughout the entire pH range [95]. The negative charging character of the faces therefore dominates the overall particle charge, conferring a net negative charge to the particles even at very low pH values. The pure titania particles used here for reference are comprised mainly of anatase, with traces of rutile. The titania shows an isoelectric point near pH 7, which is in good agreement with the literature values reported for anatase [91]. The results after one complete $TiCl_4 + H_2O$ reaction cycles are represented by the curve marked kaolin(1). The titania deposition has influenced the overall particle charging by causing an increase in the measured electrophoretic mobility for the region below about pH 7. In addition, the treated particles now possess an isoelectric point in the region of pH 3.5 – 4.0. The overall electrokinetic behavior, however, still resembles that of the untreated kaolin. The results after three complete deposition cycles are illustrated by the curve marked kaolin(3). These results clearly indicate that after three deposition cycles the kaolin surface is dominated by the presence of titania. The results mimic those of the pure titania sample, and yield and isoelectric point in the 6.5 – 7.0 range. These results correspond quite well with the spectroscopic data, which also reveal that three complete $TiCl_4 + H_2O$ cycles are needed to completely cover the starting kaolin material.

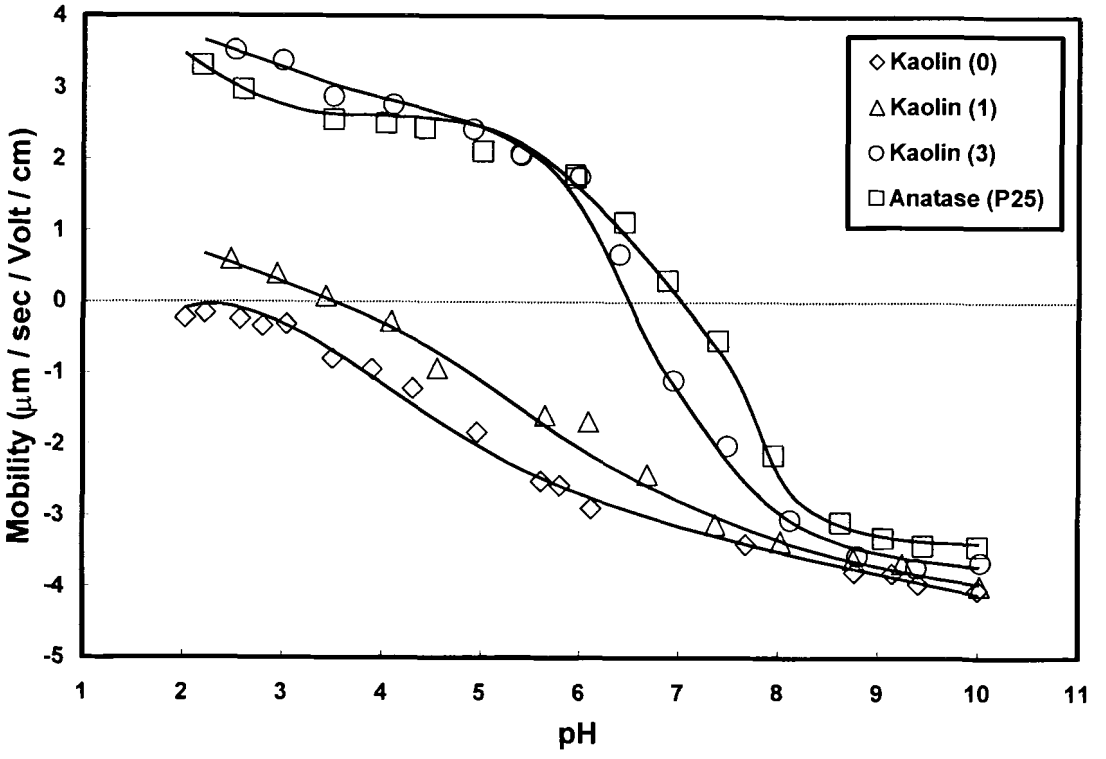

Figure 5.11. Influence of the number of deposition cycles on the electrophoretic mobility of the kaolin particles.

As mentioned previously, the dual-charging behavior of kaolin platelets can lead to flocculation of the particles and increased slurry or coating viscosity. For this reason kaolin based systems are treated with polyphosphates or polyacrylates in order to confer colloidal stability and to endure proper dispersion. Maximum dispersion of the mineral pigments in a coating system results in a reduced coating viscosity. This reduced viscosity is advantageous since it allows the coating to be applied at the highest possible solids content. High solids coatings minimize the drying requirements, limit the migration of materials with an affinity for water, and also optimize the final coating structure [2]. Figure 5.12 illustrates the effect that a titania surface coating has on the

dispersion of kaolin pigments. The pigment suspension were made up at a solids content of 10% at pH 6, mixed thoroughly for 60 minutes, then allowed to sit undisturbed for 30 minutes. The untreated kaolin begins to settles almost immediately after the mixing has been stopped, and after 30 minutes almost al of the particles have settled. The kaolin particles that have been coated with the titania remain in suspension, with only the largest fraction of the particle size distribution settling after 30 minutes. This increased stability should result in a reduction of the dispersant demand in the preparation of high solids coatings. The now uniform particle charging of the kaolin particles will also affect the particle packing, and therefore influence the final consolidated structure of the coating layer.

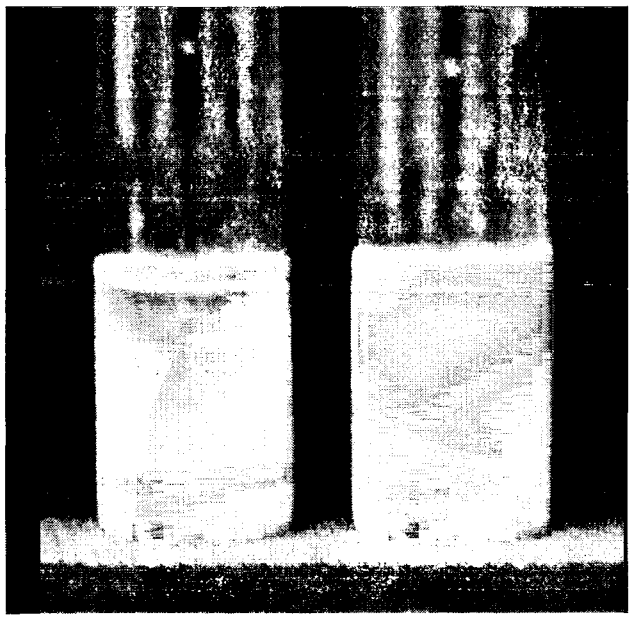

Figure 5.12. Dispersion stability of untreated kaolin (left) and titania-coated kaolin (right).

5.5. Summary

Atomic layer deposition (ALD) has been used to deposit a TiO_2 layer onto both silica and kaolin pigments using the reactive vapors of $TiCl_4$ and H_2O. The chemical attachment of the titania layer to the silica is confirmed through the formation of surface Si–O–Ti bonds, and complete coverage of the surface is accomplished after three reaction cycles. The multitude of lattice vibrations of the kaolin in the low frequency region makes the determination of surface bonding difficult. However, the difference in the structure of adsorbed water between the crystalline kaolin and the amorphous titania allow the surface coverage of the kaolin to be followed. Again it requires three complete reaction cycles before the kaolin surface has been covered by the titania coating. For both pigments the Raman spectra after the TiO_2 deposition does not reveal the presence of any crystalline forms of TiO_2. After calcining both pigments to a temperature of 500° C, the Raman spectra reveal the presence of TiO_2 in its anatase crystalline form. Investigation of the electrophoretic mobility shows the treated kaolin, after three deposition cycles, behaves like a TiO_2 particle when dispersed in water.

CHAPTER 6. THESIS SUMMARY

6.1. Conclusions

The major conclusions, which are drawn from the work presented in this thesis, are summarized below with respect to the corresponding chapter.

CHAPTER 3:

- Fourier transform infrared – attenuated total reflection spectroscopy (FTIR-ATR) is a powerful tool for studying the molecular adsorption properties occurring at the pigment – aqueous solution interface.
- The use of a polyethylene binder to anchor colloidal silica particles to the surface of an internal reflection element (IRE) does not impede the study of small molecule adsorption, either from the gas or aqueous phase.
- The polyethylene binder has been shown to only weakly perturb about 25% of the reactive surface sites on the colloidal silica particles. However, these perturbed sites are still able to participate in the gas phase reaction with silanes.
- An evacuable, gas-phase ATR cell has been designed which allows the surface reactions occurring on the surface modified IRE to be followed.
- The surface density of the aminosilane APDMES is shown to have an impact on the number of free carboxylic acid groups emanating from the silica surface after reaction with succinic anhydride.
- The results of Chapter 3 would not have been possible without the expanded spectral range advantages and the enhanced surface area afforded by using colloidal silica particles and a ZnSe IRE.

CHAPTER 4:

- The formation of a thin TiO_2 layer on the surface of a ZnSe internal reflection element is accomplished through the deposition of a fumed TiO_2 colloidal dispersion.
- The deposited pigment layer is indefinitely stable in an aqueous environment, and does not require the use of a polymeric binder.
- The adsorption dynamics of the cationic surfactant cetyltrimethylammonium bromide ($C_{16}TAB$) at the TiO_2 – aqueous solution interface have been followed using ATR spectroscopy
- The equilibrium adsorption isotherm is determined through measurement of the particle's electrophoretic mobility.
- The underlying microstructure of the adsorbed cationic surfactant is uncovered through the use of anionic probe molecules.
- The enhanced surface area of the deposited TiO_2 layer allows the distinction to be made between different adsorbed surfactant molecules based on their differing polar head groups.
- The addition of the anionic surfactant sodium dodecyl sulfate (SDS) to the pre-adsorbed $C_{16}TAB$ layer results in the formation of a highly ordered microstructure at the interface.
- The cationic surfactant $C_{16}TAB$ is shown to adsorb at the TiO_2 – aqueous solution interface as isolated islands with a "defective" bilayer structure.
- The addition of the anionic polyelectrolyte sodium polyacrylate (NaPA) to the pre-adsorbed $C_{16}TAB$ layer results in removal of the bilayer portion of the adsorbed surfactant.

- The results indicate that it is the structure of the adsorbed surfactant layer, and not the amount of adsorbed surfactant, which dictates the subsequent adsorption behavior of the system.

CHAPTER 5:

- Atomic Layer Deposition (ALD) has been successfully applied to create a thin TiO_2 layer on the surfaces of both silica and kaolin pigments.
- The reactive vapors of $TiCl_4$ and H_2O are used in a cyclic reaction sequence to form the TiO_2 surface layer.
- The formation of Si–O–Ti surface bonds, through reaction with the surface silanols of silica, is detected via FTIR spectroscopy. The results show that three complete reaction cycles are necessary to completely cover the silica surface with a TiO_2 layer.
- Detection of a covalent surface bond to the kaolin is difficult due to the intensity and number of kaolin lattice vibrations in the low frequency region. Therefore, differences in the structure of water adsorbed to the surfaces of kaolin and TiO_2 is used to monitor the extent of titania surface coverage on the kaolin pigment.
- Like the silica pigment, it was found that three complete reaction cycles is necessary to completely cover the kaolin surface with a TiO_2 layer.
- After three complete deposition cycles the surface modified kaolin displays the same surface charging as a pure TiO_2 particle, as determined by measurement of the zeta potential.
- The TiO_2 coated kaolin particles display an enhanced colloidal stability, as compared to the parent kaolin, when dispersed in water.

6.2. Recommendations for Future Work

Throughout this research the guiding principle has been to investigate the importance of molecular interactions in the context of these complex pigmented systems. Many new techniques have been developed which will allow the surface phenomena occurring in these systems to be investigated. A few introductory studies utilizing these various techniques have illustrated the applicability to aqueous-based adsorption studies. However, a lot of unsolved questions remain regarding not only the techniques, but also the impact on more complex coating systems. Therefore the following areas of research are suggested to be taken into consideration.

- Explore the influence that the polyethylene binder has on adsorption studies in systems containing long-chain molecules (polymers, surfactants, polyelectrolytes).
- Investigate the entire concentration region of the adsorption isotherm for surfactant molecules adsorbed to the surface of pigment particles.
- Determine the differences in the adsorbed microstructure of a family of surfactants, differing only in the length of their hydrocarbon tail.
- Explore the feasibility of flowing pigment particles across an adsorbed surfactant layer, in order to study the redistribution of adsorbed species between two different pigments.
- Expand upon the influence of solution conditions during the adsorption process (ionic strength, temperature, pH).

- Scale up the pigment surface modification techniques so that enough pigment can be produced to study bulk coating properties.

REFERENCES

[1] R.W. Hagemeyer, Pigments for paper, Technical Association of the Pulp and Paper Industry, Atlanta, 1984.

[2] T.W.R. Dean, The Essential Guide to Aqueous Coating of Paper and Board, Paper Industry Technical Association, Lancashire, 1997.

[3] W.P. Hsu, R. Yu and E. Matijevic, J. Colloid Interface Sci., 156 (1993) 56.

[4] R.W. Johnson, E.S. Thiele and R.H. French, Tappi J., 80 (1997) 233.

[5] D.M. Chapman, Coating Structure Effects On Ink-Jet Print Quality, TAPPI Coating Conference Proceedings, (1997) 73.

[6] A. Foissy, A. El Attar and J.M. Lamarche, J. Colloid Interface Sci., 96 (1983) 275.

[7] M.R. Böhmer, Y.E.A. Sofi and A. Foissy, J. Colloid Interface Sci., 164 (1994) 126.

[8] M. Mäkinen and A. Laakso, Nord. Pulp & Pap. Res. J., 1 (1993) 59.

[9] H.J. Hakkanen and J.E.I. Korppi-Tommola, Anal. Chem., 70 (1998) 4724.

[10] L. Järnström and P. Stenius, Colloids Surf. A, 50 (1990) 47.

[11] J.R. Boylan, Tappi J., 80 (1997) 68.

[12] T.F. Tadros, J. Colloid Interface Sci., 64 (1978) 36.

[13] L. Järnström, J. Nickel and M. Rigdahl, Nord. Pulp & Pap. Res. J., 2 (1993) 250.

[14] M. Whalen-Shaw, Tappi J., 67 (1984) 60.

[15] P. Stenius, J. Kuortti and B. Kronberg, Tappi J., 67 (1984) 56.

[16] B.J. Ninness, D.W. Bousfield and C.P. Tripp, Appl. Spectrosc., 55 (2001) 655.

[17] B.J. Ninness, D.W. Bousfield and C.P. Tripp, Colloids Surf. A: Physicochem. Eng. Aspects, (2001), In Press.

[18] B.J. Ninness, D.W. Bousfield and C.P. Tripp, Colloids Surf. A: Physicochem. Eng. Aspects, (2001), Submitted for Publication.

[19] N.J. Harrick, Internal Reflection Spectroscopy, John Wiley & Sons, New York, 1987.

[20] J.J. Kellar, W.M. Cross and J.D. Miller, Separation Science and Technology, 25 (1990) 2133.

[21] K.P. Ishida and P.R. Griffiths (1991): Adsorption of Proteins and Polysaccharides at Aqueous-Solid Interfaces by Infrared Internal Reflection Spectrometry. In: Fourier Transform Infrared Spectroscopy in Colloid and Interface Science. (: D.R. Scheuing) American Chemical Society, Boston, 208-224.

[22] R.P. Sperline, J.S. Jeon and S. Raghavan, Appl. Spectrosc., 49 (1995) 1178.

[23] J.J. Kellar, W.M. Cross and J.D. Miller, Appl. Spectrosc., 43 (1989) 1456.

[24] R.P. Sperline, S. Muralidharan and H. Freiser, Langmuir, 3 (1987) 198.

[25] S. Ross and I.D. Morrison, Colloidal Systems And Interfaces, John Wiley & Sons, New York, 1988.

[26] T.F. Tadros, Solid/Liquid Dispersions, Academic Press Inc., London, 1987.

[27] M.D.A. Bolland, A.M. Posner and J.P. Quirk, Clays Clay Miner., 28, No. 6 (1980) 412.

[28] H. van Olphen, An Introduction to Clay Colloid Chemistry, John Wiley & Sons, New York, 1963.

[29] P.C. Hiemenz and R. Rajagopalan, Principles of Colloid and Surface Chemistry, Marcel Dekker, New York, 1997.

[30] Malvern Instruments (2000): Making Zeta Potential Measurements. Zeta Potential Measurements, Manual number MAN0150, Issue 2.0.

[31] R.K. Iler, The Chemistry of Silica, John Wiley & Sons, New York, 1979.

[32] M.L. Hair, Infrared Spectroscopy in Surface Chemistry, Marcel Dekker, New York, 1967.

[33] A.V. Kiselev and V.I. Lygin, Infrared Spectra of Surface Compounds, John Wiley & Sons, New York, 1975.

[34] H.E. Johnson and S. Granick, Macromolecules, 23 (1990) 3367.

[35] J. Drelich, W.-H. Jang and J.D. Miller, Langmuir, 13 (1997) 1345.

[36] M.L. Free and J.D. Miller, Langmuir, 13 (1997) 4377.

[37] D. Neivandt, M.L. Gee, C.P. Tripp and M.L. Hair, Langmuir, 13 (1997) 2519.

[38] D.J. Neivandt, M.L. Gee, M.L. Hair and C.P. Tripp, J. Phys. Chem. B, 102 (1998) 5107.

[39] C.E. Giacomelli, M.G.E.G. Bremer and W. Norde, J. Colloid Interface Sci., 220 (1999) 13.

[40] C.P. Tripp and M.L. Hair, Langmuir, 7 (1991) 923.

[41] S.J. Hug and B. Sulzberger, Langmuir, 10 (1994) 3587.

[42] P.E. Poston, D. Rivera, R. Uibel and J.M. Harris, Appl. Spectrosc., 52 (1998) 1391.

[43] L. Han, T.M. Niemczyk, D.M. Haaland and G.P. Lopez, Appl. Spectrosc., 53 (1999) 381.

[44] K. Kajihara, K. Nakanishi, K. Tanaka, K. Hirao and N. Soga, J. Am. Ceram. Soc., 81 (1998) 2670.

[45] M. Schena, Microarray Biochip Technology, Eaton Publishing, Natick, MA, 2000.

[46] C.P. Tripp and M.L. Hair, Langmuir, 11 (1995) 149.

[47] G. Curthoys, V.Y. Davydov, A.V. Kiselev, S.A. Kiselev and B.V. Kuznetsov, J. Colloid Interface Sci., 48 (1974) 58.

[48] J.R. Combes, L.D. White and C.P. Tripp, Langmuir, 15 (1999) 7870.

[49] L.D. White and C.P. Tripp, J. Colloid Interface Sci., 232 (2000) 400.

[50] L.J. Bellamy, The Infra-red Spectra of Complex Molecules, Chapman and Hall Ltd., Thetford, UK, 1975.

[51] D. Myers, Surfactant Science and Technology, VCH, New York, 1992.

[52] M.J. Rosen, Surfactants In Emerging Technologies, Marcel Dekker, New York, 1987.

[53] M.J. Rosen, Surfactants and Interfacial Phenomena, John Wiley & Sons, New York, 1978.

[54] R. Zana, Surfactant Solutions, Marcel Dekker, New York, 1987.

[55] C.H. Giles, A.P. D'silva and I.A. Easton, J. Colloid Interface Sci., 47 (1974) 766.

[56] P. Somasundaran, T.W. Healy and D.W. Fuerstenau, J. Phys. Chem., 68 (1964) 3562.

[57] P. Somasundaran and D.W. Fuerstenau, J. Phys. Chem., 70 (1966) 90.

[58] J.H. Harwell, J.C. Hoskins, R.S. Schechter and W.H. Wade, Langmuir, 1 (1985) 251.

[59] M.A. Yeskie and J.H. Harwell, J. Phys. Chem., 92 (1988) 2346.

[60] J.F. Scamehorn, R.S. Schechter and W.H. Wade, J. Colloid Interface Sci., 85 (1982) 463.

[61] Y. Gao, J. Du and T. Gu, J. Chem. Soc. Faraday Trans., 83 (1987) 2671.

[62] B.-Y. Zhu and T. Gu, J. Chem. Soc. Faraday Trans., 85 (1989) 3813.

[63] J. Leimbach, J. Sigg and H. Rupprecht, Colloids Surf. A, 94 (1995) 1.

[64] R.A. Johnson and R. Nagarajan, Colloids Surf. A, 167 (2000) 21.

[65] R.A. Johnson and R. Nagarajan, Colloids Surf. A, 167 (2000) 31.

[66] S.C. Biswas and D.K. Chattoraj, J. Colloid Interface Sci., 205 (1998) 12.

[67] L. Ghosh, K.P. Das and D.K. Chattoraj, J. Indian Chem. Soc., LXIII (1986) 144.

[68] R. Stratton-Crawley and H.L. Shergold, Colloids and Surf., 2 (1981) 145.

[69] W.A. Ducker and E.J. Wanless, Langmuir, 15 (1999) 160.

[70] B.G. Sharma, S. Basu and M.M. Sharma, Langmuir, 12 (1996) 6506.

[71] S. Nishimura, P.J. Scales, S.R. Biggs and T.W. Healy, Colloids Surf. A, 103 (1995) 289.

[72] G. Ceotto, E.F. de Souza and O. Teschke, J. Mol. Cat. A, 167 (2001) 225.

[73] B. Li, M. Fujii, K. Fukada, T. Kato and T. Seimiya, Thin Solid Films, 312 (1998) 20.

[74] P.K. Singh, J.J. Adler, Y.I. Rabinovich and B.M. Moudgil, Langmuir, 17 (2001) 468.

[75] L. Huang and P. Somasundaran, Colloids Surf. A, 117 (1996) 235.

[76] P. Somasundaran, X. Yu and S. Krishnakumar, Colloids Surf. A, 133 (1998) 125.

[77] T. Persson, L. Jarnstrom and M. Rigdahl, Tappi J., 80 (1997) 117.

[78] J.H. Braun, J. Coat. Technol., 69 (1997) 59.

[79] S. Doeuff, M. Henry, C. Sanchez and J. Livage, J. Non-Cryst. Solids, 89 (1987) 206.

[80] P.A. Connor, K.D. Dobson and A.J. McQuillan, Langmuir, 11 (1995) 4193.

[81] P.A. Conner, K.D. Dobson and A.J. McQuillan, Langmuir, 15 (1999) 2402.

[82] P.A. Connor and A.J. McQuillan, Langmuir, 15 (1999) 2916.

[83] K.D. Dobson, A.D. Roddick-Lanzilotta and A.J. McQuillan, Vib. Spectrosc., 24 (2000) 287.

[84] H.B. Klevins, J. Am. Oil Chem. Soc, 30 (1953) 74.

[85] B.W. Barry, J.C. Morrison and G.F.J. Russell, J. Colloid Interface Sci., 33 (1970) 554.

[86] E.A. Simister, R.K. Thomas, J. Penfold, R. Aveyard, B.P. Binks, P. Cooper, P.D.I. Fletcher, J.R. Lu and A. Sokolowski, J. Phys. Chem., 96 (1992) 1383.

[87] J.R. Lu, I.P. Purcell, E.M. Lee, E.A. Simister, R.K. Thomas, A.R. Rennie and J. Penfold, J. Colloid Interface Sci., 174 (1995) 441.

[88] M.E. Montgomery Jr and M.J. Wirth, Langmuir, 10 (1994) 861.

[89] J.G. Weers and D.R. Scheuing (1991): Micellar Sphere to Rod Transitions. In: Fourier Transform Infrared Spectroscopy in Colloid and Interface Science. (: D.R. Scheuing) American Chemical Society, Washington, DC, 87-122.

[90] D.R. Scheuring and J.G. Weers, Langmuir, 6 (1990) 665.

[91] G.D. Parfitt, Progr. Surf. Membr. Sci., 11 (1976) 181.

[92] D.A. Myrzakozha, T. Hasegawa, J. Nishijo, T. Imae and Y. Ozaki, Langmuir, 15 (1999) 3595.

[93] A. Sridharan and P.V. Satyamurthy, Clays Clay Miner., 44 (1996) 479.

[94] B. Braggs, D. Fornasiero, J. Ralston and R. St. Smart, Clays Clay Miner., 42 (1994) 123.

[95] D.J.A. Williams and K.P. Williams, J. Colloid Interface Sci., 65 (1978) 79.

[96] R.M. Davis, Tappi J., (1987) 99.

[97] M.G. Reichmann and A.T. Bell, Langmuir, 3 (1987) 111.

[98] J. Retuert, R. Quijada and V.M. Fuenzalida, J. Mat. Chem., 10 (2000) 2818.

[99] M. Holgado, A. Cintas, M. Ibisate, C.J. Serna, C. López and F. Meseguer, J. Colloid Interface Sci., 229 (2000) 6.

[100] X.-C. Guo and P. Dong, Langmuir, 15 (1999) 5535.

[101] E.L. Lakomaa, S. Haukka and T. Suntola, Appl. Surf. Sci., 60/61 (1992) 742.

[102] K. Schrijnemakers, N.R.E.N. Impens and E.F. Vansant, Langmuir, 15 (1999) 5807.

[103] B.A. Morrow (1990): surface groups on oxides. In: Spectroscopic Analysis of Heterogeneous Catalysts, Part A: Methods of Surface Analysis. (: J.L.G. Fierro) Elsevier, Amsterdam.

[104] K. Wada, Clay Miner., 7 (1967) 51.

[105] R.L. Frost and A.M. Vassallo, Clays Clay Miner., 44 (1996) 635.

[106] E. Mendelovici, R. Villalba, A. Sagarzazu and O. Carias, Clay Miner., 30 (1995) 307.

[107] B.A. Morrow and A.J. McFarlan, Langmuir, 7 (1991) 1695.

[108] J.P. Blitz, Colloids and Surf., 63 (1992) 11.

[109] B.A. Morrow and A.J. McFarlan, J. Non-Cryst. Solids, 120 (1990) 61.

[110] J.B. Kinney and R.H. Staley, J. Phys. Chem., 87 (1983) 3735.

[111] J.F. Lambert, W.S. Millman and J.J. Fripiat, J. Am. Chem. Soc., 111 (1989) 3517.

BIOGRAPHY OF THE AUTHOR

Brian Ninness was born in Carnegie, Pennsylvania on December 21, 1971. He was raised in Carnegie and graduated from Chartiers Valley High School in 1990. He studied Chemical Engineering at the University of Dayton and the University of Pittsburgh, where he graduated Summa Cum Laude in May, 1995 with a Bachelors of Science degree. Brian began his graduate work at the University of Maine in September of 1995 and graduated with a Master of Science degree in May 1997. After graduating he worked as a Research and Development Engineer with the Beloit Corporation in Rockton, Illinois.

In May of 1999 he enrolled in the graduate program at the University of Maine. Brian is a candidate for the Doctor of Philosophy degree in Chemical Engineering from The University of Maine in December, 2001.